The Effect of Porefill on Pre- and Post-stack Seismic Data in a Dutch Buntsandstein Reservoir.

M.Sc. Thesis;
By:

Aaron E. Auduson

IDEA-League Universities: TU Delft/ETH Zurich/RWTH Aachen, And Wintershall Noordzee B.V., the Netherlands.

Supervisors:
Prof. Dr. Ir. Rob Arts, TU Delft
Andries Wever, Wintershall Noordzee B.V

August, 2010

Copyright ©2010: Applied Geophysics group
All rights reserved;
No part of this publication may be reproduced, stored in a retrieval system or transmitted in any form or by any means-electronic, mechanical, photocopying, recording or other formats, without prior written permission from the Applied Geophysics and Petrophysics group.

ABSTRACT

Wintershall is operating a number of Buntsandstein fields in the Southern North Sea. It has proven a major exploration challenge in the area to predict the reservoir quality of these fields based on seismic data only. The effect of salt present in the area plugging the pore space leads at first sight to similar seismic responses on post-stack data as for gas filled reservoirs. This study aims to gain better insight into the (subtle) differences in seismic response induced by water-, gas- or salt-fill scenario. The approach adopted is by studying the seismic response at various existing wells in one of the fields and the corresponding seismic responses of the processed 3D seismic survey. First a thorough analysis of the log responses of 13 wells is made and the effect of a.o. depth trends, compaction, diagenesis and facies changes to the seismic response is qualitatively investigated. Then, a match between the log data and the poststack seismic data is established by creating synthetic seismic data. Finally by using fluid substitution and more recent solid substitution theory, subtle changes in seismic response, both pre-stack and post-stack, between the different porefills are predicted. Based on these modeled predictions recommendations are made concerning the type of data analysis that should be carried out to discern the different porefills on the seismic data. The results of this research should lead to an improved characterization of the Buntsandstein reservoirs and as a consequence, to a higher success rate in drilling (i.e. less “dry wells”).

DEDICATION:

To God, my father; Vick (Edomi; Queen Victoria De Great), my wife; and Paulina, my mother (posthumous);

CONTENTS ***PAGE***

CHAPTER ONE: INTRODUCTION----------7

CHAPTER TWO: GEOLOGICAL SETTING

2.1.0 Location----------9

2.2.0 Stratigraphic successions----------10

2.3.0 Sedimentology of the Triassic Volpriehausen Formation----------12

2.5.0 Petroleum system of the Triassic Volpriehausen Formation----------12

CHAPTER THREE: THEORETICAL BACKROUND-WELL-TO-SEISMIC CALIBRATION

3.1.0 The Original Gassmann's Algorithm----------15

3.1.1 The Extended Gassmann's Algorithm For Solid-filled Media----------16

3.1.2 Verification of the Extended Gassmann's Theory----------17

3.2.0. The Shuey's Approximation of Zoeppritz equation----------18

3.3.0 Well Logs: A Review----------19

CHAPTER FOUR: WELL LOG ANAYSES

4.1.0 Workflow----------23

4.2.0 Well Data Analysis----------24

4.2.1 Deterministic cross plot analysis----------29

4.3.0 Rock Physics Framework ----------42

CHAPTER FIVE: SYNTHETIC SEISMOGRAM

5.1.0. Data Input and Quality Control----------45

5.2.0 Initial Well Tie ----------47

5.3.0. Wavelet Estimation Procedure ----------48

5.4.0 Results and Interpretation: Initial wells ----------49

5.5.0 Synthetics from Substituted wells (Predictive Modelling) ----------58

5.6.0 Results and Interpretation-Substituted well ----------62

5.7.0 AVO Behaviours----------62

5.8.0 AVO: Initial Wells ----------63

5.8.1 AVO: Substituted Wells----------63

5.8. 2 AVO Classification ----------65

5.9.0 Integrated Interpretation and Remarks----------67

***CHAPTER SIX**:* CONCLUSION.

6.1.0 CONCLUSIONS----------68

6.2.0 RECOMMENDATION----------69

ACKNOWLEDGEMENT----------70

REFERENCES----------71

APPENDICES ----------73

CHAPTER ONE

INTRODUCTION

The quality of Buntsandstein fields with the Volpriehausen sandstone as the main producing unit in the Southern North Sea suffers often from salt plugging. It has proven a major exploration challenge in the area to predict the reservoir quality of these fields based on seismic data only. The effect of salt presence in the area plugging the pore space leads at first sight to similar seismic responses on post-stack data as for gas filled reservoirs. This study aims to gain better insight in the (subtle) differences in seismic response induced by water-, gas- or salt-fill.

Pacek (2009) has studied a limited number of wells in this area trying to predict seismic responses for gas-, water- or salt filled reservoirs. To that end, she applied an extension of the Gassmann theory (R. Ciz et al, 2008) for porefill replacement by solids (i.e. salt) to predict the seismic responses. Application of the theory from one well to another did not give satisfactory results (i.e. for example predicting from a water well the response of a salt well). For a single well however, with a water-filled reservoir compartment plugged by salt only partially, a very good prediction of the sonic and density properties in these different zones has been achieved with the theory. The major conclusion of Pacek was that, the extended Gassmann theory works, but that variability in the input parameters between the different wells prevents a universal application in the area. One of the recommendations was to investigate possible depth trends in the input parameters and take these into account in the theory.

This study starts from the work of Pacek (2009). The approach adopted is by studying the seismic response at various existing wells covering different reservoir depths. A thorough analysis of the log responses of 13 wells is made and the effect of not only depth trends, but also of compaction, diagenesis and facies changes to the seismic response is qualitatively investigated. The consequences for the extended Gassmann theory are described.

As a next step, a match between the log data and the poststack seismic data is established by creating synthetic seismic data. Finally by using fluid substitution and the recent solid substitution theory, subtle changes in seismic response, both pre-stack and post-stack, between the different pore-fills are predicted. Based on these modeled predictions recommendations are made concerning the type of data analysis that should be carried out to discern the different pore-fills on the seismic data.

The results of this research must lead to an improved characterization of the Buntsandstein reservoirs and as a consequence, to a higher success rate in drilling (i.e. less “dry wells”).

This thesis is built up as follows: **Chapter two** gives the **geologic overview** of the work area. This includes the location of the work area, lithostratigraphic setting and the general petroleum system of the work area. C**hapter three** provides the **theoretical basis** and assumptions used within the limits of reasonable boundary conditions for the thesis work. C**hapter four** gives the details of the well log analyses. In **chapter five** the synthetic seismic modelling exercise is presented with the results. **Chapter six** wraps

up the thesis work giving the **conclusions and recommendations** of the work, based on the results and interpretations.

CHAPTER TWO

GEOLOGICAL SETTINGS

2.1.0 Location

The Volpriehausen petroleum system is found within the Northern part of the Southern North Sea, Offshore, the Netherlands (Figure1).

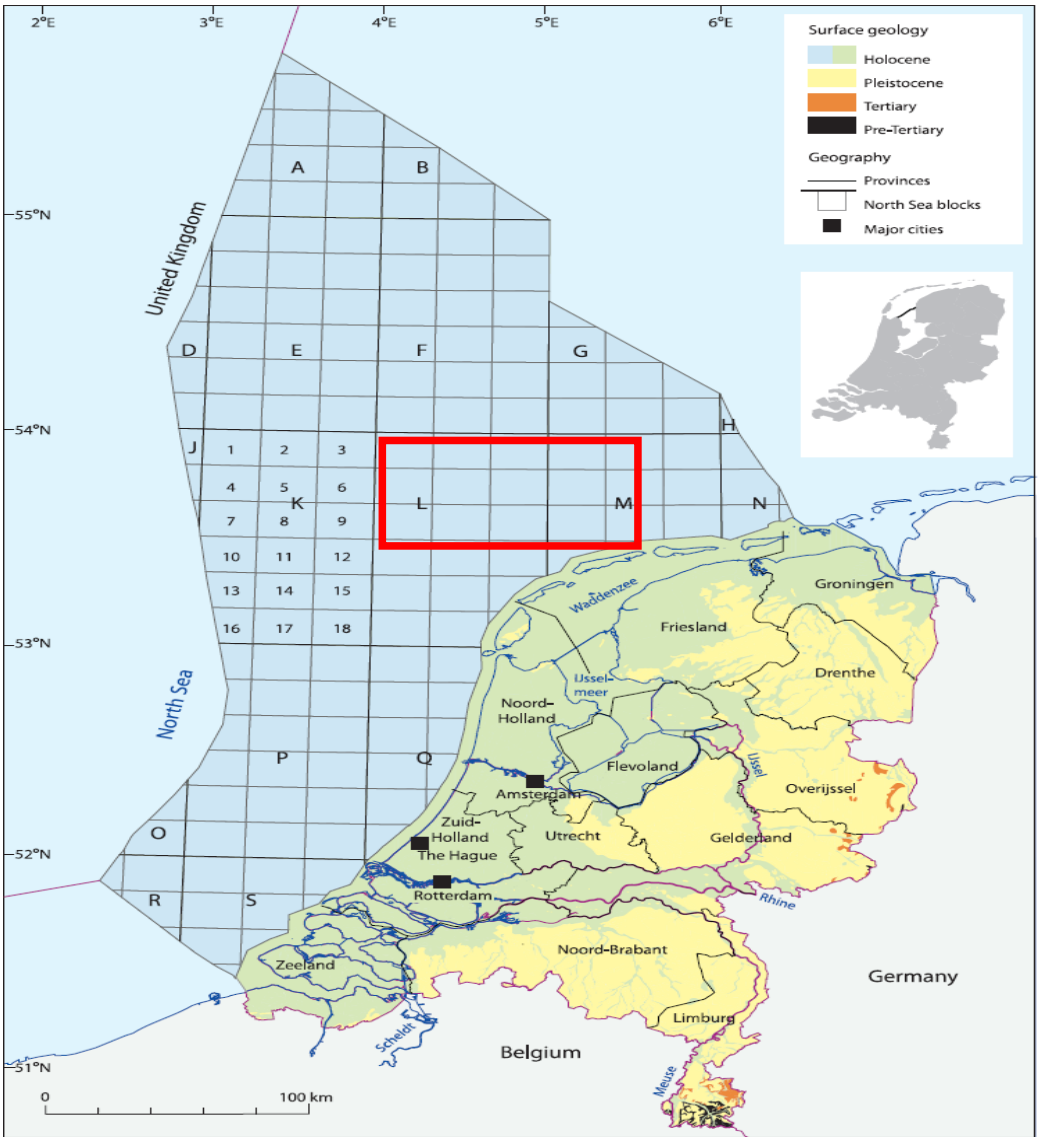


Figure 1. General map of the geography and geology of the Netherlands (2007 version, courtesy TNO data). T.E. Wong et al,2007. The red rectangle indicates the study area.

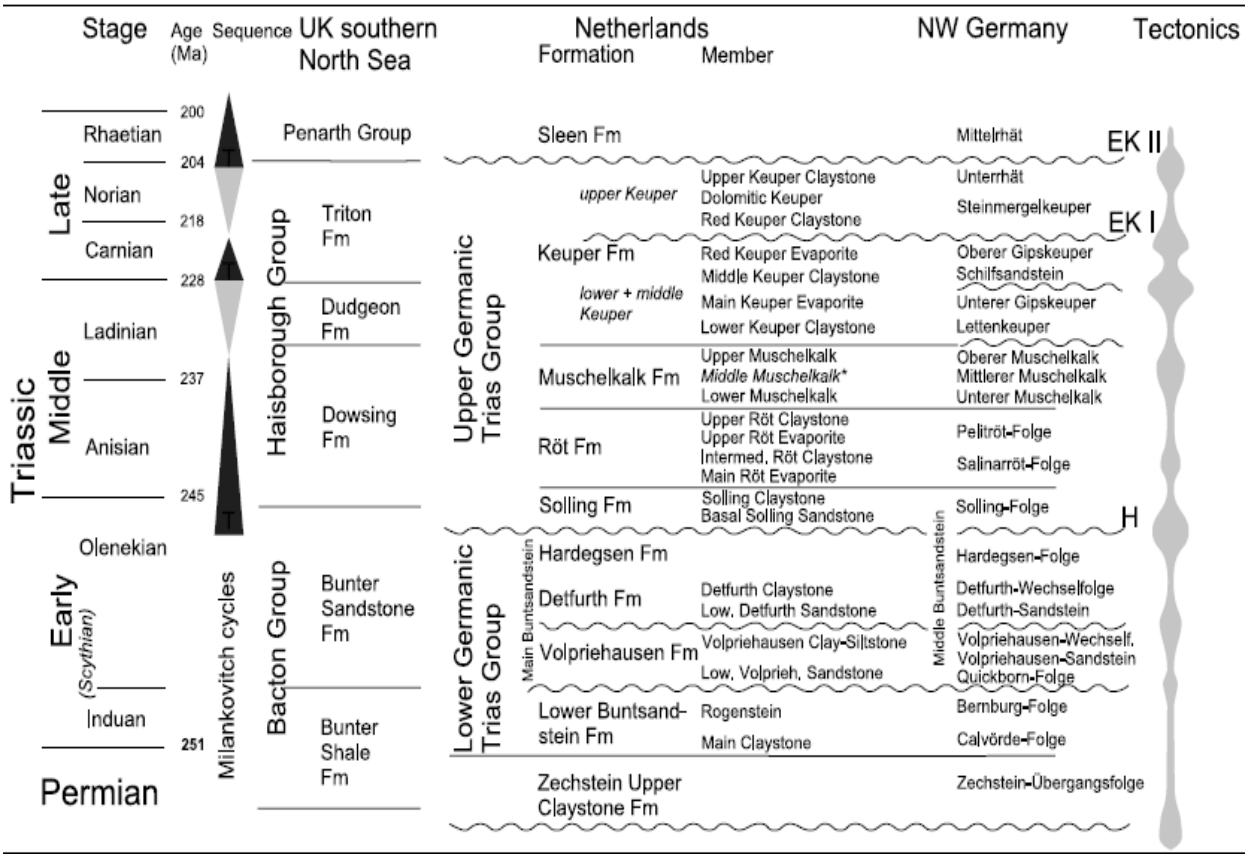
2.2.0 Stratigraphic successions

The general stratigraphic successions are summarized in table 1 (Van Adrichem Boogaert et al, 1994; Johnson et al. 1994; Geluk 1999 and Kozur, 1999). The Triassic is subdivided into two groups with the following lithostratigraphic descriptions:

1. The Lower Germanic Trias Group (latest Permian– Olenekian), comprising mainly fine-grained clastic deposits with sandstone and oolitic intercalations, with predominantly a content of sandstones at the southern basin margin;
2. The Upper Germanic Trias Group (Olenekian–Norian) comprising an alternation of fine-grained clastics, carbonates and evaporites with subordinate sandstones.

The boundary between these groups is formed by the Hardegsen or Base Solling Unconformity, which forms a regionally well-correlatable event (Ziegler, 1990; Geluk & Rohling, 1997, 1999; Geluk, 2005). The Volpriehausen Formation, which is our primary target in this case study, is located in the Triassic Lower Germanic group.
The top of the Upper Germanic Trias Group, i.e. the base of the Rhaetian Sleen Formation, forms an excellent marker on both seismic data and well logs. The Sleen Formation, representing the youngest Triassic, belongs to the Altena Group (Wong et al., 1994).

Table 1: Stratigraphic subdivision of the Triassic in the Netherlands and adjacent countries



After Van Adrichem Boogaert et al (1994), Johnson et al. (1994), Geluk (1999) and Kozur, 1999. Ages after ISC (2003); Sequences after Gianolla & Jacquin (1998); transgressive sequences in black, regressive sequences in grey. EK I: main Early Kimmerian Unconformity, base Norian; EK II: Early Kimmerian II Unconformity, base Rhaetian; H: Hardegsen Unconformity. * The Middle Muschelkalk is an informal unit and comprises the Muschelkalk Evaporite and Middle Muschelkalk Marl.

The Volpriehausen Formation is divided into two Members:

1. The Lower Volpriehausen Sandstone (clean sandstone) and
2. The Upper Volpriehausen Clay-Siltstone (several claystone intercalations).

There is no clear interface between the Lower Volpriehausen Sandstone and the Upper Volpriehausen Clay-Siltsone, but more of a gradual transition.

The Volpriehausen Formation displays its largest thickness, over 200m, in the Dutch Central Graben and the Broad Fourteens Basin. It reaches 100 m in the Ems Low and 150 m in the Roer Valley Graben. The Volpriehausen Unconformity at the base of the formation locally cuts up to several tens of meters into the Lower Buntsandstein Formation. In our study area, the Volpriehausen reservoir thickness ranges from a minimum of 4m (water well) to a maximum of 41m (gas well).

2.3.0 Sedimentology of the Triassic Volpriehausen Formation

The wells analyzed in this study are from the L and M blocks of the Southern North Sea. The cores and cuttings show that the Volpriehausen Sandstone is characterized by a pale orange to orange brown colour; with an average porosity of 10 - 15%.The interval is intercalated with silty sandstone cemented with dolomite, anhydrite and ankerite. The salt-plugged intervals show poor porosity (Core-log data) as further discussed in Chapter 4..

The Lower Volpriehausen sandstone is arkosic, with quartz content slightly below 50%. It is cemented by high percentages of calcite and dolomite, especially in its lower part. In the Dutch Central Graben, salt plugging of the pores in the sandstone is common (Fontaine et al., 1993; Dronkert & Remmelts, 1996; Purvis & Okkerman, 1996).

The Volpriehausen Clay-Siltstone forms a succession of predominantly lacustrine siltstones and marls, with subordinate sandstones.

2.4.0 Petroleum system of the Triassic Volpriehausen Formation

The Triassic sandstones are widely distributed in the Netherlands and form, after the Rotliegend, the second most important gas reservoirs in the Netherlands (de Jager et al, 2007).

In the southern part of the West Netherlands Basin, where no or very little inversion occurred, gas generation continues to present day. Although the Triassic play in the basin is largely a gas play, in several accumulations (Papekop, Pernis West, Spijkenisse Oost, Waalwijk Zuid and Botlek) an oil leg was found underneath the gas, and the Ottoland structure probably contains oil only. The oil has been correlated to the source rocks of the Lower Jurassic Posidonia Shale (Figure 2), with probably some contribution from the Lower Jurassic Aalburg and uppermost Triassic Sleen formations. This oil migrated into the older reservoirs from down-thrown blocks across faults.

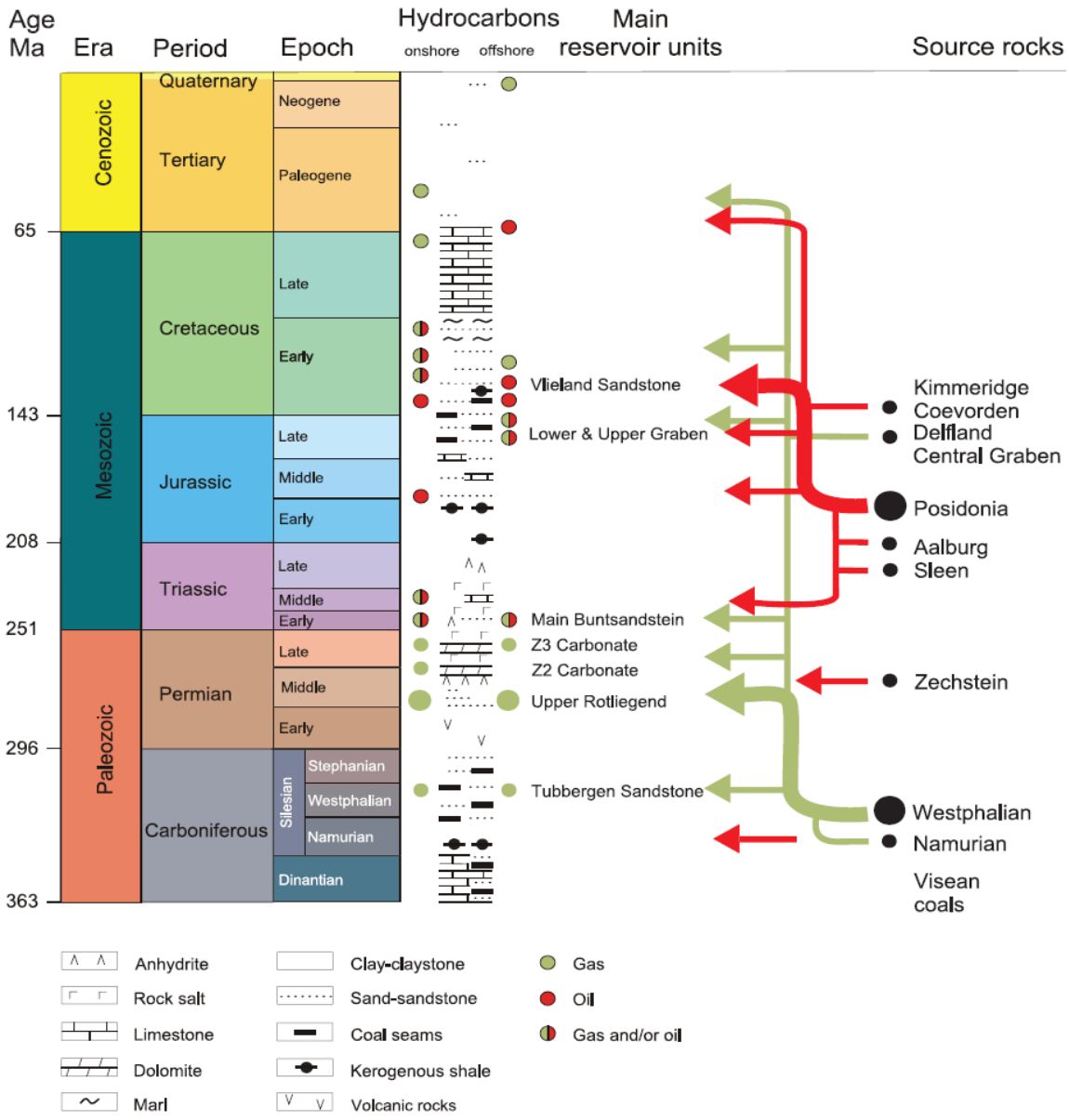


Fig. 2. Hydrocarbon systems in the Dutch subsurface. Arrows show from which source rocks the main reservoirs have been charged with gas and/or oil. The Upper Permian Zechstein salt, present in much of the subsurface, provides a regional seal between a Paleozoic gas and a Mesozoic oil and gas system.

Offshore, the Volpriehausen and Detfurth sandstones are gas reservoirs encountered in the northern Vlieland Basin, Terschelling Basin, Schill Grund High and southern Dutch Central Graben area.
In the northern part of the Western Netherlands basin, for example in block L6, similar reservoirs, that are of high quality in the Southern part, appear to be salt-plugged. The large thickness of the reservoir in part of block L9 suggests a unique depositional setting. Extensive core coverage indicates that the reservoir is made up mainly of eolian sandstones, with locally made sediments deposited as a result of glaciomarine sedimentation.

Well and seismic data show that the reservoir interval is wedge-shaped, thickening into listric normal fault that detaches onto the top of the Zechstein salt, adjacent to a salt wall.
Salt plugging of the reservoirs is a serious risk to the Triassic plays in the northern offshore (Purvis & Okkerman, 1996), hence the essence of this investigation. Salt-plugged reservoirs have been encountered in particular near salt walls and along fault planes, and are often characterized by a phase reversal of the seismic response at the top reservoir.

CHAPTER THREE

THEORETICAL BACKROUND-WELL-TO-SEISMIC CALIBRATION

In this chapter, background theory and assumptions relevant for this project are discussed including; the Gassmann theory extended for solid substitution; the verification of this relatively new theory; and the consequences for AVO analysis. Finally a short overview of well logging techniques used in this study is provided.

3.1.0 The Original Gassmann's Algorithm

As stated in the introductory chapter, rock physics is an essential link connecting seismic data to the presence of hydrocarbons and to reservoir characteristics. Modeling the effects of fluid on rock velocity and density is the common method used to ascertain the influence of pore fluids on seismic data. Gassmann's (1951) equations are the relations most widely used to calculate seismic velocity changes resulting from different fluid saturations in reservoirs.
The theory is based on the pore-pressure changes induced relative to the incompressibility (or bulk) and rigidity (or shear) moduli of the medium, by passing acoustic waves over the subsurface area. Thus, we can transform the moduli from the initial fluid saturation to the dry state, and then from the dry state to another fluid-filled state during the process of fluid substitution (equations 1 and 2).

$$K_{dry}^{-1} = \frac{K_{sat}^{-1}\left((\frac{\phi K_0^{-1}}{K_{fl}^{-1}} + 1 - \phi) - K_0^{-1} \right)}{\frac{\phi K_0^{-1}}{K_{fl}^{-1}} + \frac{K_{sat}^{-1}}{K_0^{-1}} - 1 - \phi} \text{----------(1)}$$

$$K_{sat}^{-1} = K_{dry}^{-1} + \frac{(1 - \frac{K_{dry}^{-1}}{K_0^{-1}})^2}{\frac{\phi}{K_{fl}^{-1}} + \frac{1-\phi}{K_0^{-1}} - \frac{K_{dry}^{-1}}{K_0^{-2}}} \text{----------(2)}$$

$$\mu_{dry} = \mu_{sat} \quad (3)$$

Where;

K_0 = bulk modulus of mineral material making up the rock.

K_{dry} = effective bulk modulus of dry rock.

K_{sat} = effective bulk modulus of the rock with pore fluid

K_{fl} = effective bulk modulus of the pore fluid

ϕ = Porosity

Despite the popularity and wide application of Gassmann's equations and their incorporation into most software packages for seismic reservoir interpretation, it is worth noting that a number of the underlying assumptions are not valid for common reservoir rocks and fluids (De-hua Han and Michael L. Batzle*,* 2004*).*Such assumptions include*:*

1. The porous frame is macroscopically and microscopically monomineralic, elastic, homogeneous and isotropic (all minerals making up the rock have the same bulk and shear moduli and that the fluid-bearing rock is completely saturated).
2 All pores are interconnected and that the pore pressure is in equilibrium within the pore space.
3 The medium is a closed system with no pore-fluid movement across boundaries.
4 There is no chemical interaction between fluids and rock frame
5 Sufficiently low frequencies 100Hz (to give enough time for the pore fluid to flow and eliminate wave-induced pore pressure gradients; also implying 'no frequency dependency).

Many of these assumptions may not be valid for hydrocarbon reservoirs and depend on rock and fluid properties and the in-situ conditions. For example, most rocks are anisotropic to some degree, invalidating assumption (1). The work of Brown and Korringa (1975) provides an explicit form for an anisotropic fluid substitution. In such cases, seismic frequencies may still be too high for the application of Gassmann's equation. Pore pressures may not have enough time to reach equilibrium, and the rock remains unrelaxed or only partially relaxed. A Gassmann-type calculation provides an estimate of relaxed velocity at zero frequency, which is a lower bound of the fluid-saturation effect.
In the Volpriehausen case, the reservoir is normally very clean and homogeneous. A thick clean (i.e. very low Gamma Ray) interval honours most of the rock frame conditions. However, a shaley sand, or sand with intercalated shale layers results in the violation of assumption 1.

3.1.1. The Extended Gassmann's Algorithm For Solid-filled Media

The original Gassmann theory was further extended recently by Ciz and Shapiro (2008) for the case where the pore space is filled with anisotropic, elastic solid material. Example is halite grains plugging into the reservoir pores spaces which is the case study here.
The basic operational theory is summarized hereafter as follows:

$$K_{sat}^{*-1} = K_{dry}^{-1} - \frac{\left(K_{dry}^{-1} - K_{gr}^{-1}\right)^2}{\phi\left(K_{if}^{-1} - K_{\phi}^{-1}\right) + \left(K_{dry}^{-1} - K_{gr}^{-1}\right)} \quad (4)$$

And

$$\mu_{sat}^{*-1} = \mu_{dry}^{-1} - \frac{\left(\mu_{dry}^{-1} - \mu_{gr}^{-1}\right)^2}{\phi\left(\mu_{if}^{-1} - \mu_{\phi}^{-1}\right) + \left(\mu_{dry}^{-1} - \mu_{gr}^{-1}\right)} \quad (5)$$

Where

K_{sat}^{*-1} and μ_{sat}^{*-1} are solid saturated bulk and shear moduli;

K_{dry} and μ_{dry} denote drained bulk and shear moduli of the porous frame;

K_{gr} and μ_{gr} represent bulk and shear moduli of the grain material of the frame;

K_{if} and μ_{if} are bulk and shear moduli related to the solid body of the pore infill;

K_{ϕ} and μ_{ϕ} are the bulk and shear moduli related to the pore space of the frame.

As one might expect, the major change is observed for the shear modulus, where the assumption of no shear stresses is no longer valid.
Expressions 4 and 5 represent the new isotropic Gassmann equations for a solid-saturated porous rock (cf. equations 1 and 2).

3.1.2 Verification of the Extended Gassmann Theory

This new generalized Gassmann model has been verified against real data
In the attempt to validate the new Gassmann theory, R. Cis et al (2008) made a comparison between the extended theory with experimental data using samples filled with viscous heavy oil in rock physical laboratory. The latter is considered as a solid, particularly at low temperatures. Han et al. (2007) have performed a number of experiments on heavy oils and heavy oil rocks and the results of the measured ultrasonic velocities of heavy oil in dependence of temperature are shown in figure 2a (left). They show that for a wide range of temperatures the measured data correlates very well with classical Gassmann's equations. This is seen for temperatures 60° C and higher. The linear increase with temperature is shown at temperatures lower than 50° C, where we observe deviation between measured data and the classical Gassmann's equations. The shear velocity of the heavy oil becomes non-zero. In R. Cis et al 2008 show(figure 2a to the right) that the application of the new generalized Gassmann's equations improves the results obtained by Han et al. (2007) using classical Gassmann's equations. Our results also show that the new model implementing the corrected infill moduli can provide an almost exact match with measured data. In this case, the value of P- and S-wave velocity at the lowest temperature is used for the calibration of the infill properties. This result confirms applicability of the new Gassmann's equations for the heavy oil modeling.

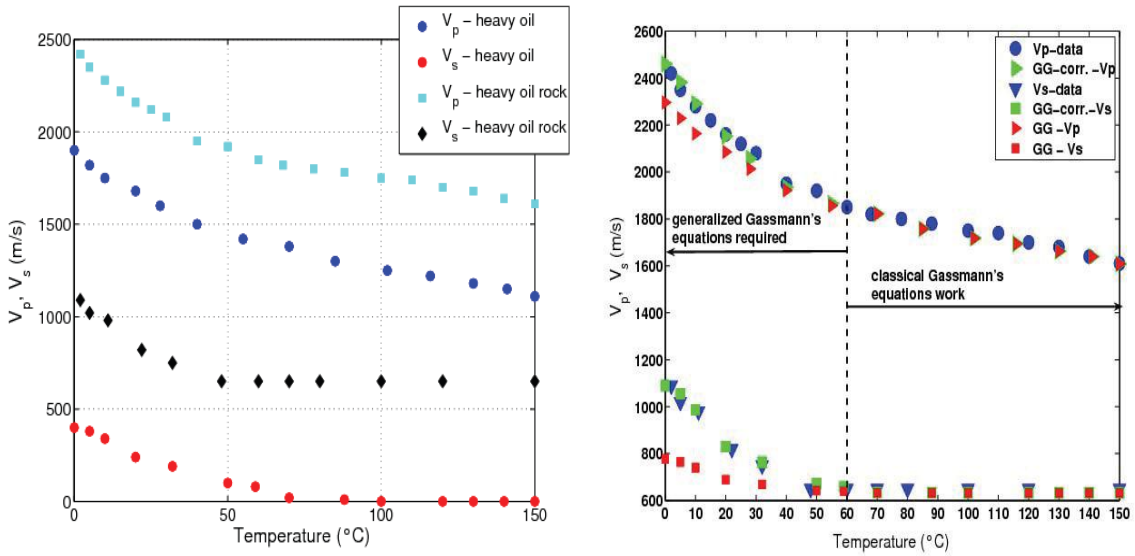


Figure 2a.Measured P- and S-wave velocities for heavy oil and heavy oil rocks on the left and the comparison with the application of new Gassmann's model (GG and GG-corr) based on equations 1 and 2. After Cis et al,2008

More recently Pacek (2009) has applied this theory to predict solid (salt) substitutions in water-filled Volpriehausen reservoirs in our study area. For a single well with a water-filled reservoir compartment plugged by salt only partially, a very good prediction of the sonic and density properties in these different zones has been achieved with the theory. The major conclusion of Pacek was, the extended Gassmann theory works, but that variability in the input parameters between the different wells prevents a universal application in the area. One of the recommendations was to investigate possible depth trends in the input parameters and take these into account in the theory.

3.2.0. The Shuey's Approximation of Zoeppritz equations

To investigate the behaviour of pre-stack seismic amplitudes versus offset (or angle of incidence) at the top reservoir, we use the Shuey's approximation (Hampson-Russell, 2004), a simplified linearization of the full Zoeppritz' equations, in this study.

Shuey's (1985) approximation assumes small layer contrasts and is described briefly as follows:

$$R(\theta) = R_P + \left[R_P A_0 + \frac{\Delta\sigma}{(1-\sigma)^2} \right] \sin^2\theta + \frac{\Delta\alpha}{2\alpha}(\tan^2\theta - \sin^2) \qquad (6)$$

Where: $\sigma = (\sigma_1 + \sigma_2)/2$

$$\sigma = \sigma_2 - \sigma_1$$

$$A_0 = B - 2(1+B) * \frac{1-2\sigma}{1-\sigma}$$

$$B = \frac{\Delta\alpha/\alpha}{\Delta\alpha/\alpha + \Delta\frac{\rho}{\rho}}$$

Further simplifications result in:

$$R(\theta) = R_P\left[1-\sin^2\theta\right] + \frac{9}{4}\Delta\sigma\sin^2\theta = R_P + [\frac{9}{4}\Delta\sigma - R_P]\sin^2\theta = R_P + G\sin^2\theta \qquad (7)$$

Where: $\Delta\sigma = \frac{4}{9}(R_P + G)$ = Poisson's ratio;

R_P is intercept (normal incidence) and G is the gradient (Poisson reflectivity). Hence, with appropriate determination of these parameters, the acoustic and elastic impedance can be calculated, from which the seismic attributes for reservoir characterization are extracted.

3.3.0 Well Logs: A Review

In reservoir characterization, attributes such as porosity, permeability and fluid saturation, are the basic parameters of a reservoir to look out for in the assessment of reservoir quality. This section provides the petrophysical characteristic parameter measurements and extractions requisite for the 2D forward modeling for the synthetic-to-seismic ties. Figure 3 below shows the basic input parameters that can be measured during the logging operations. For the purpose of this study, the parameters needed for the modelling are as follows: **Gamma radiation, density, porosity, sonic, the compressional velocities, shear wave velocities. T**he respective logs and their analyses are carried out briefly as follows:

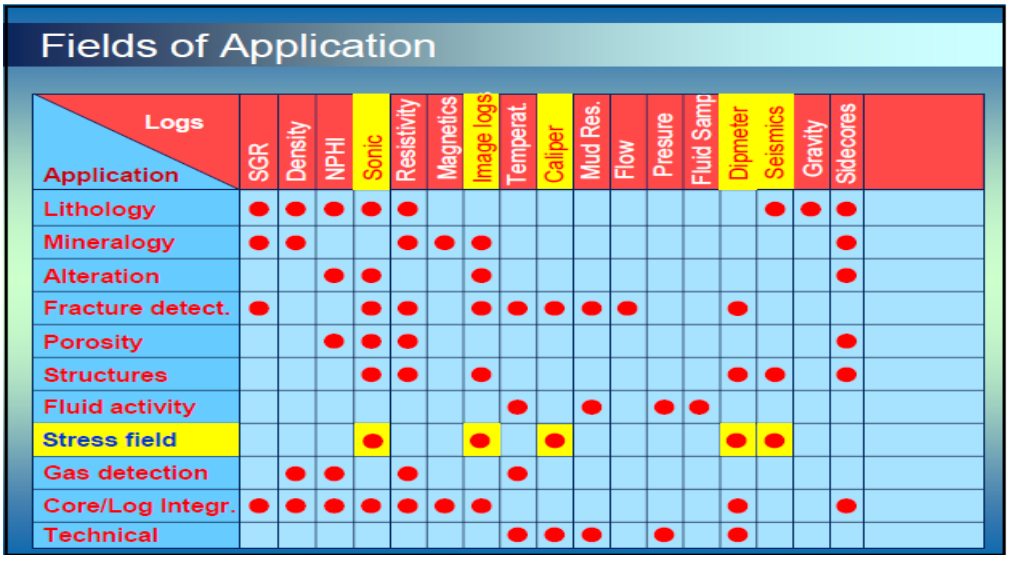


Figure 3: Geophysical log and their application. Courtesy geophysical logs and interpretation course work 2009.

The Gamma-Ray (GR) Logging: The Gamma-Ray tool is capable of detecting variations in the natural radioactivity originating from changes in concentration of the trace **elements** uranium (U), thorium (Th) and potassium (K); hence it is used in the GR measurements. The tool is sensitive to sodium iodide scintillation counter and a photo-multiplier. The Compton scattering, is driven by the electron density of material which is relatively constant and can hence be ignored. However, salt does not follow the sedimentary trend. The tool is calibrated in API (American Petroleum Institute) unit (Figure 4 below).
Since the concentration of these radioactive elements varies between different rocks types, gamma-ray logs are used for lithological mapping (commonly accepted is that high Gamma-ray reading is an indication of shale).

The Density logging; Density Measurement is based on gamma radiation and Compton scattering – scattering by the electron sheath; attenuation of which proportional to the electron density. The measurement of the formation's density is a sum of matrix and fluid density and porosity as given by Wyllie equation (Wyllie et al 1963).Hence, porosity logs also derived from the density logging operation.
Although, Compton scattering depends on electron density and not bulk density, density-logs are calibrated (counts/s; SI unit in g/cm³) to give the correct bulk density in the majority of sedimentary rocks (Figure 5).

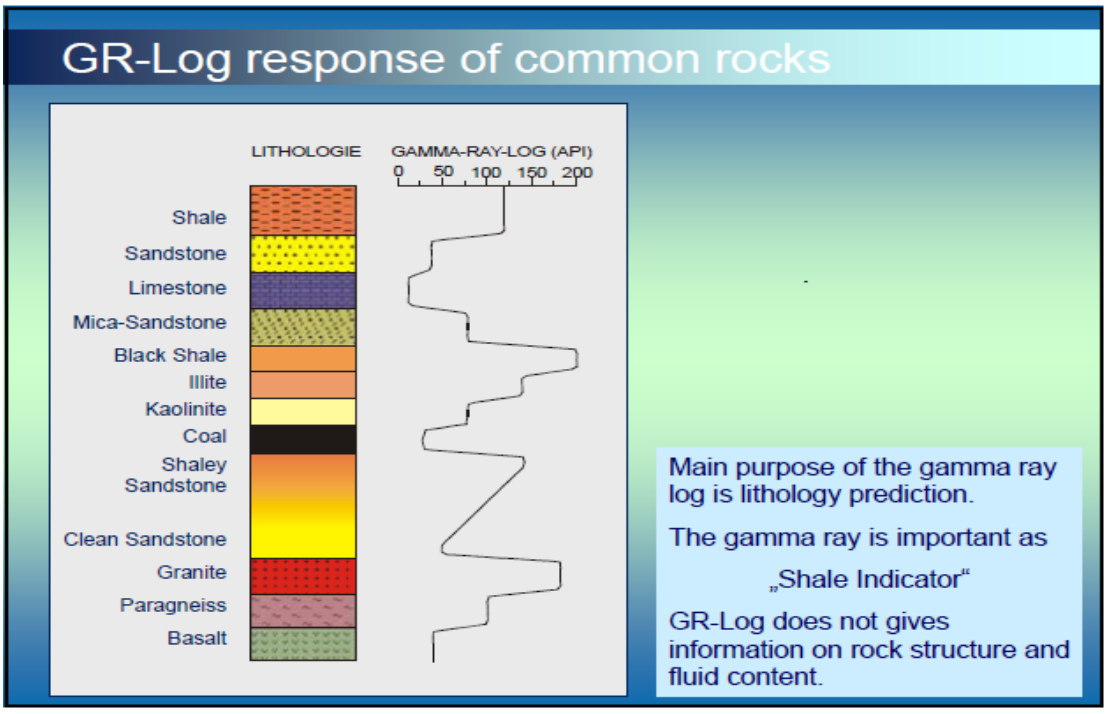


Figure 4: Gamma Ray logs as lithologic mapper. Courtesy geophysical logs and interpretation course work 2009.

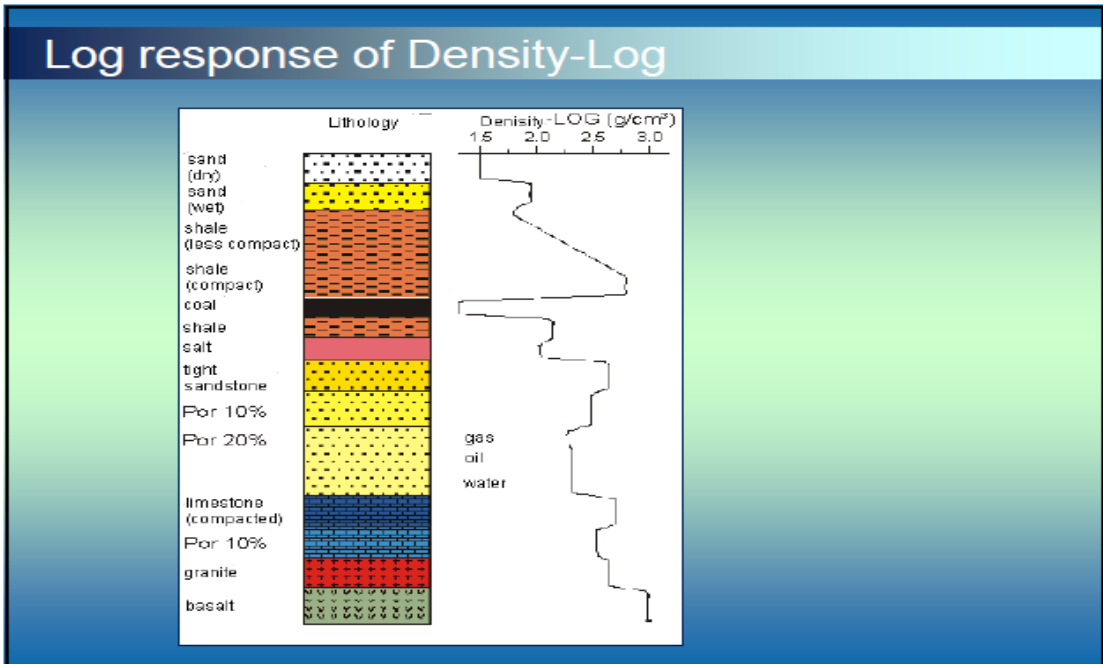


Figure 5: Density log sedimentary profile response. Courtesy geophysical logs and interpretation course work 2009.

The Sonic Logging: The sonic logging tool is capable of measuring and recording the compressional slowness based on the transit time between transmitter and receiver. An acoustic transducer emits a sonic signal between 10 and 30 kHz which is detected at two receivers (Figure 6 and 7). The time between emission and reception is measured for each receiver, and subtracted to give the travel time in the interval between the two receivers (Figure 6).

If the receivers are two feet apart, then this time is divided by two to give the interval transit time, or slowness, of the formation. The depth of investigation depends on the slowness, the transmitter-to-receiver spacing and the presence or absence of an alternated zone.

The sonic tool is calibrated in units of Δt [μs/m] which are converted into Vp, Vs and Vs_int [km/s].Hence, the requisite velocity for the modelling operation are obtained from the sonic logging tools. Log response of the sonic logging is as shown in Figure 8.

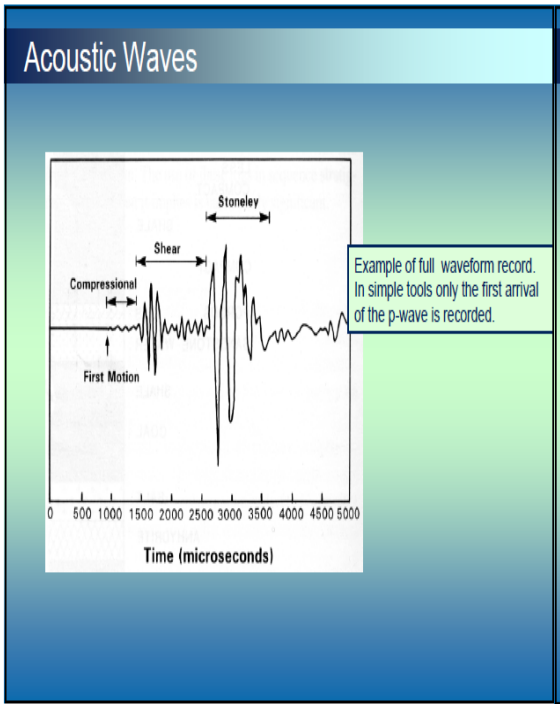


Figure 6 Left acoustic wave form

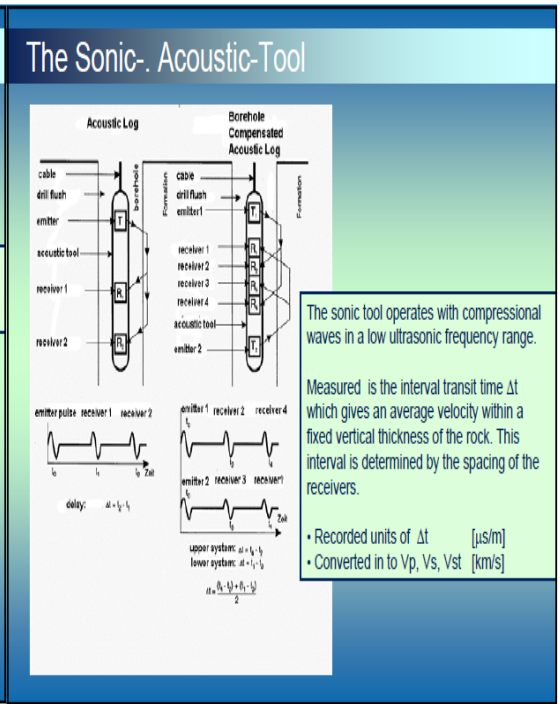


Figure 7.Transmiting and receiving of sonic signal. Courtesy geophysical logs and interpretation course work 2009.

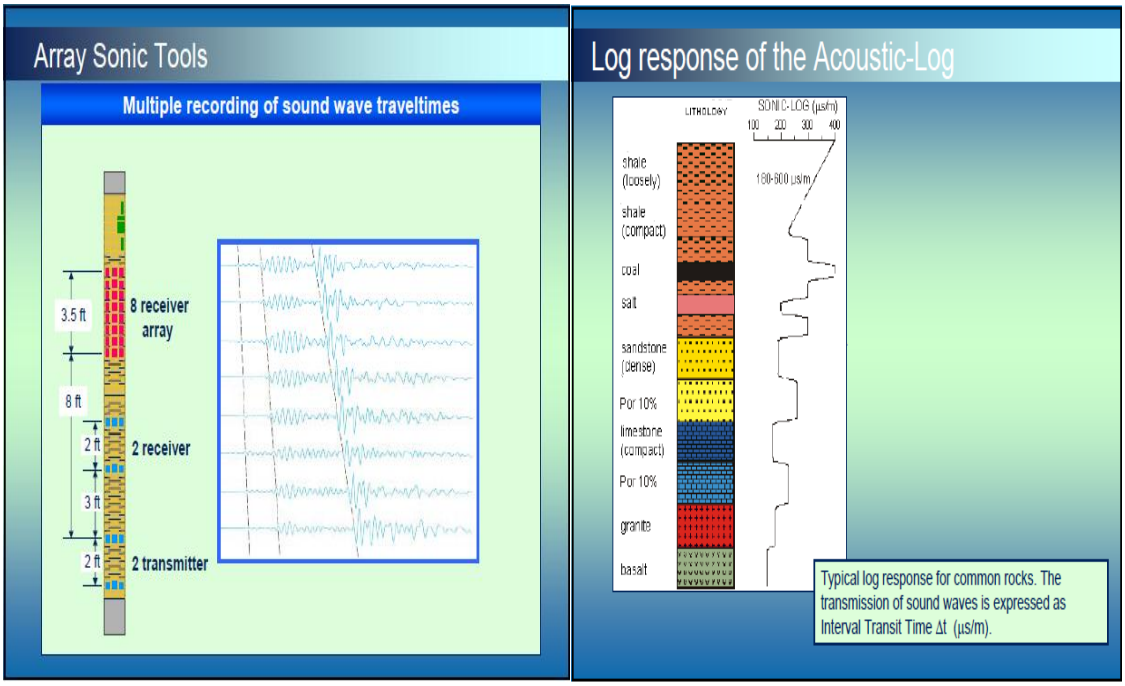


Figure 8.Left: example of multiple recording of interval transit time. Right: Sonic-response log. Courtesy geophysical logs and interpretation course work 2009.

CHAPTER FOUR

WELL LOG ANALYSES

Based on the standard principles of well logs reviewed above, wells used for the synthetic models are here by analyzed for proper data verification.

4.1.0 Workflow

The following steps are used within my workflow for both the well and the seismic data sets (figure 9):

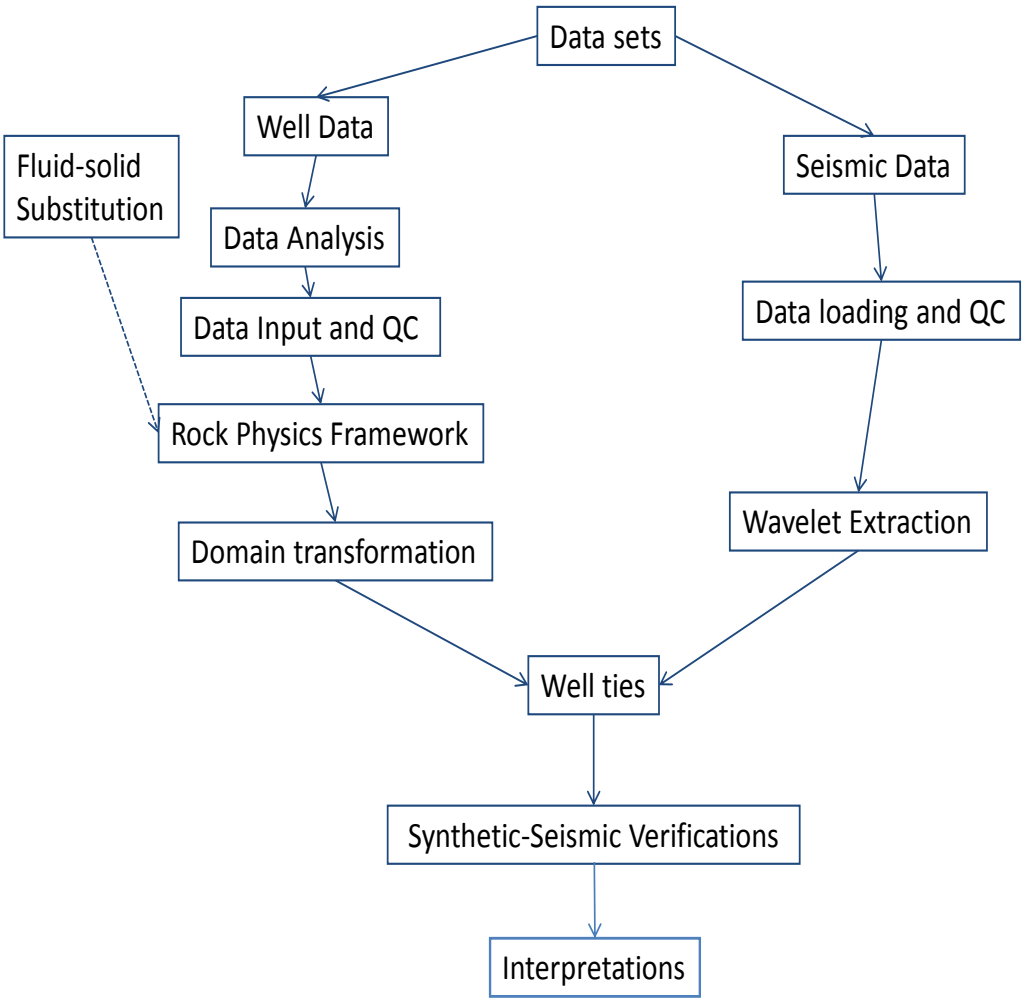


Figure 9.Workflow, indicating the major sequences of procedures followed in the work.

4.2.0. Well Data Analysis.

The key parameters for our analysis are probably the density and velocity (or sonic) measurements, since these are directly linked to the seismic response and are required input for our rock physics fluid/solid replacement modeling. Therefore a thorough qualitative assessment is required.

Pacek (2009) observed in her study inconsistencies between the logged bulk densities, the measured core densities and the densities derived from the logged porosities and saturations. The latter is important, since our rock physics model requires consistent input between saturations, porosities and densities. Pacek (2009) decided to use the densities derived from the porosity logs in her study for fluid replacement. Required matrix densities were derived from core data.

The starting point for this study is to verify the consistency between the different log and core data observations particularly for the density. To that end the formation bulk density was plotted against the measured (equation 9) core density. Furthermore, the bulk density against the depth of the reservoir intervals has been analyzed to study potentially systematic density variations with depth.

$$\rho_{B-Core} = (1-\phi) * \rho_{M_a} + \phi(\rho_x * S_x + \rho_y * S_y + \rho_z * S_z) \qquad (9)$$

Where: ρ_{B-Core} = Core bulk density in the well in analysis; ϕ = porosity; ρ_{M_a} is the matrix density of the reservoir material; ρ_x, ρ_y and ρ_z refers respectively to the corresponding solid or fluid filling the reservoir interval; S_x S_y S_z refers respectively to saturation of the corresponding solid and fluid in the interval.

These parameters mainly matrix density and porosity occur variably for each of the well as provided by the core data information table in back-up report by the logging companies.

The corresponding core porosity at each depth interval of the wells were also derived (in fraction) and loaded into the RokDoc project. RokDoc is the software package used for this work (Please, see next chapter). The water saturations in each well were extracted and averaged from the already uploaded 'las. files' in the RokDoc™ 2D well viewer. The other fluid or solid saturation in the respective well was then obtained by a difference between the water saturation and unity (1).In some cases; 100% saturation was assumed, depending on the prevailing quantity approximated from the las. file and the background information about the particular well in the back-up reports.

A total of **thirteen** were loaded into the project of the programme, for the analysis, out of which only **nine wells** had core data information classified as follows based on the predominant percentage estimation indicated in the back logging report of each well:

- Water wells (WTR,WTR2 AND WTR3)
- Gas wells (GAS,GAS2,GAS3 and GAS4)
- And salt wells (SALT2 and SALT3)

The results of the plots are as shown below grouped into the water wells (figures 9a and 10), gas wells (figures 11 and 12) and salt wells (figures 13 and 14). In a global format, the three well groups were further combined on a single plot for bulk-density versus core-density matches for linear regression analysis (figure 15) and bulk-density versus depth (16). The linear regression plots both on the group of wells and on the global scale show that the bulk density has a quarsi-linear fit with the core density (Figures 9b, 11, 13 and 15).This assertion is complemented by the data sets viewed on the histograms. Hence, the feasibility of using the calibrated bulk density logs in the reservoir is good for the purpose of this exercise.

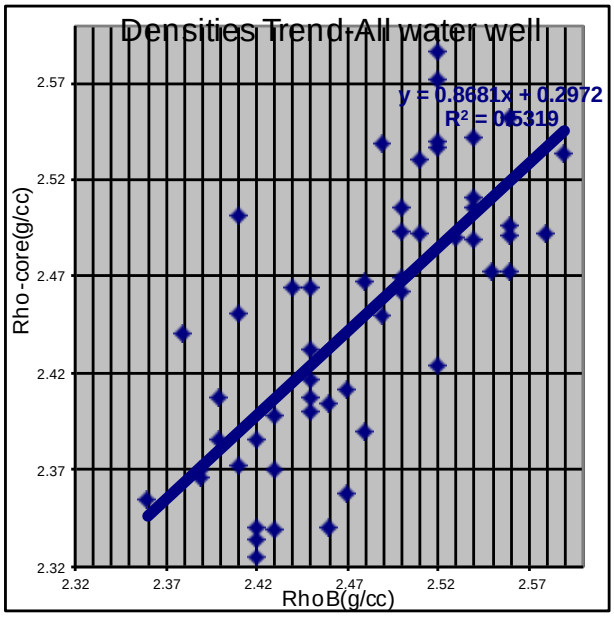


Fig.9b: Linear plot of bulk densities against core densities of the 3-water wells in a merge.

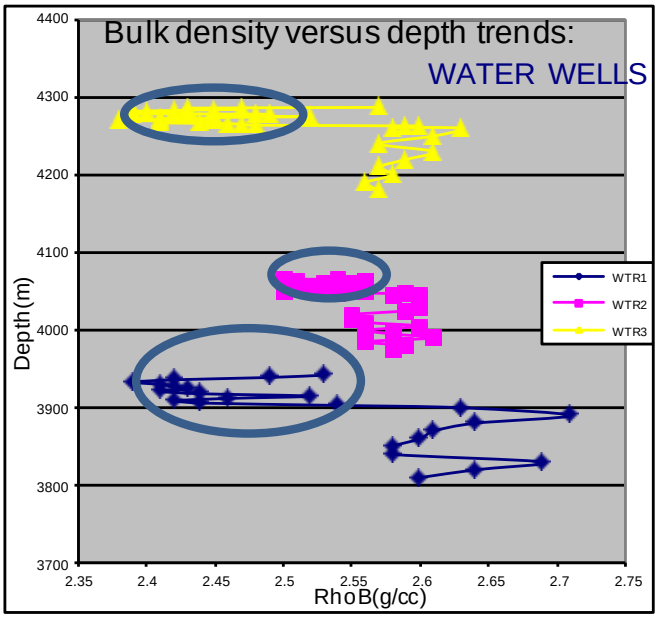


Fig.10: Bulk densities variation with depth for 3 water wells .Oval shape indicate reservoir sit for each well

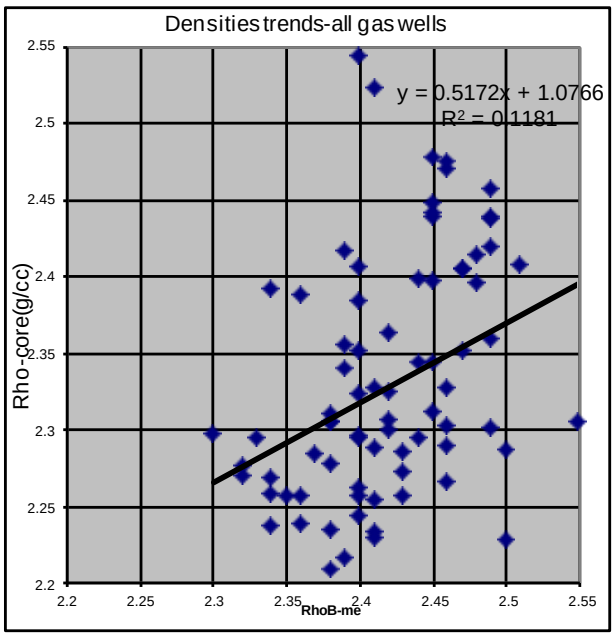


Fig.11: Linear single plot of bulk versus core densities 3 gas wells with core data.

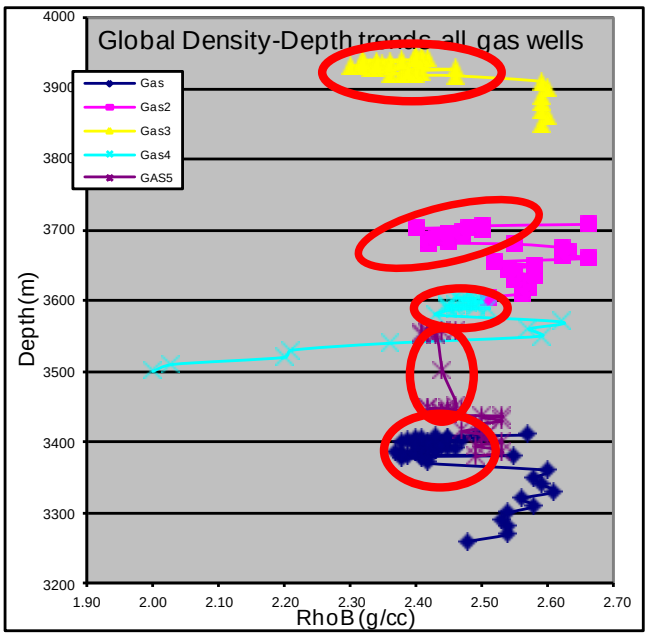


Fig.12: Bulk densities variation with depth for the 3 gas wells with core data. Oval shape indicates reservoir sit for each well.

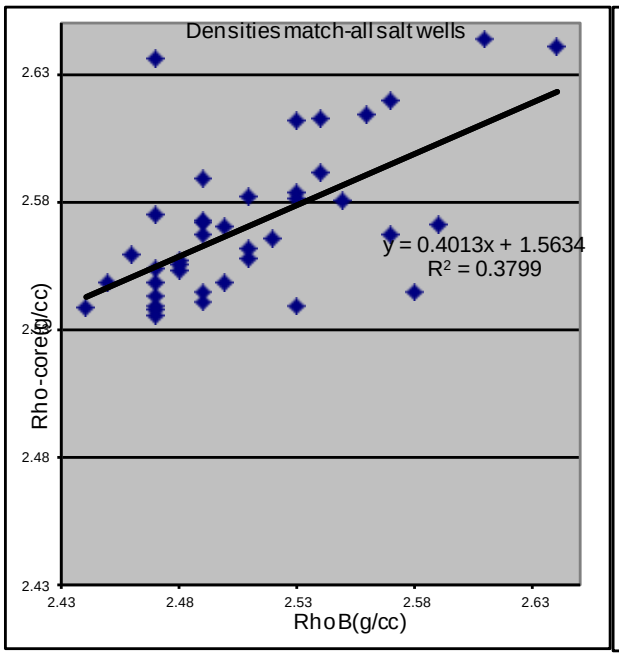


Fig.13: Single linear plot of bulk densities versus core densities of the 2-salt wells with core data

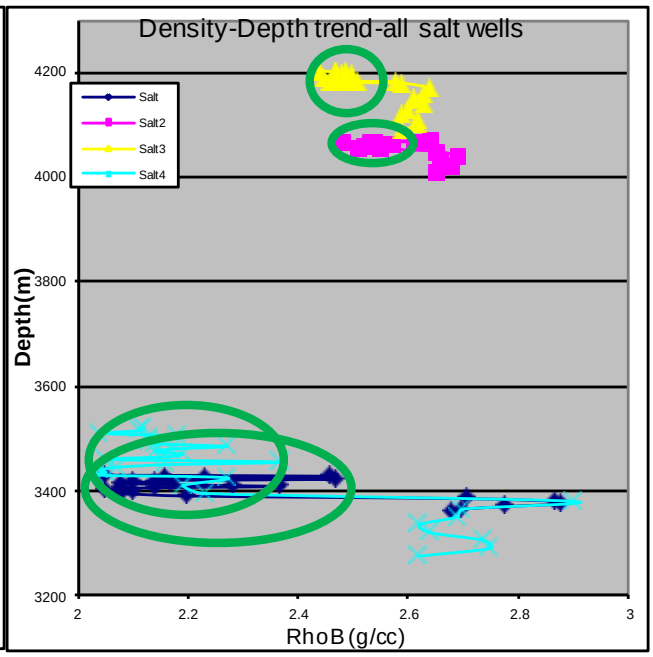


Fig.14: Bulk densities variation with depth for 4 salt wells. Oval shape indicates reservoir sit for each well

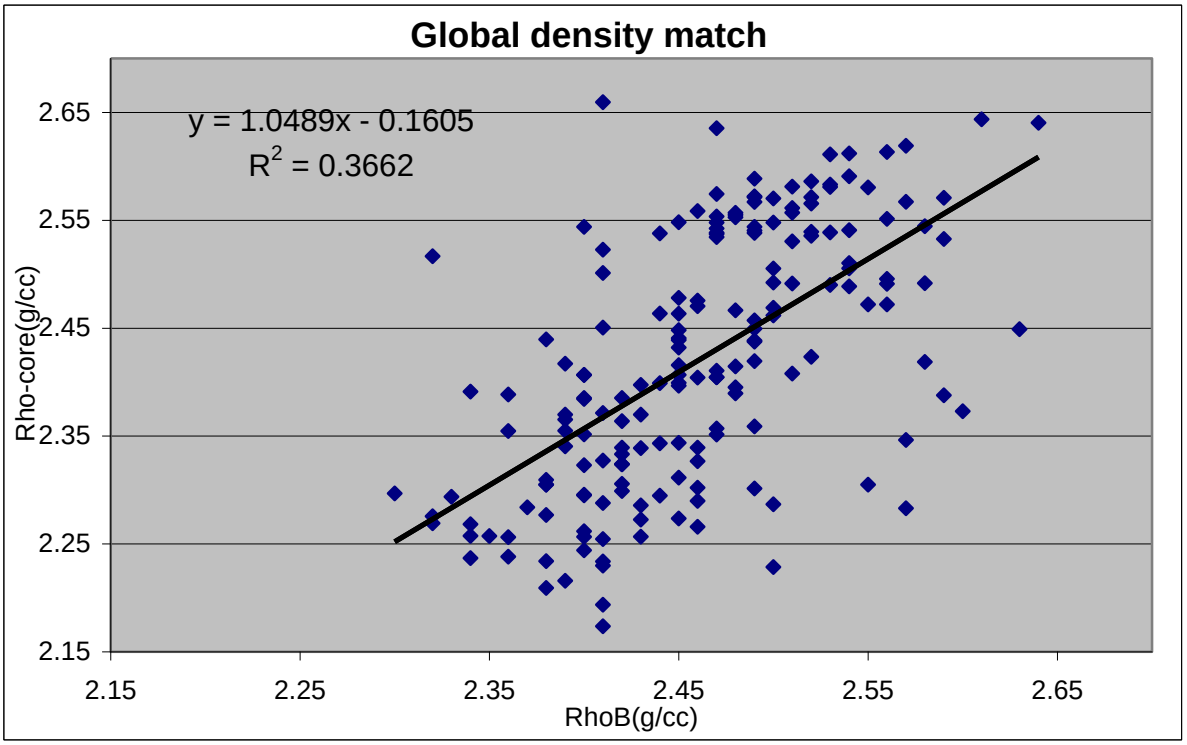


Fig 15: Linear log density versus core density trend for all the wells with core data

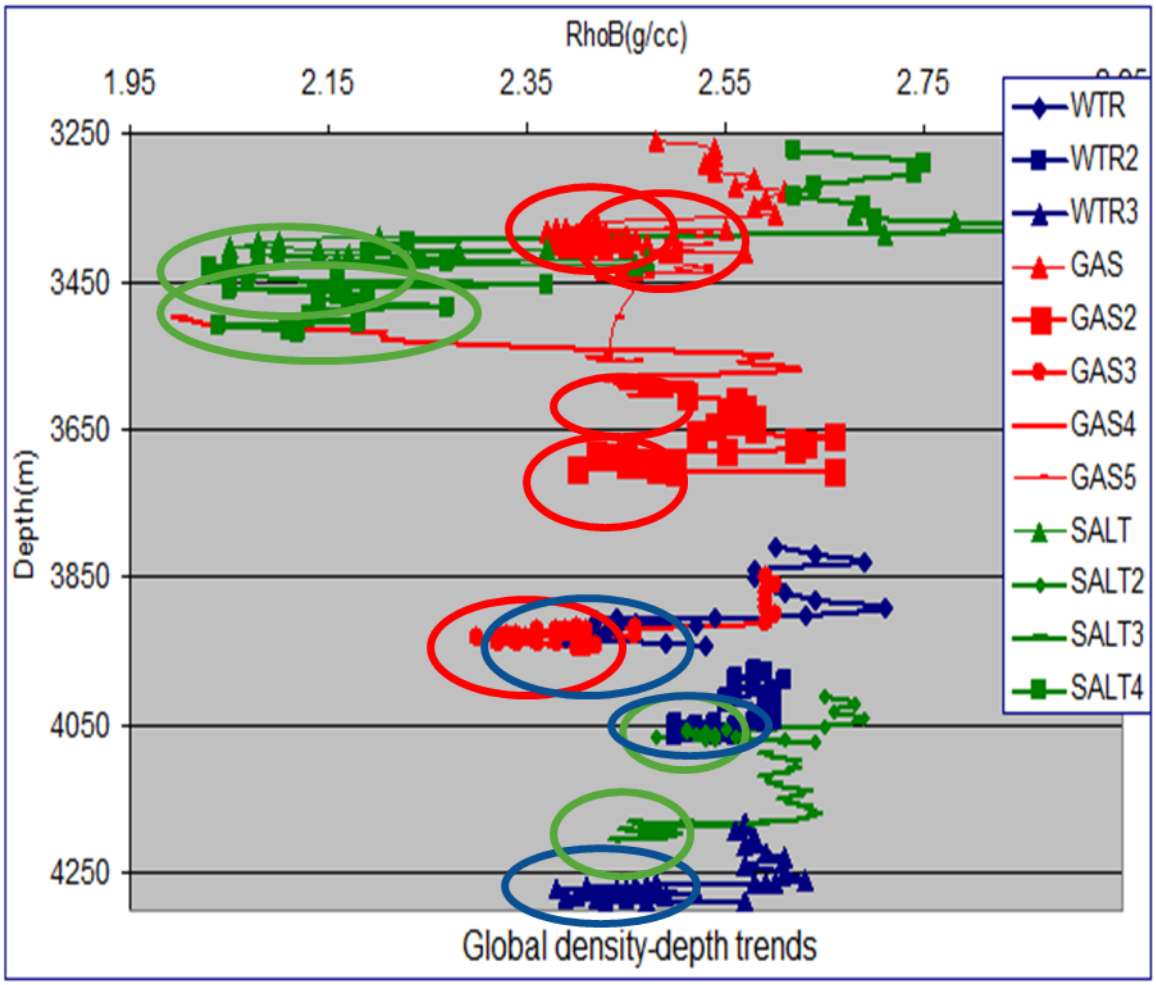


Fig.16: Global bulk densities variation with depth. NB! Oval shapes indicate the reservoir sit for each well; Blue colour oval shapes for water wells; red for as wells and green for salt wells clusters.

For the relationship between the measured bulk density and depth of reservoir interval, observation of figures 10, 12, 14 and 16 reveals a non-proportionate, non-linear and inconsistent relationship. Isabella Pacek 2009, in her thesis titled **'Extended Gassmann approach to pore-fill substitution for salt and Fluids, calibrated on Triassic Sandstone Reservoirs in the Southern North Sea'** observed a **'depth-dependent effect**' and recommended its removal for the possibility of comparing the seismic sections at different wells and within the whole reservoir.
However looking at the variations of the bulk density and core densities with the corresponding depths intervals, there seems to be no obvious relationship between the densities and depth.

Since the trends portray more zigzag or haphazard patterns between the different wells, this leads to the hypothesis, that the density values at the respective depths are rather a function of the laterally varying **lithologic characteristics of the interval.**

This is simply displaying the heterogeneous and anisotropic properties of the earth's subsurface geology, which is expected, depending on the generic and dynamic subsurface scenarios, spatial variation, differences in sedimentation regime (resulting in difference in grain size of the sandstone, compaction, cementation etc.).
In fact, spatial variation trend is confirmed by figures 16, AB (appendix-A figure) and table 2 where clusters of wells within the same range are observed with similar properties, which potentially indicates facies changes. WTR and GAS3,WTR2 and SALT2,WTR3 and SALT3 pairs coincides exactly with the inter-well pair core density-core-porosity cross plots analysis made for wells with core data(figure 25 A-C next section).

4.2.1. Deterministic cross plot analysis.

In order to ascertain the fact that both the medium and wave parameters behaviours at the different depth intervals are not depth-related, other logs such as gamma ray, sonic resistivity, clay volume and porosity were plotted and compared. This was first carried out for the water, gas and salt well group (Figures 17-19).A critical look at the logs show similar trends at depth intervals and the interest here is on the Volpriehausen Formation. This is coloured yellow in the wells. From left to right are WTR, WTR2 and WTR3. Each well displays left-right; the GR, V-Clay, PHI, resistivity, P-Sonic. Vp, Vs and Rho. The same array is displayed for gas and salt well logs. The top and bottom of the Volpriehausen reservoir are indicated by thick red and green horizontal line respectively.

Comparative analysis was carried out by plotting each log as a function of depth and visualizing the variations and behaviours both in the displayed well view and as cross plots. It was observed that the trends were similar for each of the logs compared with one another in a particular depth range.
Within the Volpriehausen Formation, density, gamma ray and resistivity logs show lower values in wells at shallower depths; high values in wells at middle or intermediate depths and again lower values in wells at deeper depths for the water wells (figure 20A-B).
P-Sonic and porosity logs are anti-correlated as expected and show higher values in wells at shallower depths; lower values in wells at middle or intermediate depths and again higher values in wells at deeper sections (Figure 20C-D).
Similar values and trends were observed for the gas and salt wells in which these logs are available in the Volpriehausen interval (Figures 21and 22).However, resistivity logs are not available for gas well GAS and GAS5. Also, the P-sonic and porosity logs are not available for GAS5 well.

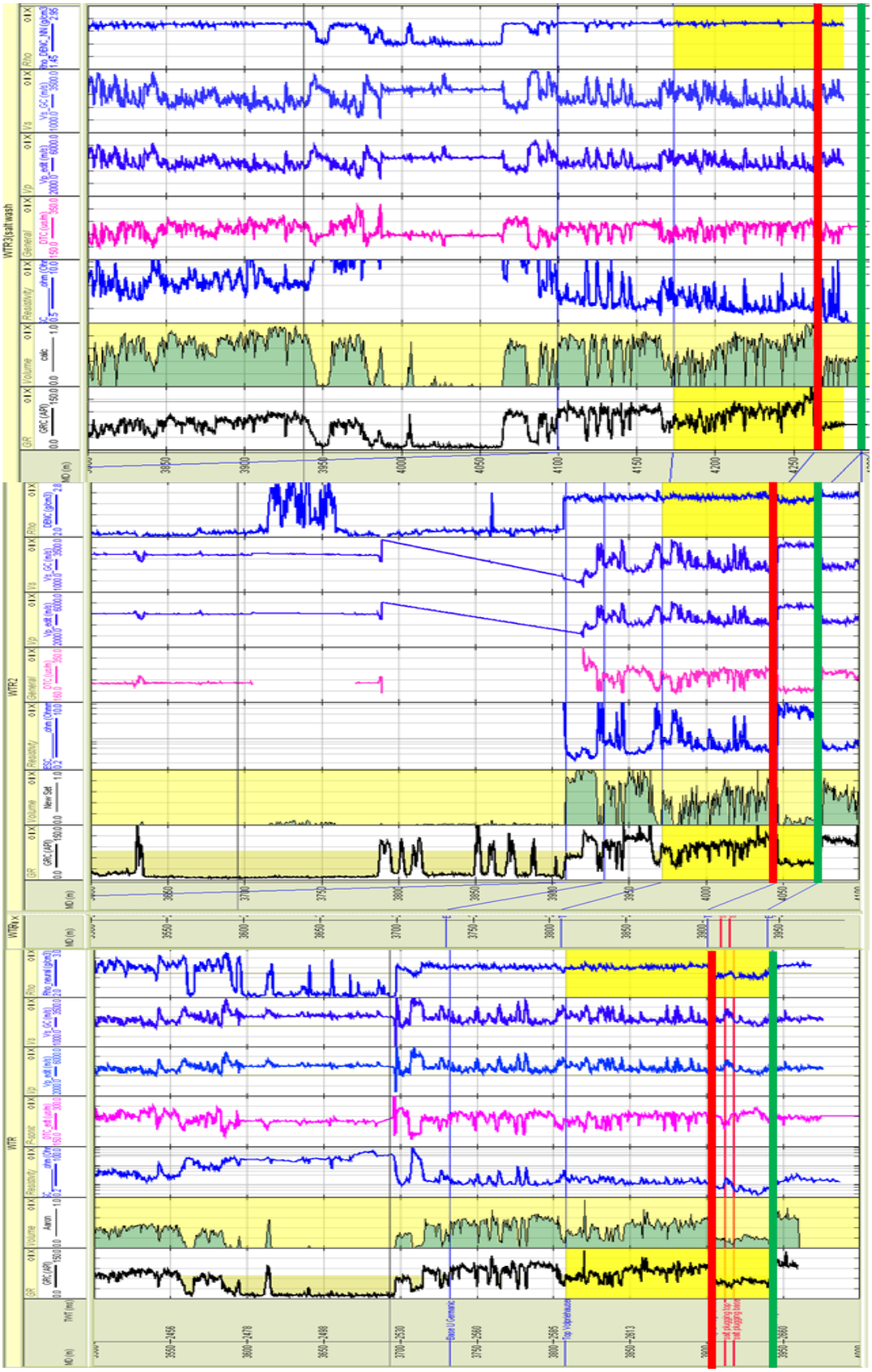


Figure 17: Logs showing the variations of medium and wave parameters at different depth intervals-water well. From left to right are WTR, WTR2 and WTR3. Thick red and green line represents top and bottom of the reservoir respectively in each well

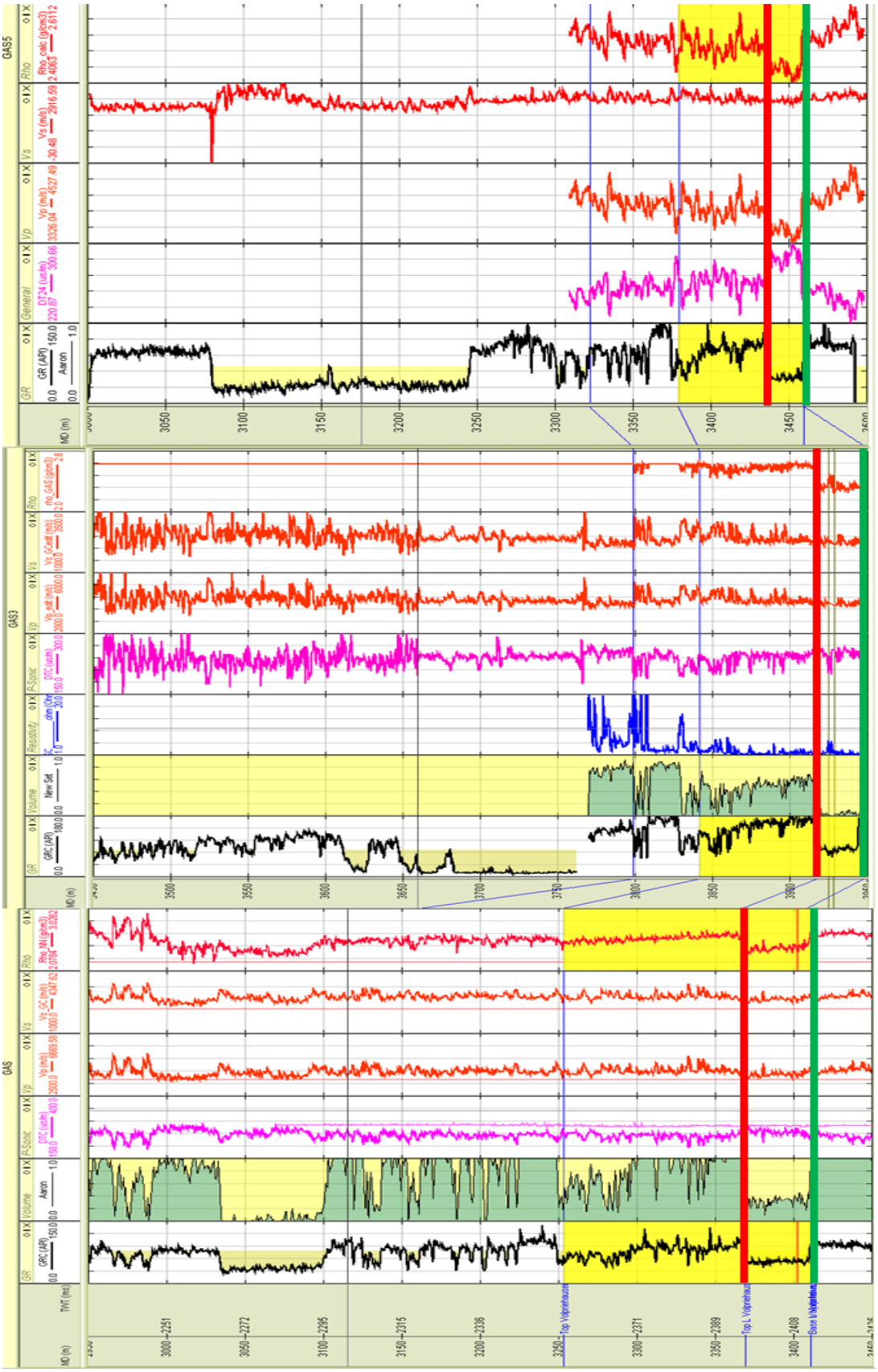


Figure 18: Logs showing the variations of medium and wave parameters at different depth intervals-gas wells. From left to right are GAS,GAS3 and GAS5. NB: GAS and GAS5 have no resistivity logs. Thick red and green line represents top and bottom of the reservoir respectively in each well.

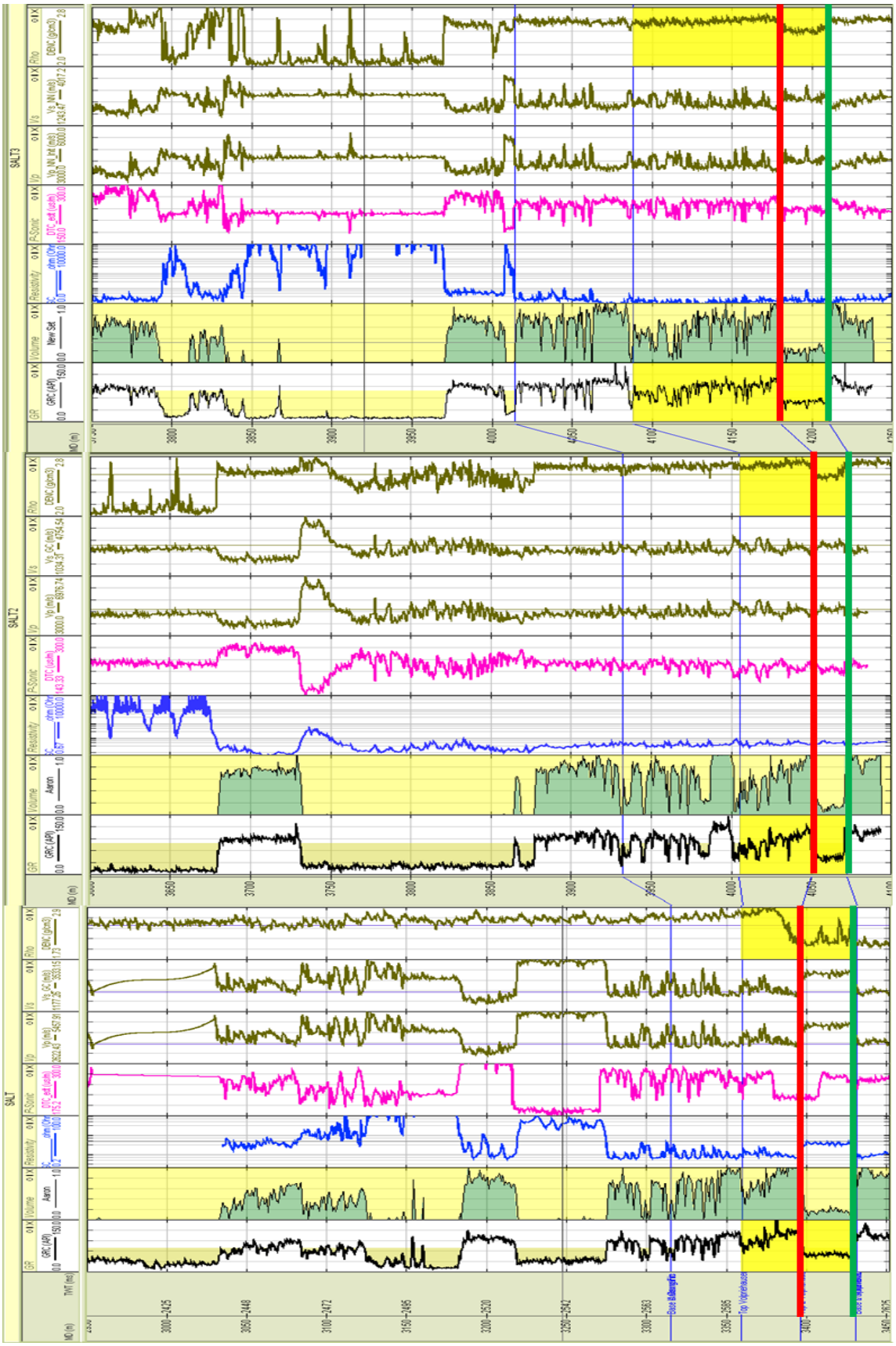


Figure 19 Logs showing the variations of medium and wave parameters at different depth intervals-salt wells. From left to right are SALT, SALT and SALT3. Thick red and green line represents top and bottom of the reservoir respectively in each well.

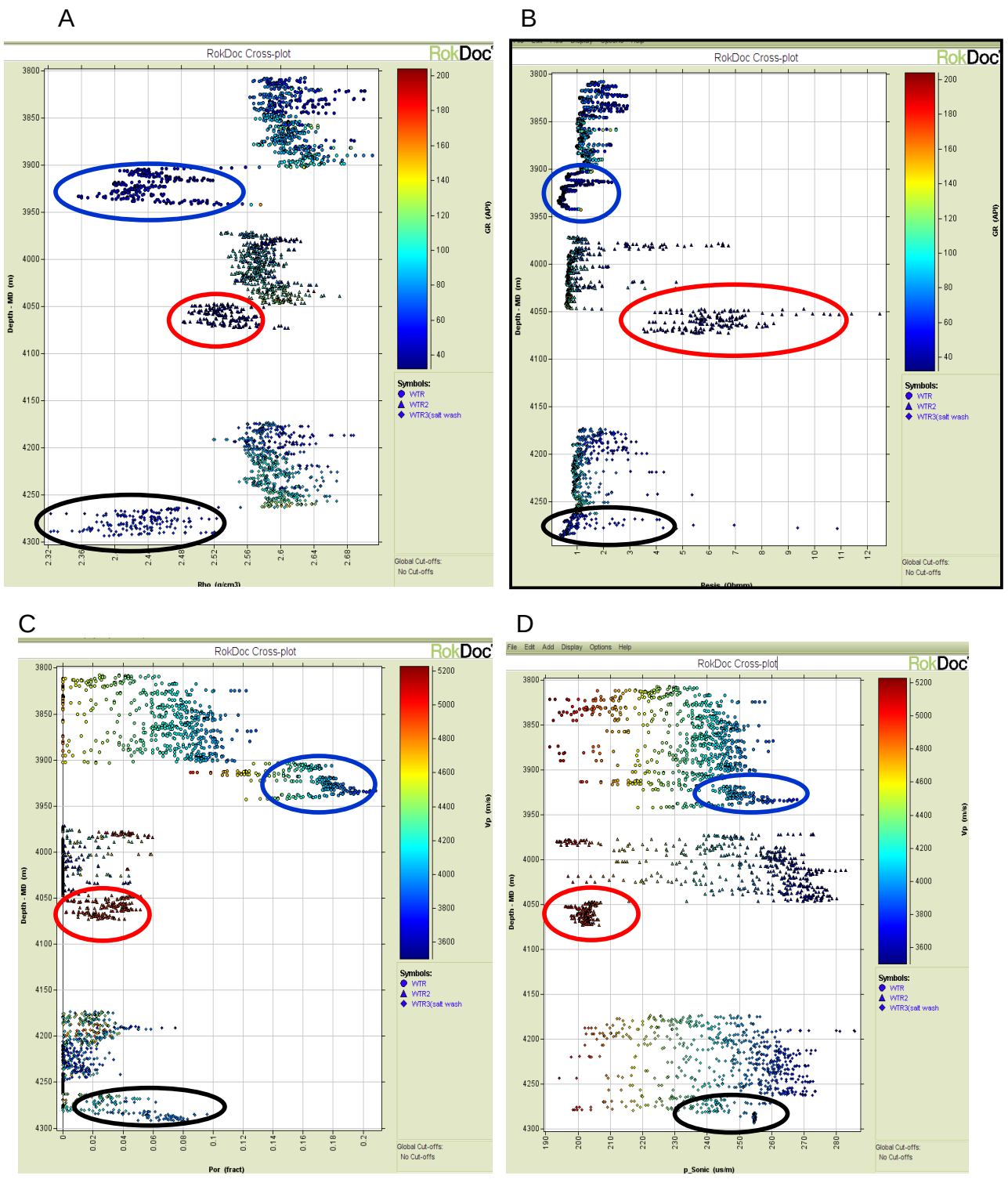


Figure 20: A=Bulk density- B=resistivity-, C= Porosity- and D = P-Sonic-depth variation respectively for water wells. The over shapes indicate the reservoir sit for each well: Blue for WTR, red for WTR2 and black for WTR3

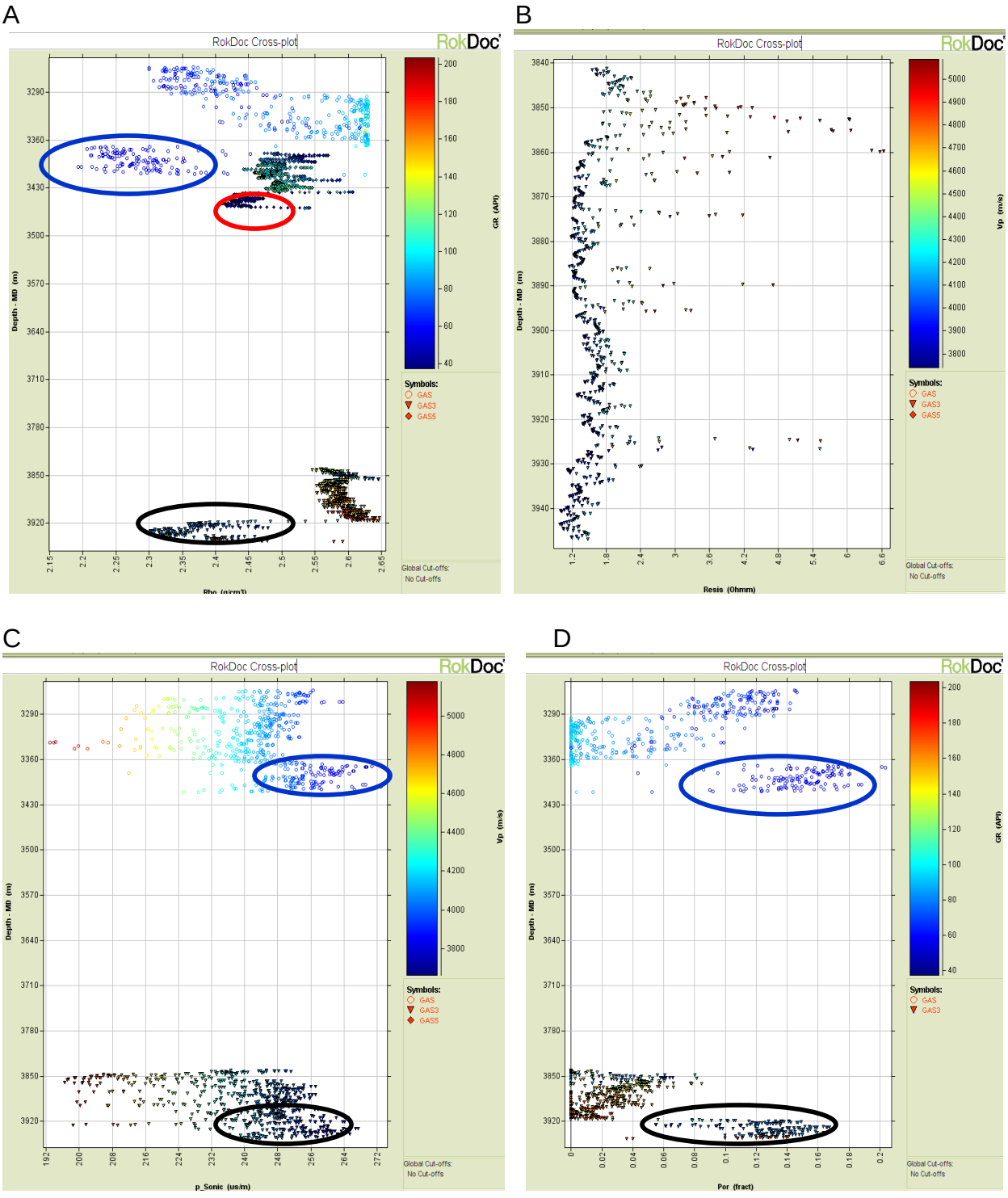


Figure 21: A=Bulk density-, B=resistivity-, C= P-Sonic- and D = Porosity-depth variation respectively for gas wells: NB: B: resistivity available only for GAS3; C: P-Sonic and Porosity not available for well GAS5. The over shapes indicate the reservoir sit for each well: Blue for GAS, red for GAS5 and black for GAS3

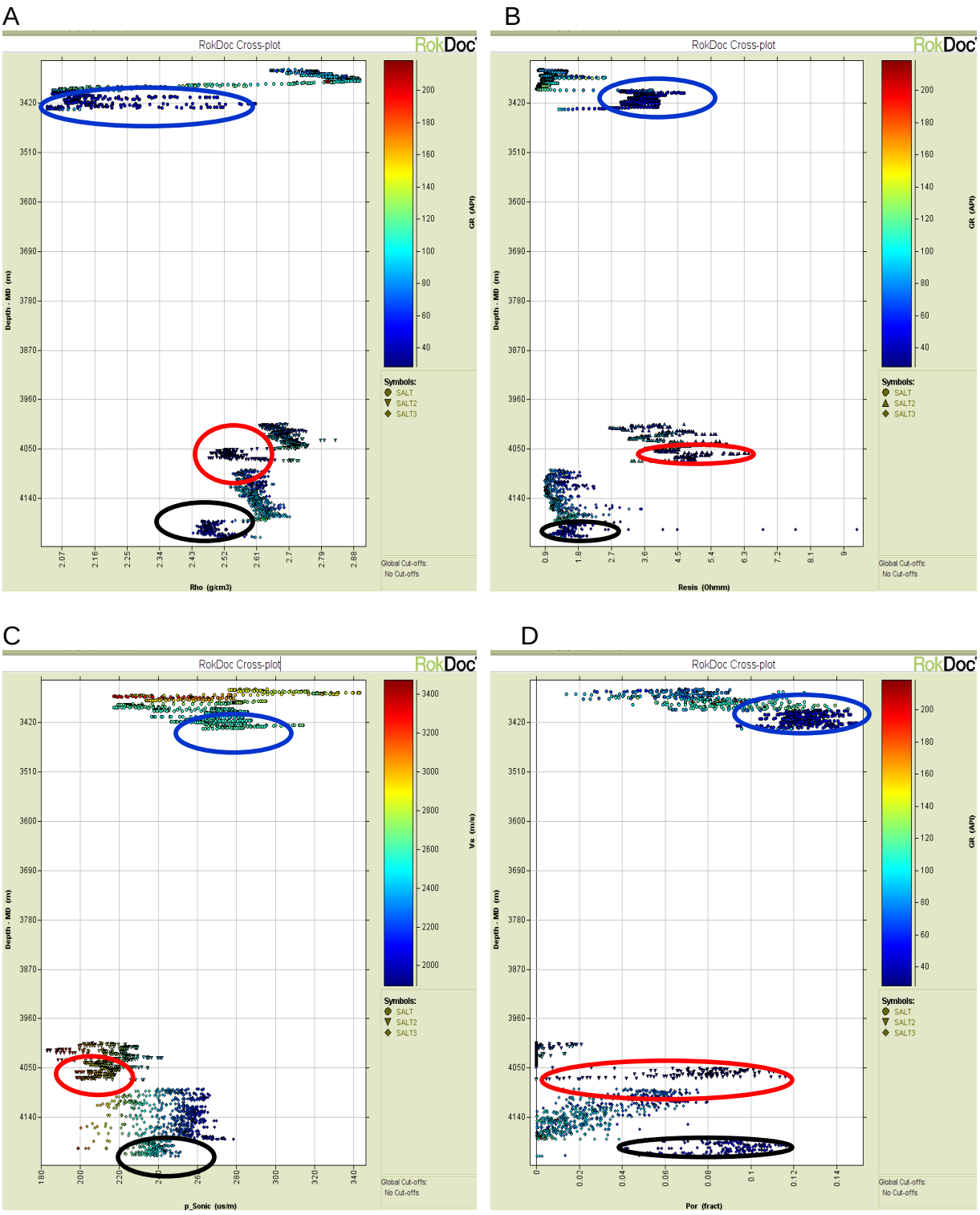


Figure 22: A=Bulk density-, B=resistivity-, C= P-Sonic- and D = Porosity-depth variation respectively for salt wells. The over shapes indicate the reservoir sit for each well: Blue for SALT, red for GAS5 and black for SALT3

Hence, we see from the cross plots and well logs that:

- The Volpriehausen interval at the intermediate depth ranges correspond to the higher density and resistivity values. Lower P-Sonic and porosity values also show that high P-wave velocity correspond to this depth range.
- The acoustic impedance contrasts between the overburden and the reservoir from the wells is not consistent. While it seems similar for WTR and WTR3, the contrast is much smaller for WTR2. Similar behavior is spotted for SALT2 and SALT3, with a much larger contrast for SALT. Again similar for GAS and GAS5, but a much smaller contrast for GAS3.

In an effort to pin-point the most likely cause of these anomalous values for these parameters in the Volpriehausen interval in wells at intermediate depth compared to the values in wells at lower and deeper depth, the **bulk density and porosity logs** were analyzed for this interval as shown in Table 2 below (The colour indicates the group of wells within approximately the same depth range). Figure 23(A-C) shows the porosity-bulk density plots. The results of these plots show that:

- WTR and GAS3 wells which occur in nearly the same shallow depth range have high porosity of similar range and lower density of similar range.
- WTR2, SALT2 and GAS5 have densities of similar range, correlating to the moderate depth where anomalous parameter values have been noticed.
- The porosities of WTR2 and SALT2 are quite low (none for GAS5 in this range).
- WTR3 and SALT3 on the other hand have moderate density and porosity values.
- These similarities in the density and porosity values point to similar lithology at the respective depth.

Table 2: Density and porosity ranges for the Volpriehausen reservoir interval. NB!'*' in bracket indicates the standard deviations density values whiles outside the bracket represent the average density values

well	Porosity	Rho	Depth(m)	Thickness	Core-data?
WTR	0.09-0.21	2.53(0.10*)	3901-3941	4	Yes
WTR2	0.00-0.05	2.56(0.03*)	4047-4072	25	Yes
WTR3	0.02-0.23	2.49(0.08*)	4263-4293	30	Yes
GAS	0.09-0.20	2.46(0.07*)	3368-3409	41	Yes
GAS3	0.06-0.17	2.42(0.10*)	3920-3946	26	Yes
GAS5	None	2.46(0.04*)	3437-3458	21	No
SALT	0.09-0.15	2.32(0.28*)	3396-3431	35	No
SALT2	0.00-0.11	2.75(0.06*)	4050-4070	20	Yes
SALT3	0.04-0.12	2.52(0.07*)	4180-4210	30	Yes

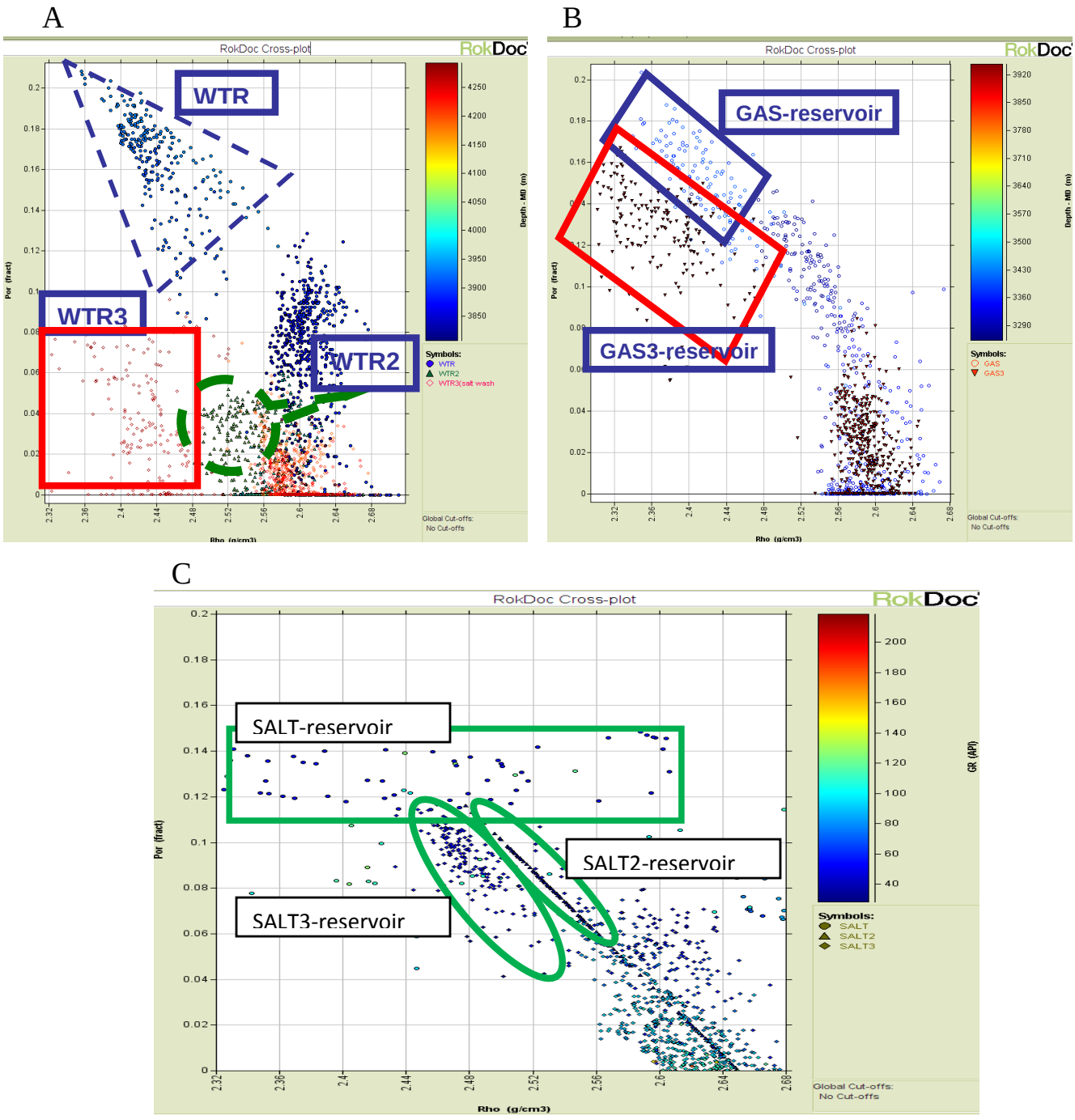


Figure 23 (A-C): A=Porosity-Rho for water well, B= porosity-Rho for gas well and C= porosity-Rho for salt wells. NB! Blue dashed triangle, green dashed call out and red square represent the reservoir sits for WTR,WTR2 and WTR3 well respectively in A; Blue and red quadrilateral shapes indicate the reservoir sit for GAS and GAS2 wells in B; Green oval shapes indicate the reservoir sits for SALT,SALT2 and SALT3 wells in C

Further, cross plots were made of **core density and core porosity** for the wells with these data. The core data were extracted from the well log report for each well and calculations were made again, using the Wyllie equation (9). The core densities and porosities were then exported into the RokDoc project as logs. Results of the plots are as shown in figures 24 A-C for the water, gas and salt wells.
These results show clearer density and porosity relationship as a function of depth:

- Again, WTR and GAS3 wells which occur in the same shallower depth range, have high porosity of similar range and lower density of similar range.
- WTR2, SALT2 have densities of similar range, correlating to the intermediate depth of anomalous parameter values.
- The porosities of WTR2 and SALT2 are very low.
- WTR3 and SALT3 also have similar values and trends (medium) as indicated in the previous plots (figure 23).
- These trends confirm the assertion made earlier, that the similarities in the density and porosity values point to **similar lithology at the respective depth.**

On the basis of co-occurrence of the reservoir interval at similar depth, inter-well cross plots were generated for checking lateral variations in these properties (figure 25 A-C):

- WTR and GAS3 (3901-3950m);
- WTR2 and SALT2 (4000-4070m);
- WTR3 and SALT3 (4100-4300m).
- GAS, GAS5 and SALT wells fall within the same depth range of 3360-3460m, but couldn't be cross-plotted as inter-well because GAS5 and SALT have no core data on the Volpriehausen reservoir intervals.

Observations from the pairs of cross plots show that the reservoir properties at the respective depths are closely related with little differences:

- GAS3 at slightly deeper depth has slightly lower porosity compared to WTR;
- WTR2 has lower porosity and at relatively deeper section compared to SALT:
- WTR3-SALT3 pair shows similar trend, but in the reverse order; WTR3 at slightly deeper depth show slightly lower density and higher porosity while SALT3 at slightly lower depth show higher density and low porosity.
- From these plots, logically, it can be interpreted that the scenarios from the WTR-GAS3 and WTR2-SALT2 points to **compaction-cementation sedimentation processes** while the WTR3-SALT3 case points to **lithofacies changes.**
- Note that these lithofacies changes are examples of reservoir heterogeneities caused by geologic processes which themselves change in time and space.

The global plot is also generated (figure 25D) to complement the pair plots.

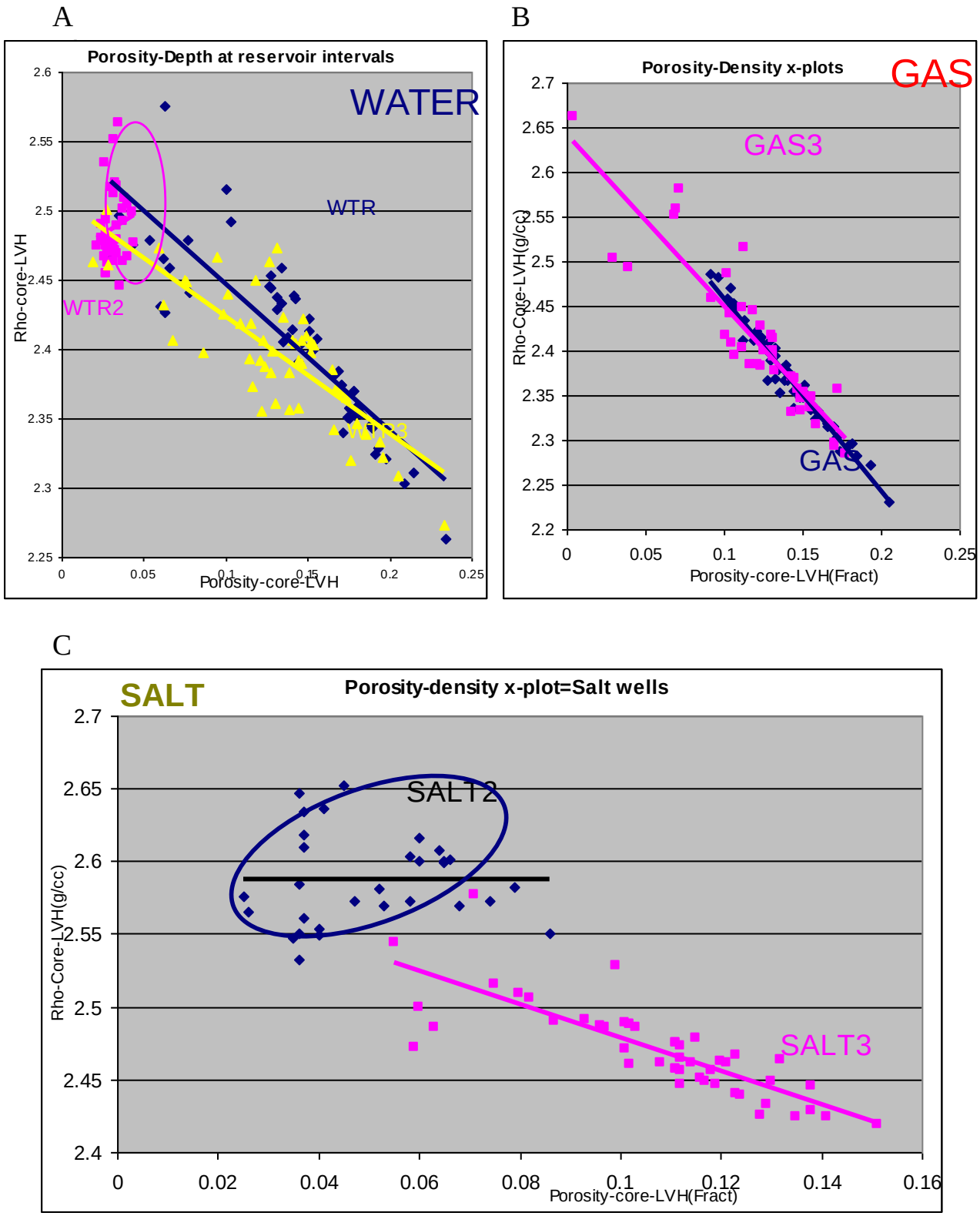


Figure 24(A-C): A= core porosity-core density for water well, B= core porosity- core density for gas well and C= core porosity- core density for salt wells. Over shapes indicate the reservoir sits. Note the similarity in the density values of WTR2 and SALT2 wells

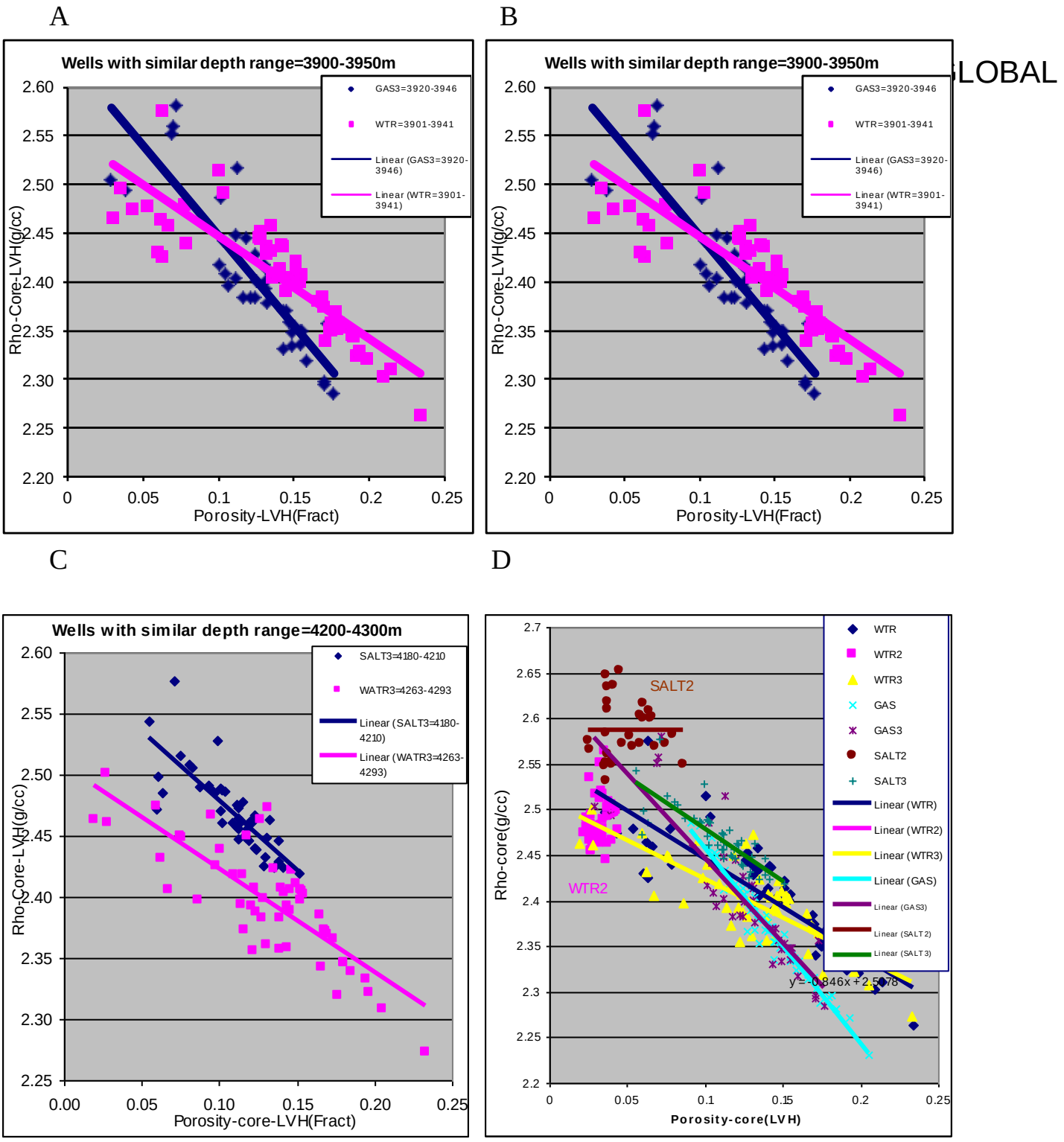


Figure 25(A-D):Inter-well cross-plots. A= core porosity-core density for GAS and WTR well, B= core porosity- core density for SALT2 and WTR2 well, C= core porosity- core density for SALT3 and WTR3 wells; and D= global plots.

The last but very important step to be taken in tracking the definite cause of the parameter values of the intermediate depths Volpriehausen reservoir intervals was to analyze their fluid contents. For this to be reliably carried out, resistivity log types such as Micro-spherically Focused Logs (MSFL), Laterolog Shallow(LLS) and Laterolog deep (LLD) are needed. These will help us to study the negative separations and infer the fluid contents. But these logs are not available for this analysis. Another alternative and/or complementary tool needed for the fluid content prediction is the FDD/NL (Formation density-neutron log). Further analysis of this type is beyond the scope of this study.

In summary for the data analytical section:

- Variation of the medium and wave parameters such as density, porosity and velocity at particular depths is not related to the depth (evidenced from logs and cross plots in figures 10, 12, 14 and 16).
- These values are similar at any particular depth, indicating similarity in lithology (evidenced by detail cross plots of bulk density and porosity of the reservoir at the depth range in question-figures 23 A-C).Core density and porosity log plots also confirm this assertion (figure 24 A-C).
- Facies changes due to cementation and compaction, as most likely syn- and post-depositional sedimentary processes are the reasons for the lateral variations in these wave and medium parameters values. This is evidenced by the results of inter-well depth-range cross plots analysis of core logs (figures 25 A-D) show slight lateral variations in the core density porosity values. Presence of older sandstones is also another possible explanation for these trends.
- Therefore, as can be clearly seen, there is no dependent effect, since no depth relationship exists with the acoustic and elastic parameters.
- Hence, synthetic seismic models can be generated at the wells in both the poststack and prestack seismic domain and their comparisons can be made with measured seismic sections for these wells with high level of confidence in the interpretation there by.

4.3.0 Rock Physics Framework

This involves the derivation and calculations made for the rock physical parameters as well as the solid-fluid substitutions needed to be incorporated into the well-to-seismic ties operational modelling. The main rock physical parameters have been derived by Isabella Pacek, 2009 and the extended Gassmann's theory was has validated based on her results of the solid and fluid substitutions. The substitution percentages of the solid and fluid material were however verified and modified where necessary with the original rock physics model intact.

The substitution is basically used to model the effects of fluids and solids (salt in our case) on log data, which will later be used to create and compare synthetic gathers. Using the new Gassmann's theory which is applicable to solid substitution in addition to fluids, substitutions were performed with the help of RokDoc Gassmann fluid substitution panel. For the salt-plugged and partially gas-filled water-bearing wells, water was first substituted for salt and then for gas. Similar procedures were followed in the cases of the salt and gas well substituting gas for water and salt and salt for gas and water respectively (see AVO modelling in the next chapter).

This resulted in observable changes in the extractable elastic parameters in response to geomechanical stress in the Formation and/or reservoir(Volpriehausen).Typical elastic properties for different materials were obtained from calculations following Mukerji et al (1998) (1975). See tables 3 and 4.

Table 3: Rock physical parameters in response to solid and fluid changes in the reservoir medium pore spaces

Substituent/parameter	GAS	WATER	SALT	SHALE_avg	SST
Vp (m/s)	3952	4001	4757	4164	6000
Vs(m/s)	2426	2228	2848	2279	4000
P(g/cm^3)	2.292	2.355	2.526	2.62	2.65
Φ (%)	15	15	3-6	<1	10
GRC(API)	50-65	40-60	44-55	>80	-
K(GPa)	17.7	22.1	28.6	27.2	38.8
μ(GPa)	13.4	11.7	18.6	13.5	42.4

Table 4: Average bulk and shear moduli in (GPa) for initial and substituted wells. In the diagonal (red) are the initial wells.

	GAS	WATER	SALT
GAS	**Kinit = 17.7** **μinit = 13.4** **Kdry = 17.1**	Ksat = 32.1 μsat = 13.4	Ksat = 25.8 μsat = 22.7
WATER	Ksat = 15.9 μsat = 11.7	**Kinit = 22.1** **μinit = 11.7** **Kdry = 15.4**	Ksat = 28.6 μsat =19.9
SALT	Ksat = 17.7 μsat = 13.4	Ksat = 22.1	$\mathbf{K_{init} = 27.5}$ $\mathbf{\mu_{init} = 20.8}$ $\mathbf{K_{drygas} = 17.3}$ $\mathbf{K_{drywater} = 15.4}$ $\mathbf{\mu_{drygas} = 13.4}$ $\mathbf{\mu_{drywater} = 11.7}$

A similar table was made for velocities and densities (tables 5), where bold letters represent the real gas, water and salt-plugged averages. The averages are derived from calculations performed on log data within one well, namely the salt substitution within GAS2 and WTR.

Table 5: Velocity and density values for different salt-plugged wells and salt-plugged zones in gas and water bearing wells.

Well	Vp(m/s)	Vs(m/s)	$\rho(g/cm^3)$
WTR2	4927	3094	2.537
SALT2	4729	2913	2.555
Salt-plugged GAS	4734	2946	2.564
Salt-plugged WTR	4665	2752	2.456
Average	4763.75	2926.25	2.528

The salt plugged scenarios in the Lower Triassic Volpriehausen sandstone reservoir are seen within the WTR and GAS2 wells marked as '**salt-plugged zones'**. Hence, they are used for the substitution experiments. The salt was considered as a normal substituent just like the fluids (though with markedly variable elastic properties). Substitutions between water and salt and then between gas and salt was performed within the same well. The solid substitutions were also performed from the new calculated salt-plugged parameters back to gas and water pore-fillings.

CHAPTER FIVE

SYNTHETIC SEISMOGRAM

As indicated in the introductory chapter, this work is essentially about understanding the effect of porefill (particularly salt fill) on the seismic response. To achieve this goal the calibration of well data to seismic data at the well location using forward seismic modeling is essential. Synthetic post-stack seismic data is simulated using a convolutional model in an iterative approach. The goal is to obtain a good tie between the well log data and the measured seismic data through an optimal match of seismic and synthetic. For that purpose, a wavelet is extracted from the seismic data. Once the calibration has been carried out properly, forward pre-stack seismic modeling has been applied to investigate the AVO response of different interfaces. Both the simulated post-stack and pre-stack models are then verified against real (measured) seismic data.

5.1.0. Data Input and Quality Control

The well data to be used were prepared and loaded into the RokDoc project (see chapter 4). The RokDoc$^{(TM)}$ software is developed by IKON Science-and is capable of linking petrophysical and rock physical properties to geophysical attributes which can help to integrate geology, well and seismic data. Log quality control was carried out where necessary as follows:

Wells representative for the geologic environment with decent to good seismic data quality around were selected

- Well log calibration (reconciling the integrated sonic log with borehole seismic measurements) was performed using the available check shot.
- The size of washout zones was calculated, and the impact on log quality was assessed (difference between caliper log and bit size)
- Removing poor points from density logs using washout curves. This was to correct for **bad-hole effects, shale effects, etc.**
- Training and application of a neural network (NN) in order to predict and infill missing density data based on Vp (compressional velocity) and GR (gamma ray). In some well cases, density and shear wave velocity logs didn't cover the desired depth range for the synthetic modelling. In such cases, NN technic was used and good desired results were obtained.
- Incomplete or non-availability of Vs logs which had to be manipulated through the neural network approach.
- Training and application of a neural network to predict Vs based on Vp, GR and density logs to predict missing data.

With the RokDoc project cross-plotting method, spikes were removed from the log data which were used in the simulations. Cut-offs was also applied to the log data in order to derive the project specific relationships in terms of sand-shale trends. With this procedure data was reviewed and adjusted for each well. Within the well viewer suspicious data could also be removed on selected intervals. Examples of such cross plots are shown in figures 26 (a and b); a shows the plot of Vp against Vs which result shows a linear fit with few erroneous points/spikes outside the reservoir indicated by the colored polygons which were removed. These plots are generated as a function of Gamma ray which indicates the sand-shale sequences. In figure 26b for example, the sand and shale trend line are indicated which show the reservoir and overburden trend respectively. These correspond to the density of each unit, thereby giving firsthand information about the lithologies of the reservoir.

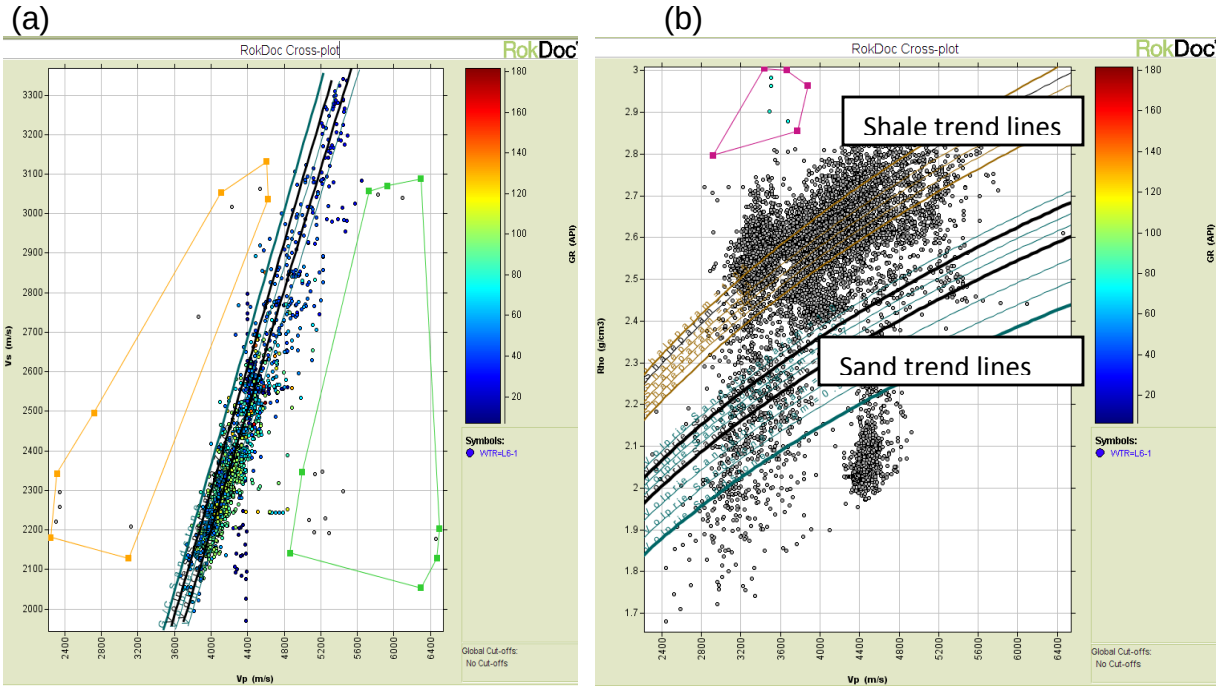


Figure 26: Cross-plot analytical results for water well WTR. (a) Vp: Vs relation; (b) Vp: Rho trend

5.2.0 Initial well Tie

Theoretically, constructing the synthetic seismogram involves creating a reflection series in time and convolving this with a wavelet. The broadband reflectivity has to be convolved with the seismic wavelet in order to tie the well log data to the seismic data. This wavelet is extracted from the seismic data around the corresponding well.
In this study, estimating the wavelet to be convolved with the reflection series, the **'Wavelet estimation through matching'** method as described in White and Simm (2003) was followed in conjunction with the RokDoc workstation technology. In fact White's algorithm for wavelet extraction is integrated in the RokDoc software. The practical procedures here include:

- Generating the reflectivity series from log data in TWT convolved with Ricker wavelet. This was done for each of the 7 wells original wells within the 3D seismic survey area and the 2 pseudo wells created. The Vp-Vs-Rho set prepared was selected for the respective well and Ricker wavelet was created using sample interval 2ms at frequency 25Hz.
- Iterative stretch/squeeze and extraction of statistical wavelets. This involve '**matching'** operation using the **digitized depth-match pairs** capable of stretching and squeezing the synthetic and composite seismic traces and applying the depth match pairs
- Analysis of PEP for assessing the degree of fitness between the synthetic and the real seismic.

This procedure results in outputs as displayed in Figures 27, 29, 31, 33, 35 and 37, enabling an effective assessment of the well tie quality:

- The shape of the wavelet
- The phase characteristics of the wavelet
- Quantitative measures related to the tie such as: (a) an estimate of the goodness-of-fit of the synthetic to seismic and (b) an estimate of the accuracy (likely phase error) of the wavelet.

In order to establish a link between the seismic impedance attributes and the geologic scenarios in the well, log elastic properties such as AI, Poisson's Ratio, EI3, LambdaRho, MuRho and Lambda/Mu were selected and their logs calculated.

5.3.0 Wavelet estimation procedure

A well-based approach to wavelet estimation was adopted in this study. This implies that after a first estimate of the wavelet, an optimal match is explored by adapting the phase of the wavelet and correlating the resulting synthetic trace with neighboring traces of the real data. The optimum wavelet is determined by the maximum correlation between the synthetic and the real traces. The procedure requires a number of input parameters described below:

- **The time window:**

  Wavelet estimation here uses the cross-correlations and is controlled mainly by the length of the input time window of seismic data 'T', how much of the correlations are used in the calculation and the length of the wavelet to be estimated 'L'. In each well tie, the input seismic time window is defined by the "cross correlation range" and for maximum output, the recommended 500msec in the cross-correlation time interval. In our data, since neural network technique was adopted where the time-converted log data was covering too little interval, to make the estimation work reliably, the time window should be at least 300ms.

- **P.E.P (Proportion of the energy predicted):** This is the energy of a trace which is the sum of squares of a segment of a time series. It simply measures how well each trace correlates with the synthetic reflectivity having added the best delay. Well tie first compares a synthetic trace with seismic traces around a well, to find the best location for wavelet estimation and then extracts a wavelet at that location. In the RokDoc package, the best location is found using P.E.P. percentage and by scanning up and down the seismic traces to allow for structural dip and imaging errors. This scan is controlled by "maximum delay in scan".
- **Delay:** This indicates the time shift that was added to each trace in order to get the best correlation for the reflectivity log.

- **Accuracy**: This is measured by the phase error within the seismic bandwidth which can be found roughly from:

$$S.E[Phase] \approx \sqrt{\left(\frac{1}{bT} * \frac{1-P}{P}\right)/2} rads \quad \text{---------- (29)}$$

  Where $\frac{1}{bT} * \frac{1-P}{P}$ is the NMSE (normalized mean squared error);
  b = seismic analysis bandwidth,
  T = time window
  P = Predictability
  S.E =squared error

- **Frequency bandwidth 'B':** The frequency bandwidth of the seismic data determines the optimum wavelet length 'L' required for a synthetic to match, which in turn limits the range of time windows 'T' that can be used as input to wavelet estimation. This seismic bandwidth is determined using a statistical wavelet estimation technique of the RokDoc programme. The more bandwidth the seismic data has, the shorter the wavelet is, and therefore the shorter the input seismic data time windows recommended for best results (Please see appendix C)

Parameter evaluation

Well tie uses 3 wavelet extraction statistics to give a measure of wavelet estimation quality. The first two statistics use 'b' ,the analysis bandwidth which is proportional to 1/L and calculated during the wavelet estimation process, along with 'B' the seismic data bandwidth.

1) B * T should be between 5 and 12
2) b / B between 0.25 and 0.5.
3) Phase errors should be < 15 degrees.

The Result tab of the RokDoc stretches and squeeze panel shows horizon maps of the P.E.P percentage and of the time delay associated with the best match found at each location. **PEP should be > 0.7 and the map should show a bull's eye or a ridge along strike for good quality well ties.**

5.4.0: Results And Interpretation-Initial wells

ASSUMPTION:

Firstly, it is assumed that the seismic data have been processed with "true amplitude" processing in order to compensate for such factors as attenuation, spherical divergence, anisotropy, source/receiver characteristics, noise effects, etc., that influence seismic amplitudes. This must be true to validate the following interpretations relative to possible DHI diagnosis; amplitudes phase definitions, peak-trough magnitude and reservoir quality.

POLARITY CONVENTION:

The North Sea normal polarity convention was used with a zero-phase wavelet by applying a 180^0 rotation for the initial tie. This zero phase wavelet matches the energy spectrum of the data window and its time shifting is expected to optimize the synthetic-to-seismic match. In the following displays, a decrease in acoustic impedance is expressed as a peak which is blue and indicates soft event; An increase in acoustic impedance is expressed as a trough which is red (white) it represents a hard event.

The columns in each of the Poststack simulations for the respective well (figures 27, 29, 31, 33, 35 and 37) from left to right show:

- Reflectivity (amplitude) series convolved with the wavelet. Exaggerated for visualization purposes to about order of 10 magnitudes.
- Real poststack seismic section displaying seismic trace along the well path.
- Seismic trace selected on PEP plot. This is used in the measurement of fitness.
- Synthetic trace using selected wavelet.
- Composite seismic trace at well location.

Displayed to right of these figures are: the 'ideal Ricker wavelet', the estimated zero phase wavelet used for poststack modelling and the cross-correlation time window between the real and synthetic seismic data at the top, middle and base respectively. Also shown at the bottom of the figures are the PEP and delay to the left and right respectively. For each of the full wavelet extracted, the time used (constant value of 500ms for all the wells except GAS well without composite seismic data along the well), time shift, b*T, b/B and the phase error (P.E) are stated at the lower right corner.

The columns in each of the Poststack and prestack seismic models calibrated with the real poststack seismic for the respective well (figures 28, 30, 32, 34, 36, and 38) from left to right show:

- Gamma ray log; used for the stratigraphical interpretation.
- Volume of shale (Vsh) indicated for N/G ratio.
- Calibrated compressional wave velocity (Vp) log from sonic.
- Calibrated shear wave velocity (Vs) log from sonic.
- Calibrated density log.
- Reflectivity (amplitude) series convolved with the wavelet.
- Real poststack seismic section displaying seismic trace along the well path.
- Seismic trace selected on PEP plot.
- Synthetic trace using selected wavelet.
- Composite seismic trace at well location.
- Real seismic wiggle traces.
- Synthetic seismic wiggle traces stacked from the gather.
- The pre-stack model to evaluate the AVO.

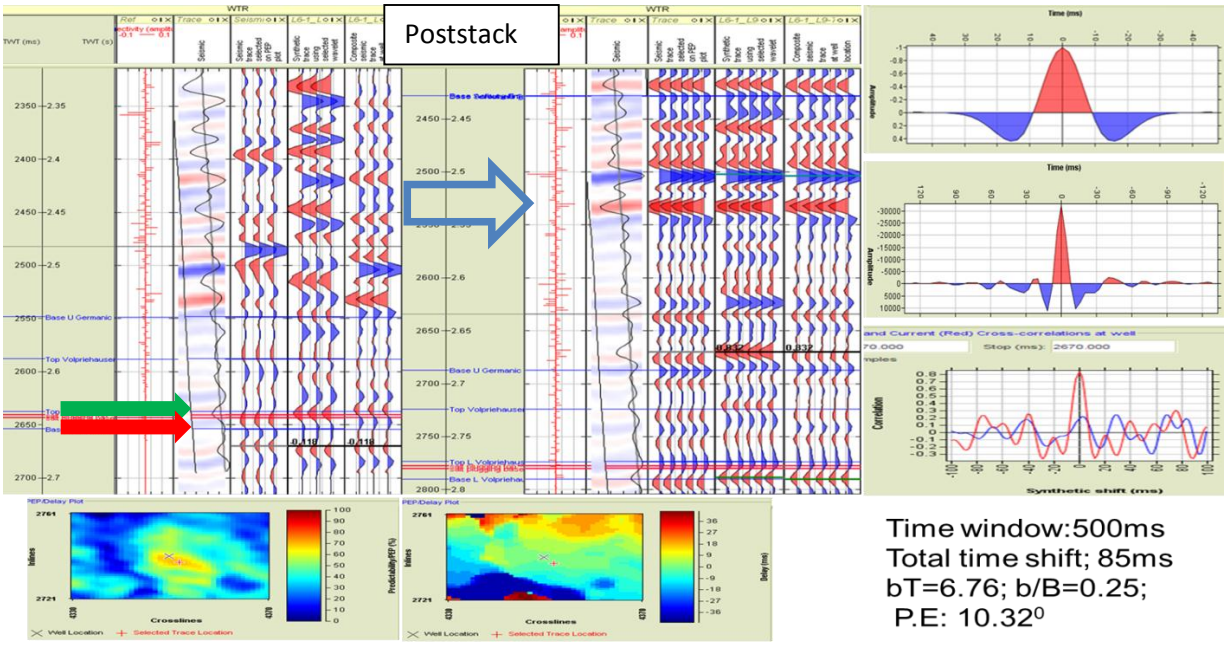


Figure 27: Well tie at WTR using a statistical zero-phase wavelet and then the white's Wavelet estimation through matching' method .NB! Time shifts are needed to match the synthetic to seismic; full wavelet extraction after depth-matching. Cross correlation: seismic & synthetic, 2170-2670ms.Initial signal function is blue; current signal is red. Green and red arrow indicate reservoir top and bottom respectively.

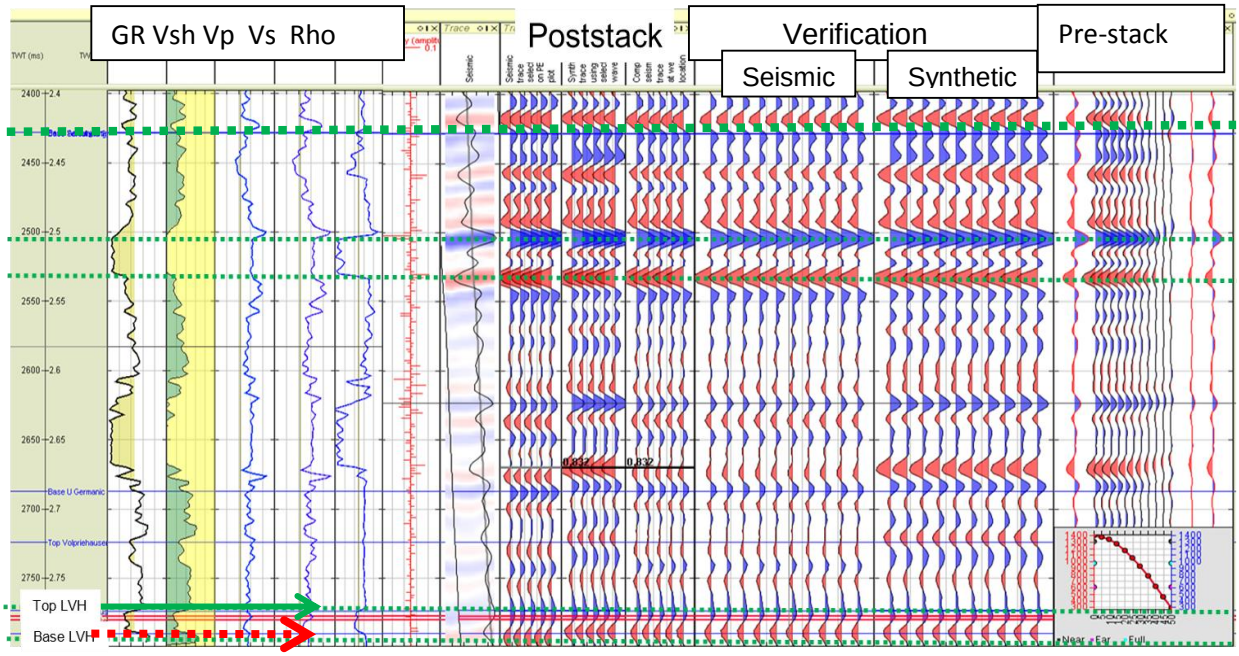


Fig. 28: Well data and synthetic-seismic verification at WTR: confirms almost a perfect match of both the poststack and prestack models with the real seismic; Similar trends in AVO of Top-Lower Volpriehausen. The horizontal dashed green lines show the matching trends. LVH =Lower Volpriehausen while blue horizontal line indicate the stratigraphical markers. Top and base of the Volpriehausen reservoir are indicated by the solid green and dashed red arrow respectively

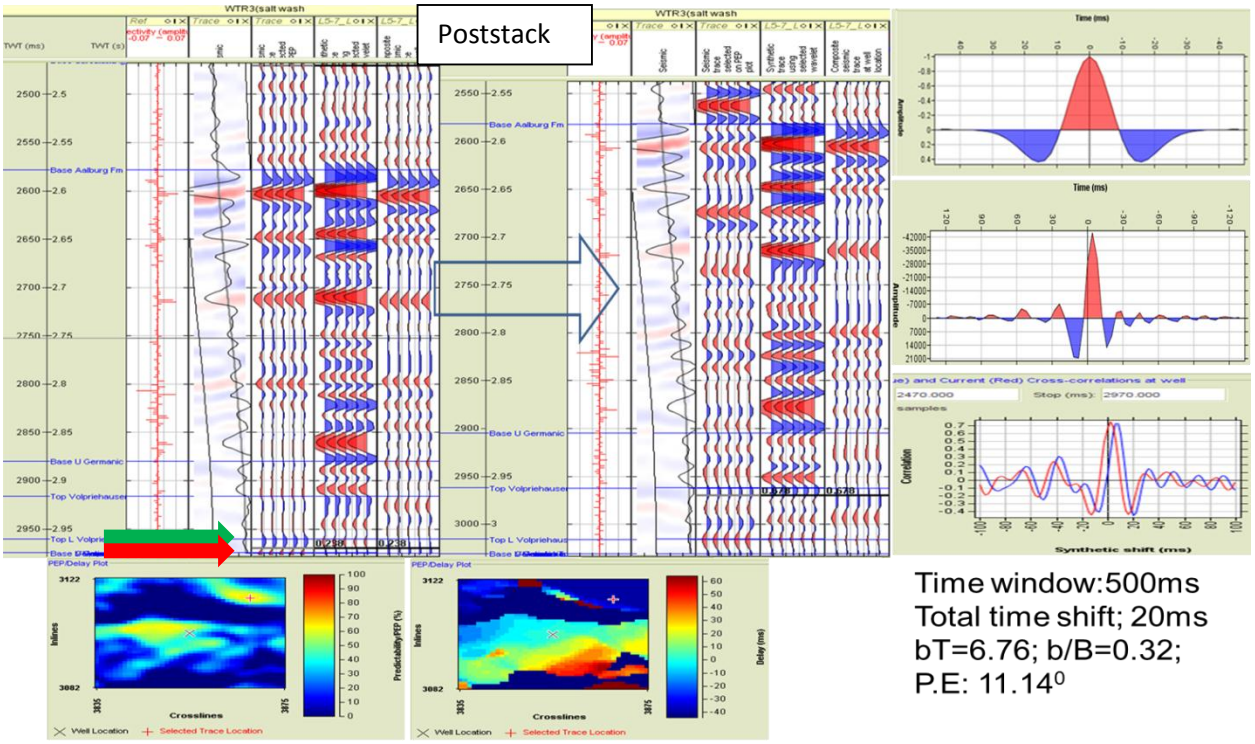


Fig. 29: Well tie at WTR3 using a statistical zero-phase wavelet and then the white's Wavelet estimation through matching' method .NB! Time shifts are needed to match the synthetic to seismic; full wavelet extraction after depth-matching. Cross correlation: seismic & synthetic, 2470-2290ms.Initial signal function is blue; current signal is red (almost a zero shift indicating perfect fit). Green and red arrow indicate reservoir top and bottom respectively.

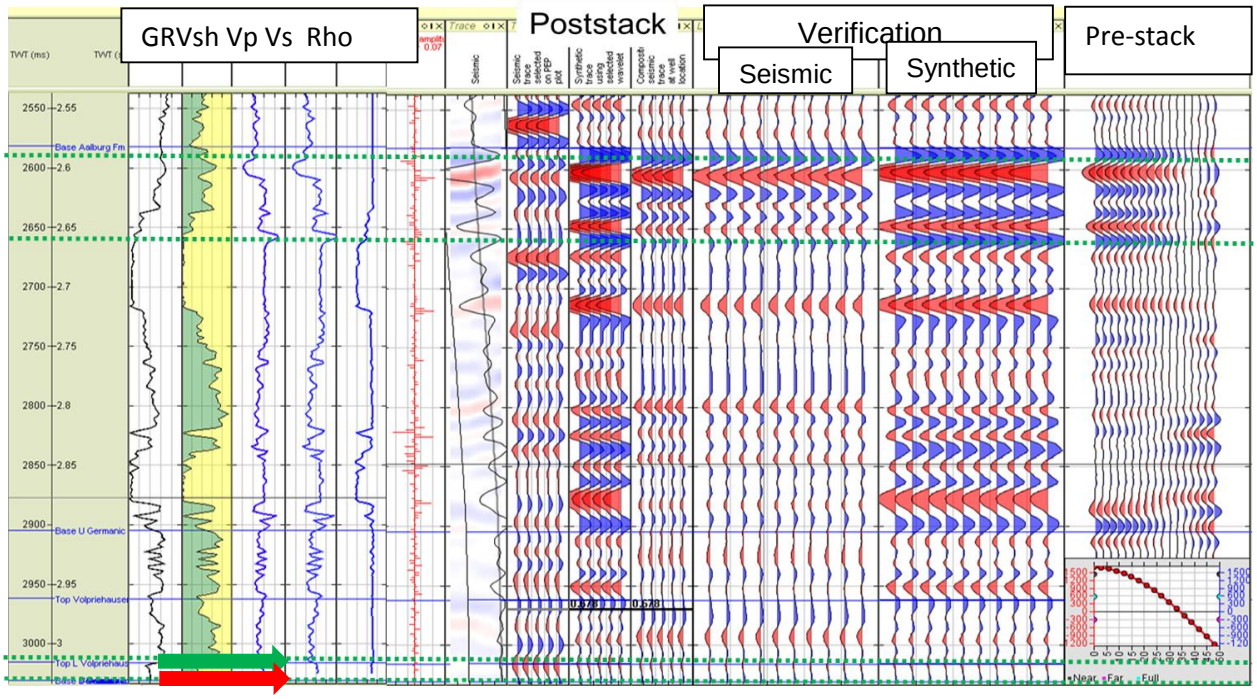


Figure 30: Well data and synthetic-seismic verification at WTR3: confirms almost a perfect match of both the poststack and prestack models with the real seismic; Similar trends in AVO of Top-Lower Volpriehausen. The horizontal dashed green lines show the matching trends, while blue horizontal lines indicate the stratigraphical markers. Green and red arrow indicate reservoir top and bottom respectively.

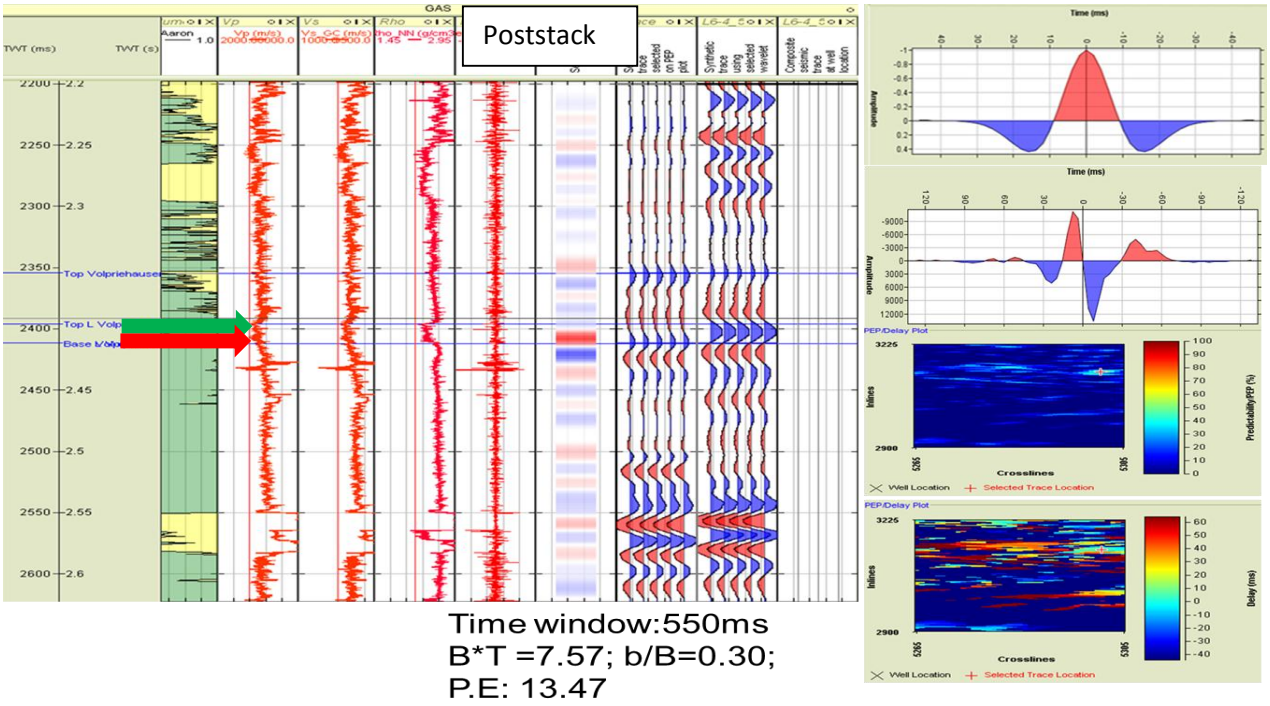


Fig. 31: Well tie at GAS using a statistical zero-phase wavelet. NB! No time shifts correction applied for lack of composite seismic along the well. Cross correlation: seismic & synthetic, 2200-2750ms.Still shows a good fit.

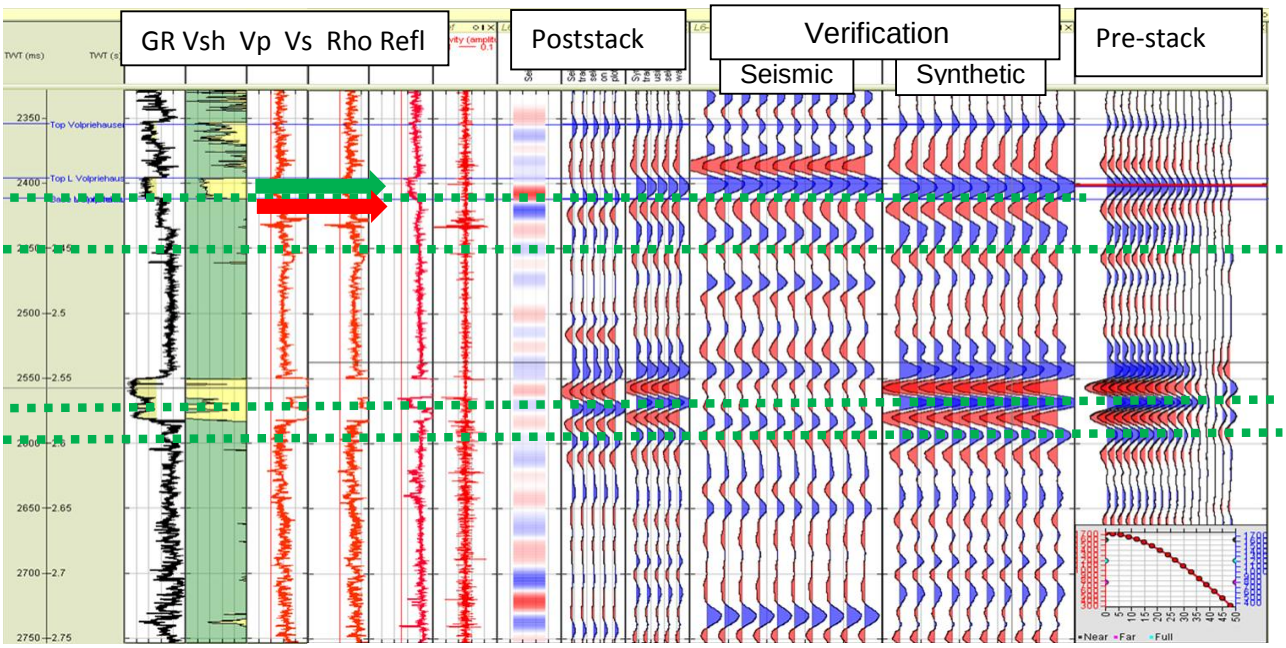


Figure 32: Well data and synthetic-seismic verification at GAS: good match of both the poststack and pre-stack models with the real seismic in spite of lack of depth-matching correction; Similar trends in AVO of Top-Lower Volpriehausen. The horizontal dashed green lines show the matching trends, while blue horizontal lines indicate the stratigraphical markers.

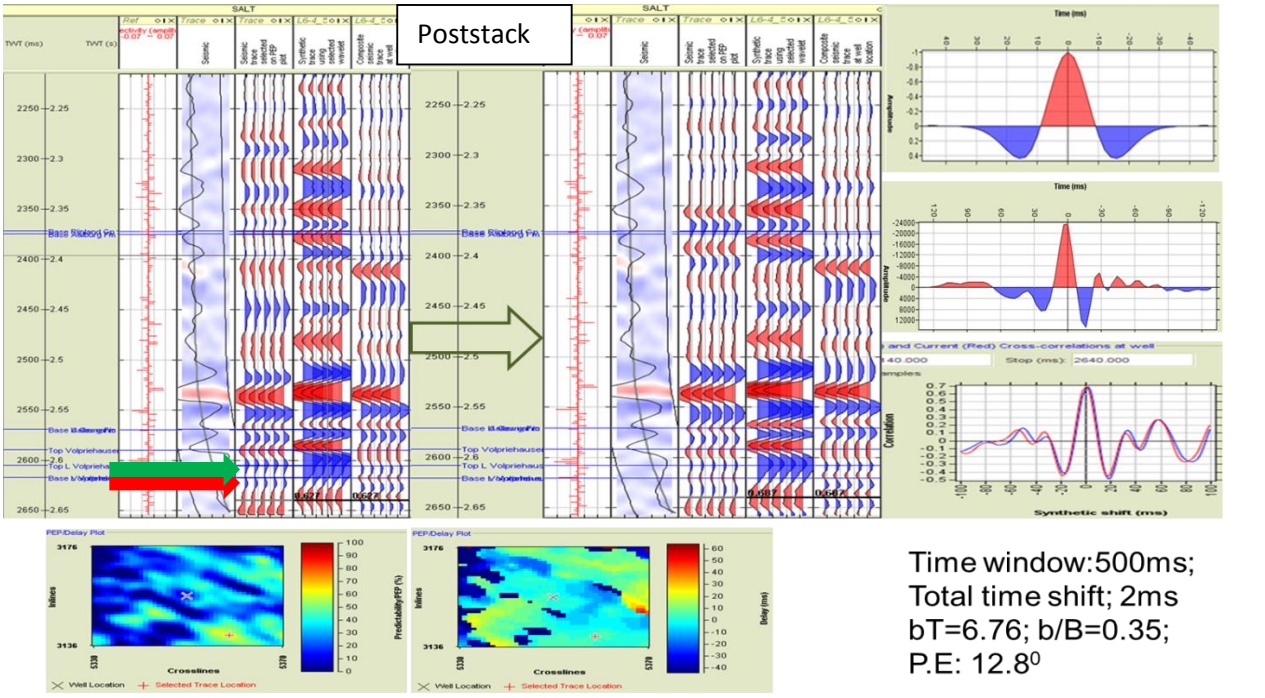


Fig. 33: Well tie at SALT using a statistical zero-phase wavelet and then the white's Wavelet estimation through matching' method .NB! Time shifts are needed to match the synthetic to seismic; full wavelet extraction after depth-matching. Cross correlation: seismic & synthetic, 2210-2260ms.Initial signal function is blue; current signal is red (almost a zero shift indicating a perfect fit). Green and red arrow indicate reservoir top and bottom respectively.

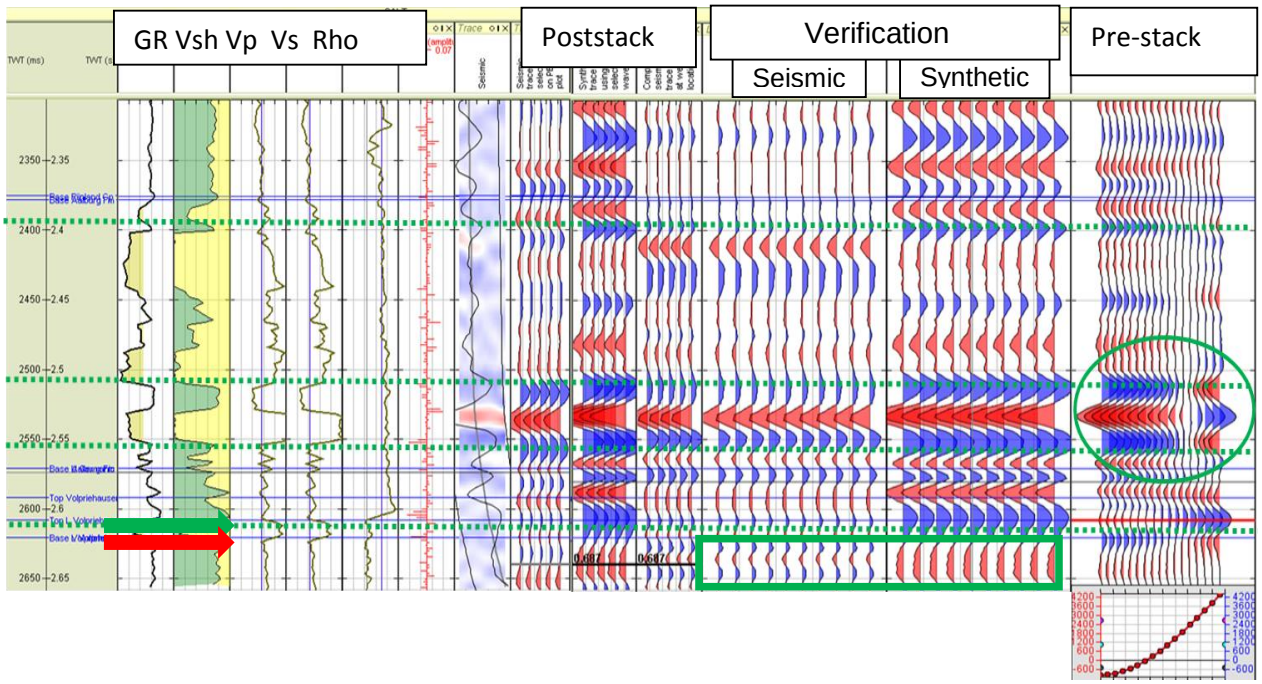


Figure 34: Well data and synthetic-seismic verification at SALT: confirms almost a perfect match of both the poststack and prestack models with the real seismic; Similar trends in AVO of Top-Lower Volpriehausen. The horizontal dashed green lines show the matching trends, while blue horizontal lines indicate the stratigraphical markers. Note a phase reversal indicated by the green circle. Green and red arrow indicate reservoir top and bottom respectively.

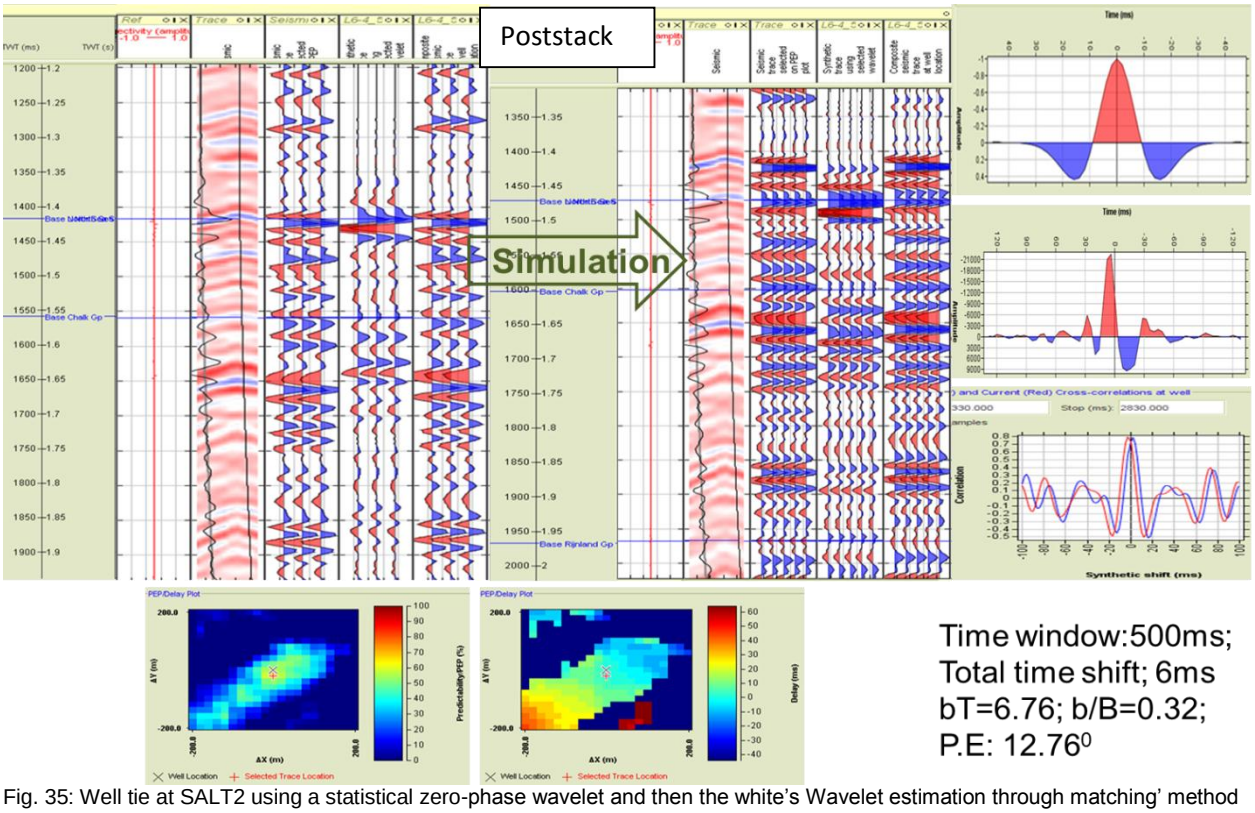


Fig. 35: Well tie at SALT2 using a statistical zero-phase wavelet and then the white's Wavelet estimation through matching' method .NB! Time shifts are needed to match the synthetic to seismic; full wavelet extraction after depth-matching. Cross correlation: seismic & synthetic, 2210-2260ms.Initial signal function is blue; current signal is red (almost a zero shift indicating a perfect fit.

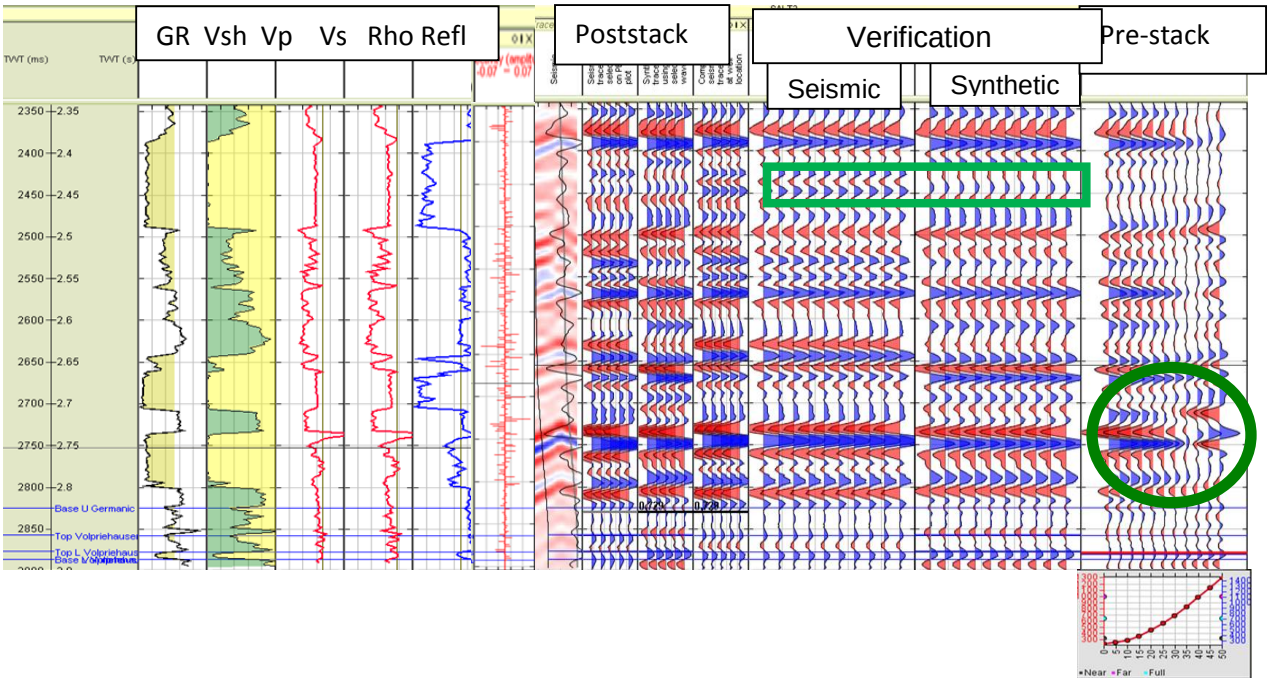


Figure 36: Well data and synthetic-seismic verification at SALT2: confirms very good match of both the poststack and prestack models with the real seismic; Similar trends in AVO of Top-Lower Volpriehausen. The horizontal dashed green lines show the matching trends, while blue horizontal lines indicate the stratigraphical markers. Note a phase reversal indicated by the smiley face. Green and red arrow indicate reservoir top and bottom respectively.

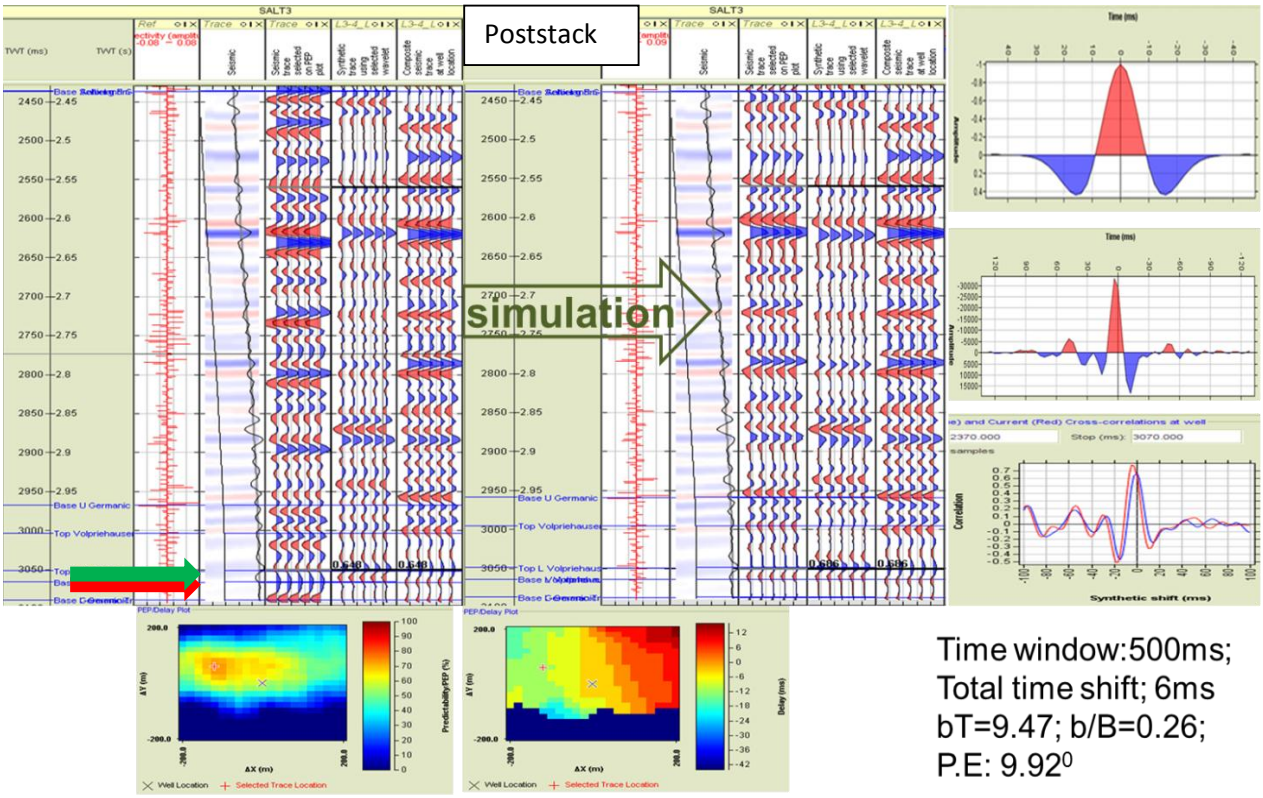


Fig. 37: Well tie at SALT3 using a statistical zero-phase wavelet and then the white's Wavelet estimation through matching' method .NB! Time shifts are needed to match the synthetic to seismic; full wavelet extraction after depth-matching. Cross correlation: seismic & synthetic, 2570-3070ms.Initial signal function is blue; current signal is red . Green and red arrow indicate reservoir top and bottom respectively.

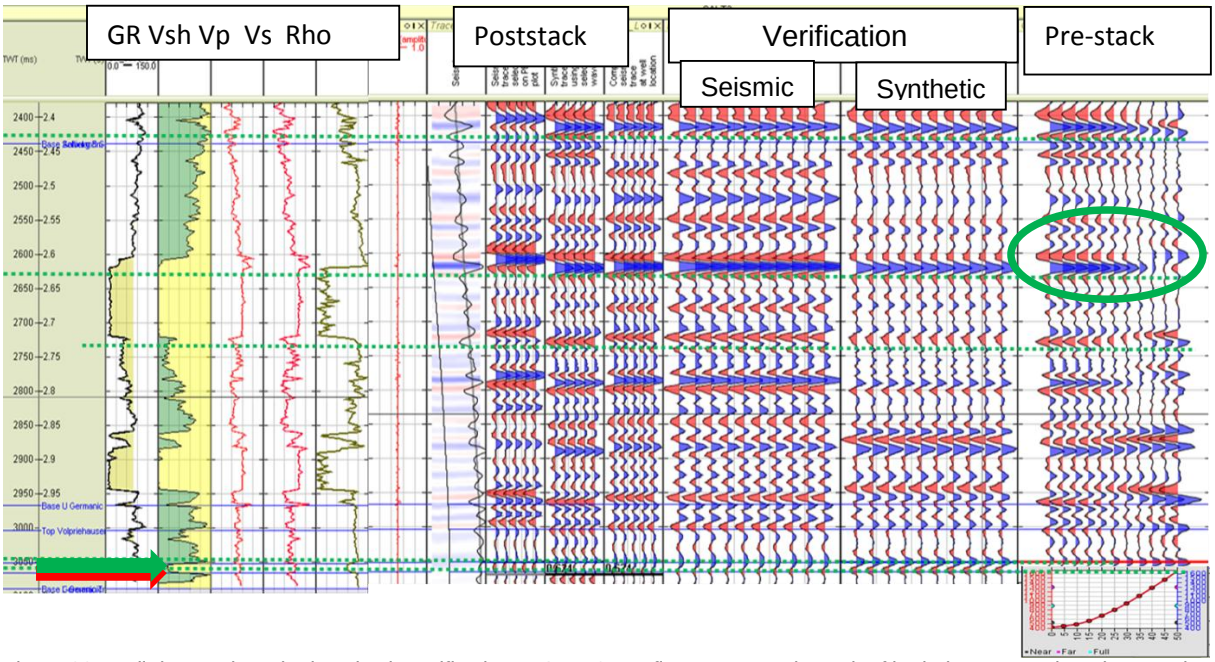


Figure 38: Well data and synthetic-seismic verification at SALT3: confirms very good match of both the poststack and prestack models with the real seismic; Similar trends in AVO of Top-Lower Volpriehausen. The horizontal dashed green lines show the matching trends, while blue horizontal lines indicate the stratigraphical markers. Note a phase reversal indicated by the smiley face. Green and red arrow indicate reservoir top and bottom respectively.

Interpreting figure 28 (WTR well), using the green horizontal dashed lines at amplitude peaks or troughs we see that:

- ❖ A perfect fit exists in the synthetic-to-seismic calibration at WTR well.
- ❖ This is true comparing poststack real seismic section in wiggle traces with both the post-stack pre-stack synthetic seismic models and correlating them with the GR, Vsh, Vp, Vs, Rho and amplitude reflectivity series as indicated on the WTR well.
- ❖ Both the logs and seismics show good correlation meaning that with synthetic seismogram operation for this well, a number of reflectors could be assigned to specific lithologies (with availability of sedimentological data).
- ❖ At the top and base Lower Volpriehausen reservoir interval, which is the interval of interest here, also exhibits the good fit between the seismics and the petrophysical logs.
- ❖ The general frequency decrease with depth due to attenuation of higher frequencies in the seismic signal in the upper layers is observed.
- ❖ These observations and interpretations hold true for all the wells relatively.

However, the following differences are observed:

- ❖ The water- and gas-filled reservoirs (Figures 28, 30 and 32) have higher velocity and lower densities than the embedding shale above and below it and the impedance of gas sand is further reduced. Hence, we see for the gas reservoir that, the amplitude is much greater.
- ❖ In the gas-filled case, a polarity reversal is observed (red oval shape in figure 32). This sounds strange in a gas reservoir, but it is a well-known scenario in salt filled reservoir in the Southern North Sea
- ❖ The amplitude signal in the salt case is much lower with polarity change phenomenon in place, though not visible in the reservoir interval, but in other sand layers especially upper sections like the Base North Sea group (figures 34, 36and 38).
- ❖ Tuning thickness effect is suspected at the WTR well due to the top and bottom reflections observed in the Volpriehausen reservoir interval in this well. It's more pronounced and clearly observable in the salt wells evidenced by the synthetic traces forming **'doublet traces'** resulting from other traces 'joining' together. This means there exist some interferences resulting from overlaps of reflections from different reflectors showing that the composite amplitude of the top and the bottom of the respective layers reached a maximum. As put by Thomas Funck and Holger Lykke-Andersen (1998), such reflectors represent thin layers, generally <2 m thick and this raises the question about the vertical resolution of the seismic data. Constructive inferences are observed here (green rectangle in figure 36 and 38).

5.5.0 Synthetics from Substituted wells (Predictive Modelling)

Here, both the Post-stack and Pre-stack synthetics were generated for two pseudo wells created as a result of fluids and solid substitutions. The pseudo logs were used in the Vs-Vs-Rho sets for synthetics when 80% of the water-bearing well became filled with gas and salt each. These are now two 'wells' referred to as 'GASintoWTR' and SALTintoWTR respectively. Figure 39 displays gathers of GAS substituted into water and salt substituted into water, compared with the originally water-filled pores spaces of the reservoir interval (Lower Volpriehausen particular).

Note that it was not possible to substitute initial salt filled wells for gas and water, due to the lower porosity condition of the salt-filled wells since the density for gas and water needs to be calculated using the porosity. The substitution from salt to gas and water was therefore performed on salt-plugged logs in water and gas bearing well which were calculated with the extended Gassmann equation. Hence, the predictive modelling here only refers to that of water well (WTR) substituted for salt and gas.

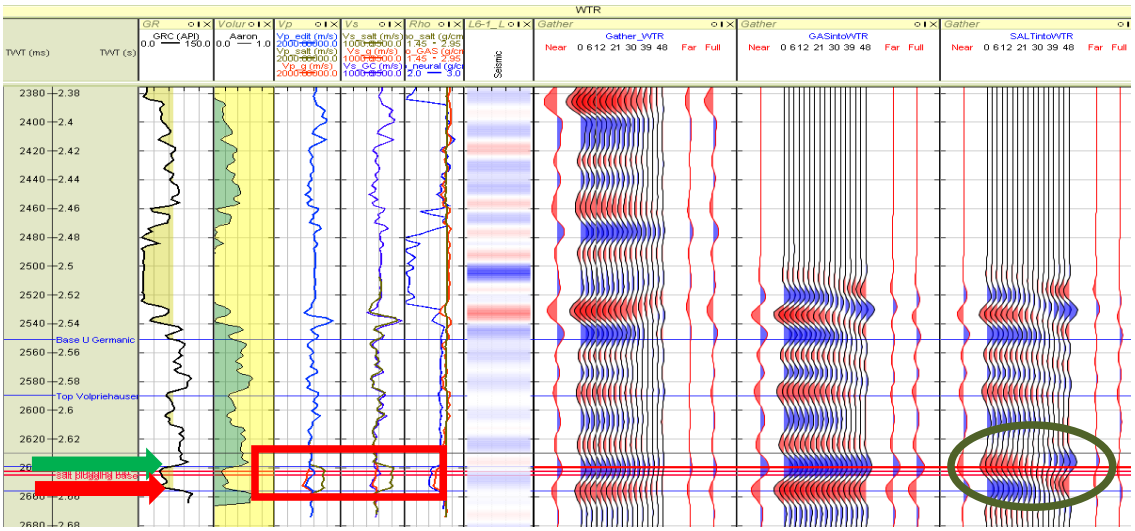


Figure 39) Well data and gather for the initial fluid log (gather WTR) and the substituted pseudo logs (GASintoWTR and SALTintoWTR) scenarios. Red rectangle and green oval shapes shows effect of substitution on Rho-Vp-Vs log sets and polarity change respectively. Horizontal lines show the position of the stratigraphical markers (red for salt-plugged zone). Green and red arrow indicate reservoir top and bottom respectively.

The columns in figure 39 show from left to right:

- Track one: holds the gamma log.
- Track two is a representation of the clay and sand volume fractions.
- Track three: the three Vp logs (blue for initial water-filled pores, and the set of substituting pseudo logs of gas (red) and salt (dark green).
- Track four: the three Vs logs (blue for initial water-filled pores, and the set of substituting pseudo logs of gas (red) and salt (dark green).
- Track five; shows the initial density log for water (blue) and a set of pseudo density logs for substituting logs of gas (red) and salt(dark green).
- Track six: 3D seismic section around the water well.
- Track seven: gather for initial water-filled reservoir.
- Track eight: gather for Water to gas substituted

- Track nine: gather for water to salt substituted

The amplitude behaviour in the initial reservoir pore spaces filled with water and those of the pseudo well logs are different, indicating the influence of fluid change (in the case of GASintoWTR) and solid (in the case of SALTintoWTR) on amplitude responses and seismic signals. The amplitude signal in the initial water-filled scenario is moderate while that of the pseudo gas-filled is high and that of the pseudo salt-filled is lower, conforming to the expectations in the normal reservoirs. Figures 39 to 43 show the poststack simulations with the poststack and prestack model verifications for these artificial water wells. The columns and the auxiliary figures are as indicated for the original wells in the previous sections.

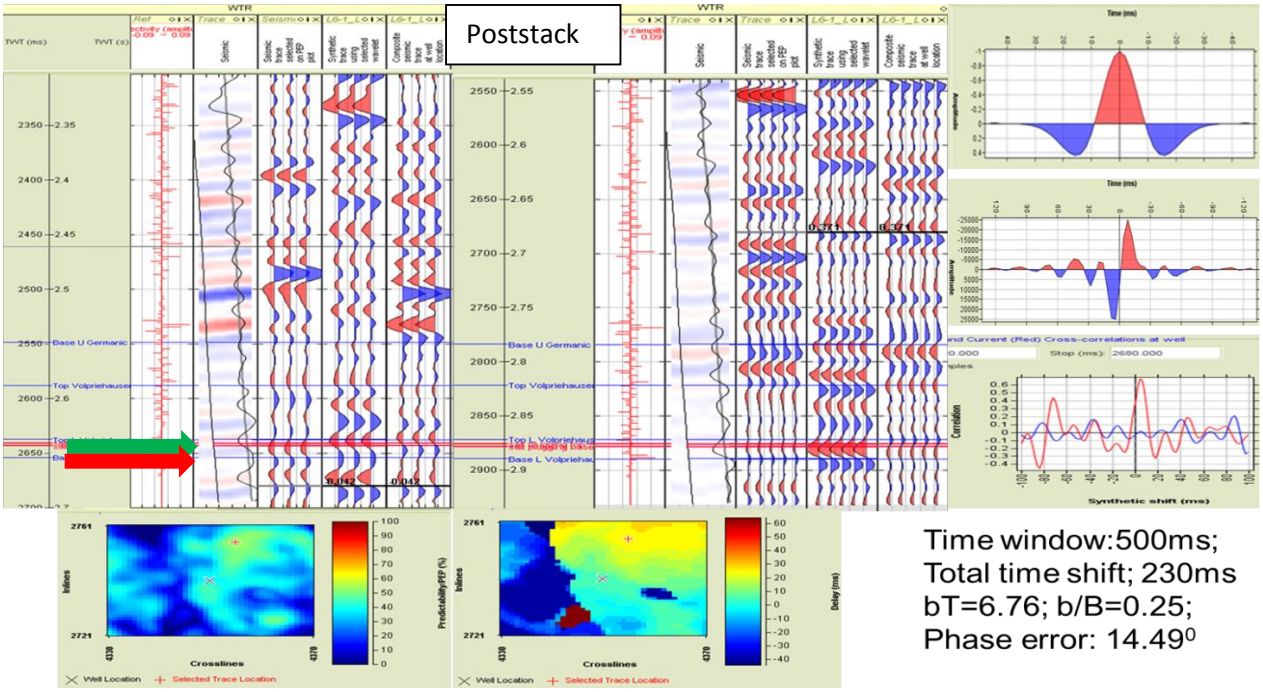


Fig. 40: Well tie at pseudo well GASintoWTR using a statistical zero-phase wavelet and then the white's Wavelet estimation through matching' method .NB! Time shifts are needed to match the synthetic to seismic; full wavelet extraction after depth-matching. Cross correlation: seismic & synthetic, 2160-2660ms.Initial signal function is blue; current signal is red. Green and red arrow indicate reservoir top and bottom respectively.

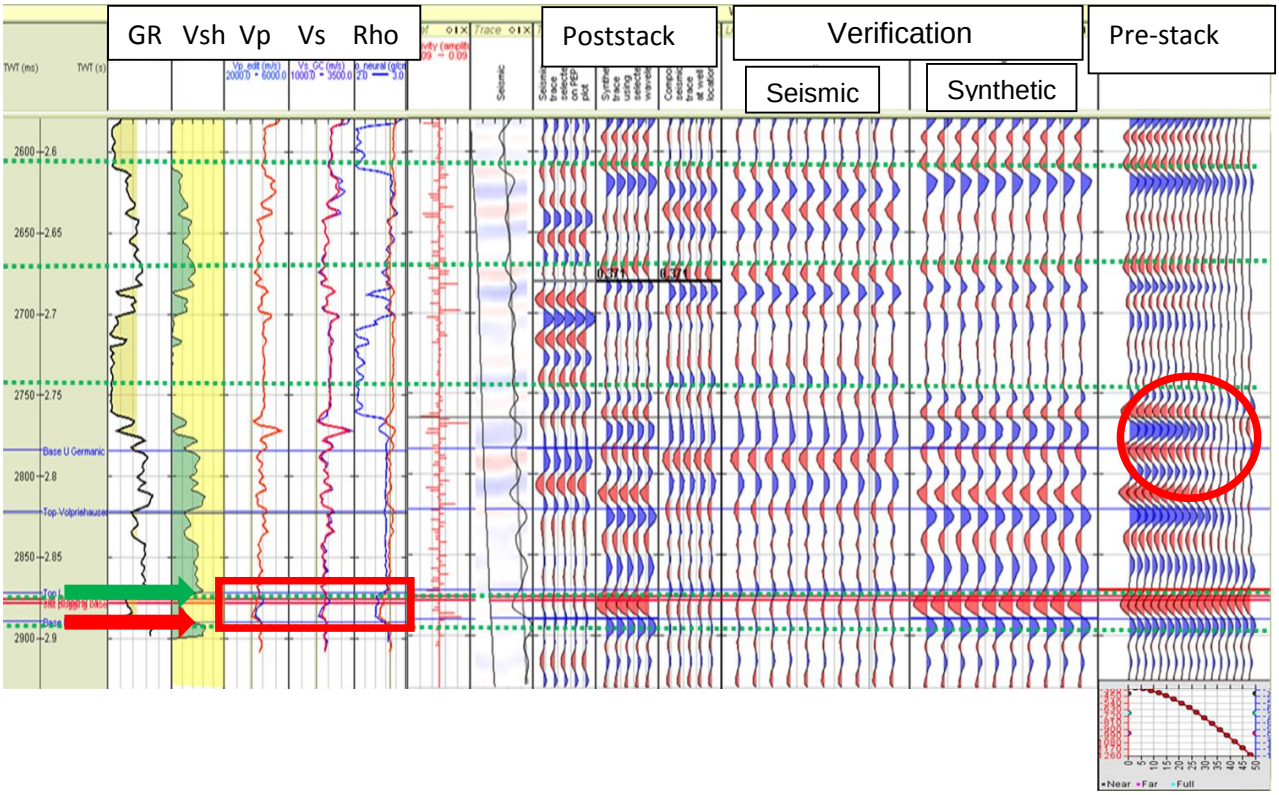


Figure 41: Well data and synthetic-seismic verification at pseudo well GASintoWTR: confirms very good match of both the poststack and prestack models with the real seismic; Similar trends in AVO of Top-Lower Volpriehausen. The horizontal dashed green lines show the matching trends, while blue horizontal lines indicate the stratigraphical markers.

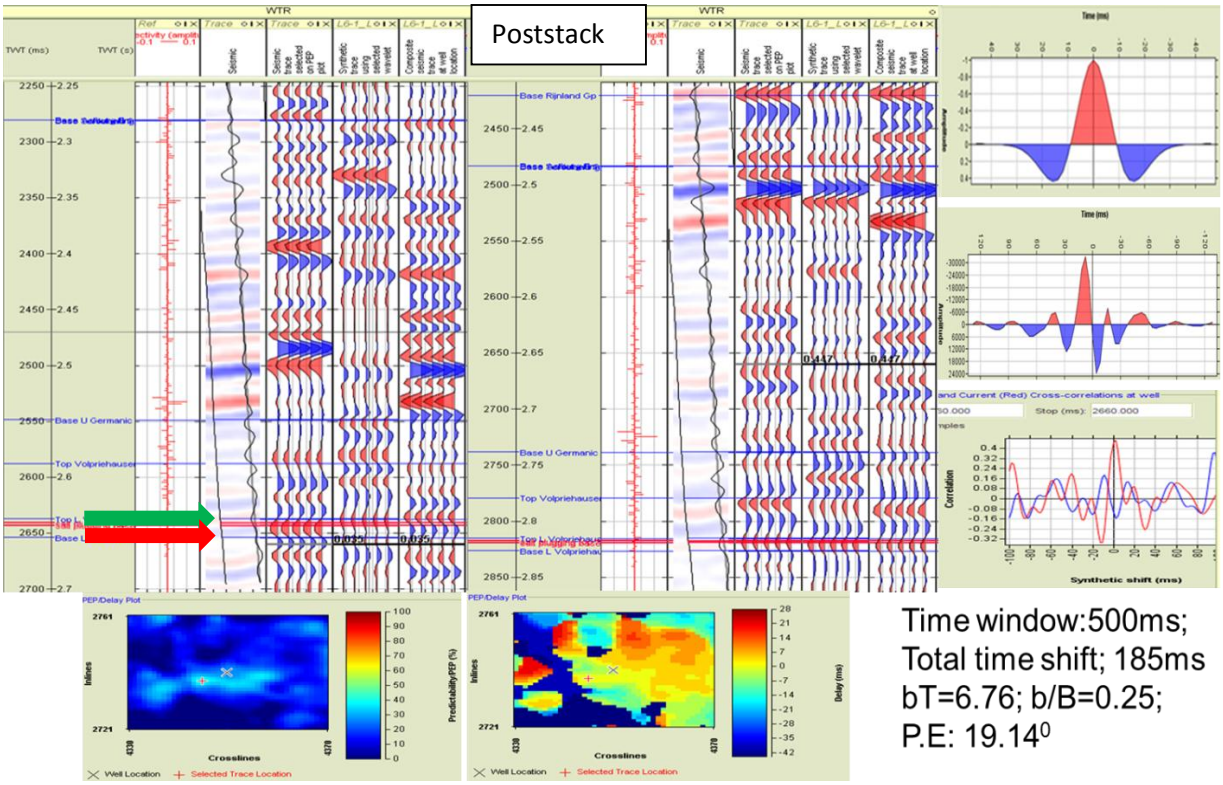


Fig. 42: Well tie at pseudo well SALTintoWTR using a statistical zero-phase wavelet and then the white's Wavelet estimation through matching' method .NB! Time shifts are needed to match the synthetic to seismic; full wavelet extraction after depth-matching. Cross correlation: seismic & synthetic, 2160-2660ms.Initial signal function is blue; current signal is red

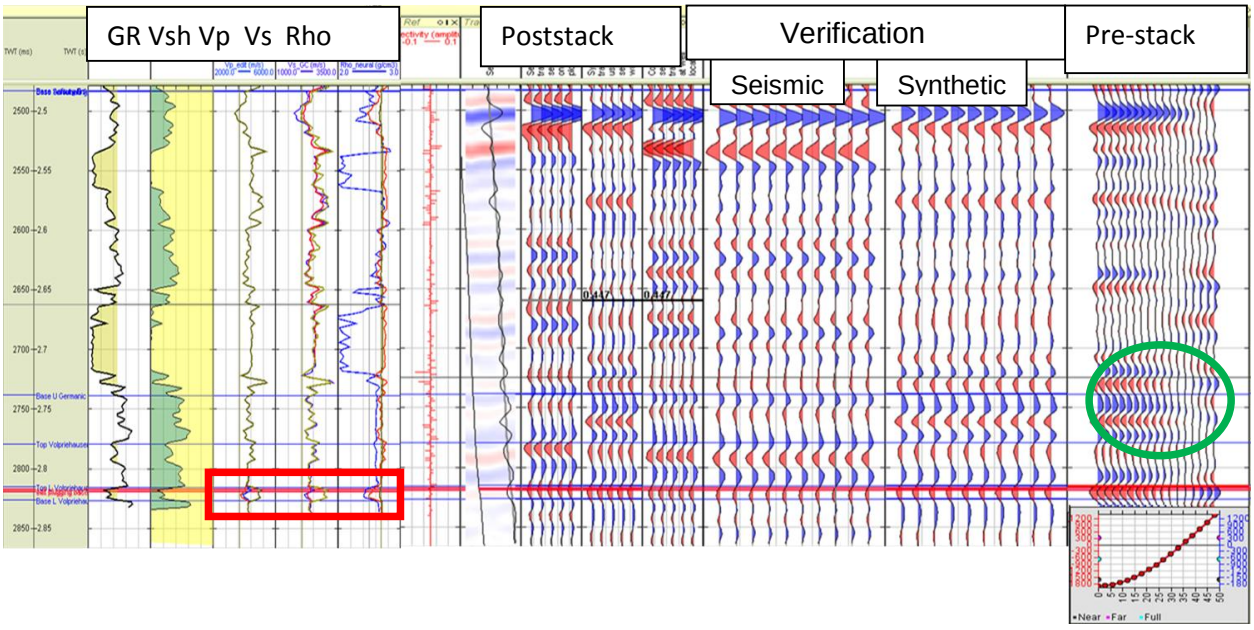


Figure 43: Well data and synthetic-seismic verification at pseudo well SALTintoWTR: confirms very good match of both the poststack and prestack models with the real seismic; Similar trends in AVO of Top-Lower Volpriehausen. The horizontal dashed green lines show the matching trends, while blue horizontal lines indicate the stratigraphical markers. Note the phase reversal indicated by the green circle. Green and red arrow indicate reservoir top and bottom respectively.

5.6.0 Results and Interpretation-Substituted well

Again, interpreting with the green horizontal dashed lines:

- The match between the seismic and the correlation with logs is not perfect, but good particularly at certain intervals
- While the frequency signal for the real and synthetic seismic show no difference.
- For the salt substituted into water artificial well, the frequency of the real seismic data is higher compared with the synthetic model and the amplitude magnitudes as observed in the original salt wells is consistent.
- The observed polarity reversal associated with the salt initial wells is evident here too.
- The substitution from initial water-filled into pseudo gas-filled reservoir shows the expected decrease in compressional velocity and density, while shear velocity remains relatively constant (Red rectangle around the Lower Volpriehausen reservoir interval in figures 39, 41 and 43).
- Also, the expected increase in compressional velocity and density, and relatively constant shear velocity in the salt substituted into water scenario is also observed.

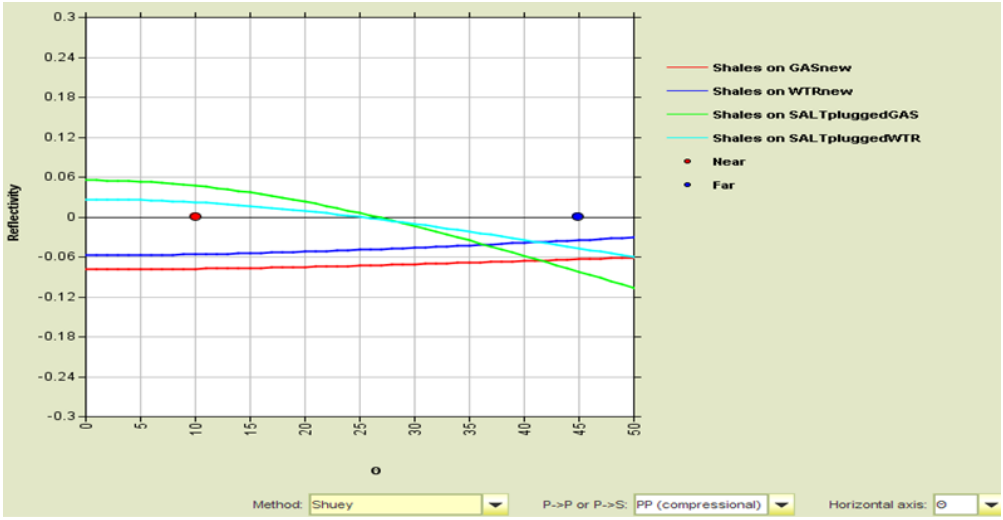
5.7.0. AVO Behaviour

As indicated in the AVO theoretical background, interpretation from AVO modeling can be used to reduce risk in exploration and development drilling as it provides unique seismic solutions for lithology, reservoir contents, and reservoir quality. The AVO modelling procedures use here are as follows:

- **Estimation of sand/shale ratio in each well and defining the well's mineral and fluids.** The Greenberg-Castagna method was used to predict Vs and Vp where shear wave velocity was not available originally. The shale volume (Vsh) was calculated using the GR log to interpret clean shale and sands lines. The mineral volume set was calculated using the Vsh and a quartz complement log, the sum of which is unity. The saturation set was calculated using the porosity log and assuming that the initial well was water-saturated, resulting in a saturation curve of Sw=1.NB!The Greenberg-Castagna method is based predominantly on the Gulf of Mexico data; Hence, the constants were calibrated to measured shear data using cut-offs.
- Deriving average interval properties from the log data using working intervals and cut-offs. This involves creating the mean properties of the Vp-Vs-Rho sets for the water, gas and salt interval in the well as the case may be.
- Using the extended Gassmann's model to carry out fluid and solid substitutions and then study the AVO responses Shuey's approximation of the Zoeppritz equation.
- Then comparisons were made between the AVO responses after a fluid-fluid or fluid-solid substitution in the particular well and the initial AVO responses. The difference in the difference in the two AVO responses are used to measure the impact of the change in fluids (say water to gas) and solid (say salt here) on AVO behaviours.

5.8.0 AVO: Initial Wells:

Four average sets were selected respectively for WTR, GAS, SALTpluggedWTR and SALTpluggedGAS intervals from the created average sets as AVO inputs and plots were generated. The near stack angle is defined at 10^0 while the far stack angle is at 50^0. Figure 44 shows the results of the reflectivity curves for the original water, salt-plugged water, original gas (GAS2 well here, though not within the survey areas but used as an example since it's the only salt-plugged gas well) and salt-plugged gas scenarios. See next chapter for full interpretation of the observation with respect to AVO classes.



Figures 44: AVO of initial gas-, water-bearing wells and salt-plugged zones (above) Red curve indicates reflectivity of a gas-bearing well; blue curve indicates that of a water-bearing well; light green curve is that of salt-plugged zone of a well GAS2 while the light blue curve is that of the salt-plugged zone of well WTR.

5.8.1 AVO: Substituted Wells:

Next, the AVO of the substituted well was studied and comparisons were made between the AVO of the respective original wells and that of the new fluid or salt substituted. The water bearing well was substituted for a salt-plugged zone after which the inverse procedure was followed for substitution from salt-plugged zone back to water. The same operation was used for gas-to-salt and salt-to-gas.
In terms of AVO classical analysis, the corresponding plots for the three substituents are as shown in figures 45, 46 and 47. Note that only WTR is used as example of synthetic generation and verification since GAS2 is out of the survey area. Table below gives the intercept (I) and gradient (G) values which are used to compare with Prestack AVO responses and classify the AVOs.

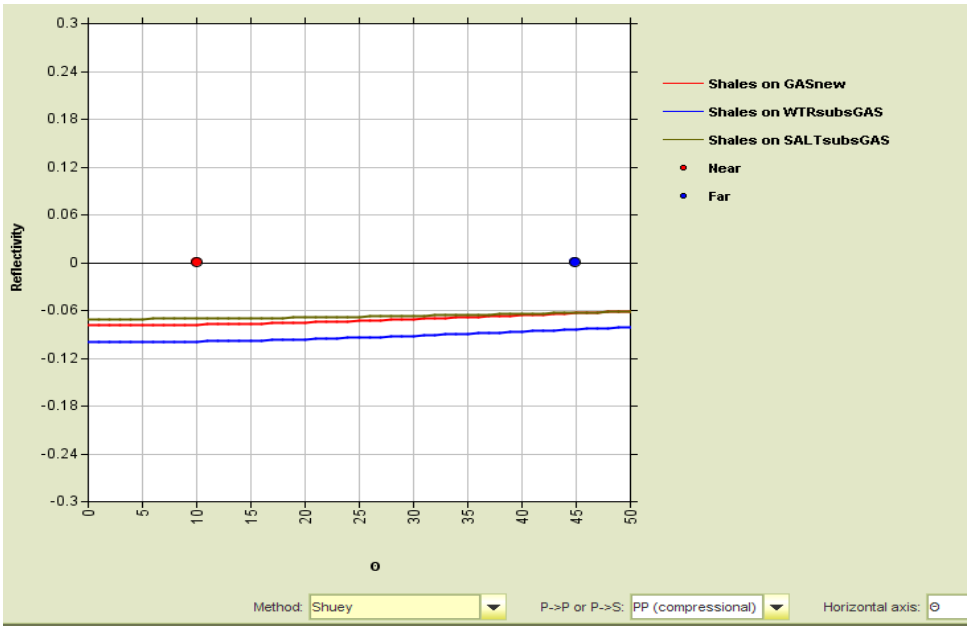


Figure 45: AVO for substitutions into gas pore-filling (above). Red curve is the real gas-bearing well. Blue is the substitution from water to gas filling and green is the substitution from salt to gas pore filling.

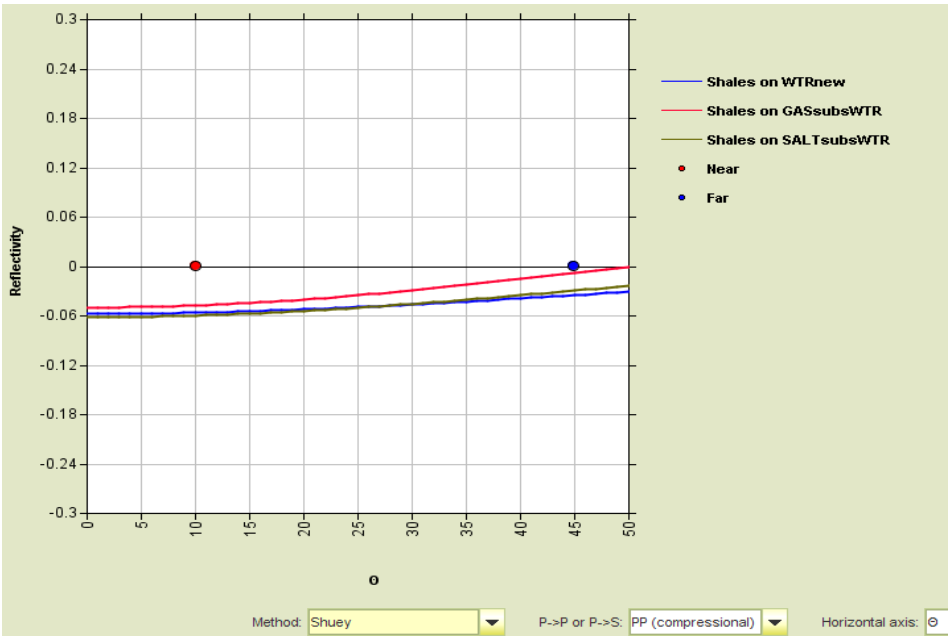


Figure 46: AVO for substitutions into water pore-filling (above). Red = real water-bearing well, the blue curve is the gas replaced by water and green the substitution from salt to water.

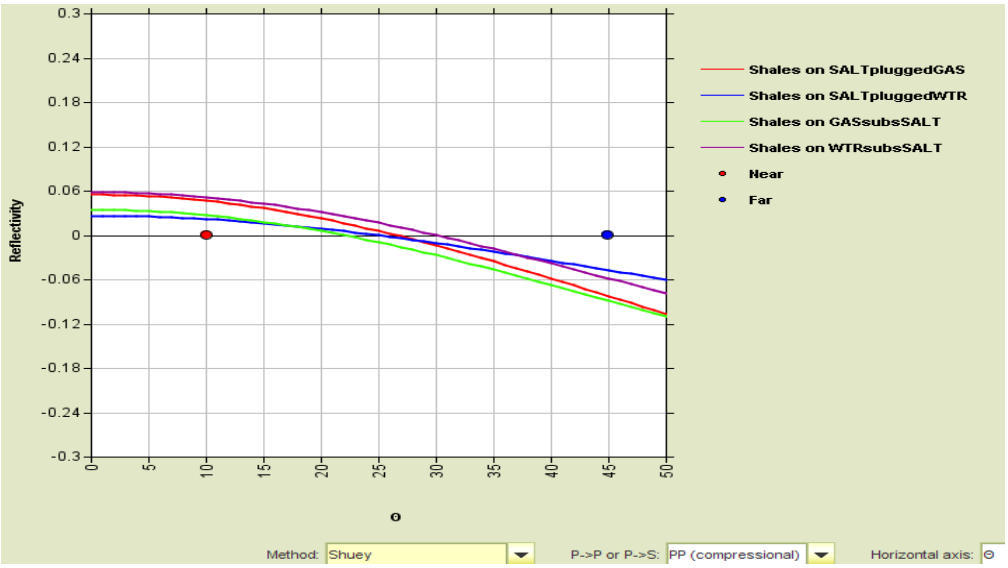


Figure 47: AVO for substitution salt pore-filling (above). Red and blue curves are the salt-plugged zones in gas and water bearing wells. Light pink is the substitution from gas to salt and light blue from water to salt pore-filling.

5.8.2 AVO Classification

Using the Castagna et al (1998) AVO interpretation based on **AVO intercept** (*A*) and gradient (*B*) cross plots, this study's results have the following AVO classes. Table 6 lists the magnitude for the intercept (I) and gradient (G) of the interfaces of interest in this analysis and interpretation.

Table 6: AVO intercepts (I) and gradients (G)

Interface and well	I	G
Shales on GAS(new)	-0.079	0.31
Shales on WTR(new)	-0.058	0.046
Shales on SALT-plugged GAS well	0.055	-0.273
Shales on SALT-plugged WTR well	-0.087	0.098
Shales on GAStoWTR	-0.101	0.032
Shales on GAStoSALT	-0.071	0.016
Shales on WTRtoGAS	-0.058	0.083
Shales on WTRtoSALT	-0.087	0.096
Shales on SALTtoWTR (inverse)	0.034	-0.245
Shales on SALTtoGAS(inverse)	-0.087	0.098

IN THE INITIAL WELLS;

- The initial gas sand (red curve) exhibits a Class IV AVO response negative impedance contrast that develop an increase from negative to positive impedance with offset(figure 44).
- The initial water-bearing well (blue curve) also falls into class IV AVO (figure 44) since it displays the same trend as in the gas-bearing well (but with higher impedance contrast that increases with offset).This is also confirmed in the I and G analysis in table 6 above. The behaviours of these two initial wells imply an amplitude decrease with offset. This is also confirmed by the observable amplitude signals in prestack seismic model (figures 28, 30, 32, 34, 36 and 38 above).
- The salt-plugged zone in the gas-bearing well (light green curve) with polarity change from positive to negative impedance contrast falls into class IIp AVO, since it exhibits a near-zero impedance that decreases with offset and a decreasing reflection magnitude with offset(figure 44).
- The salt-plugged zone in the water-bearing (light blue curve) also displays a polarity change from positive to negative impedance contrast and therefore falls into class IIp AVO(figure 44). It exhibits a near-zero impedance that decreases with offset and a decreasing reflection magnitude with offset, but with lower impedance contrast that decreases with offset.

IN THE SUBSTITUTED WELLS;

- All the curves of figure 45 above show a very small positive gradient and a negative intercept (confirmed in table 7) for the gas-bearing well.
- As observable from figure 46 above, the substituted water-bearing well show intercept magnitudes all of about -0.06 and near-positive gradients especially in the far offset.
- The inverse or back substitution of salt to water and salt to gas indicate AVO response associated with a polarity change from positive to negative, starting with a positive intercept of 0.03 - 0.06 (Figures 47 above).The gradient of the curves is between -0.1 and -0.2. This clearly begins to indicate the impact of solids (salt) on AVO behaviour.

5.9.0 Integrated Interpretation and Remarks

From the general observations of the pre-stack and post-stack synthetic seismograms with measured seismic sections at the wells used for this study, it can be inferred that a good match exist between the synthetic and the seismic data. This implies then that:

- The correlatability of both the well logs (petrophysical) and the seismics (both real and synthetic) which could be assigned to lithologic units shows that well data has been tied to the seismic data.
- The new Gassmann's model can be used for synthetic-to-seismic calibration operations.
- Full inversion can be carried out, using this extended Gassmann's model the calibration to extract the elastic and specific properties such as specific lithologies, porosity and saturation from the seismic data.

Observations for Volpriehausen reservoir interval and the upper layers based on both real and synthetic seismic data at well location how that:

- If the well is water/gas bearing, top Volpriehausen is a peak, followed by a clear trough (figures 28, 30 and 32).
- If the well is salt-plugged (or partially plugged & gas bearing), top Volpriehausen is a trough, followed by a clear peak showing polarity reversal (figures 34, 36 and 38).
- Presence of gas causes a clear brightening even when salt-plugged (figure 32)

With these interpretations of the various scenarios, the difference between the amplitude signals of the water-, gas- and salt-filled reservoir pore medium is made clearer:

- Water-filled reservoir medium shows amplitudes of moderate magnitude with normal (North Sea) polarity
- Gas-filled medium has larger amplitude magnitude with normal (North Sea) polarity; Very positive amplitudes(upper window) and Very negative amplitudes(lower window)
- Salt-filled porous medium shows lower amplitude magnitude with reversed polarity; normal-averaged negative amplitudes (upper window) and positive amplitude (lower window).

With these understanding in mind, misinterpretation risk is reduced when interpreting the top of the Volpriehausen reservoir in particular and any other hydrocarbon reservoir in general or during the interpretation of exploratory data set to detect the presence or absence of hydrocarbon. This helps to find good quality reservoir rather than poor-quality salt (solid) reservoirs.

CHAPTER SIX

CONCLUSSION AND RECOMMENDATION

6.1.0 Conclusions

This study is concluded as follows **in general:**

- This study attempted providing solution to the challenge of predicting the seismic response for a Buntsandstein reservoir in water-, gas or salt-filled investigated. The analysis is based on a real field case in the North Sea area offshore the Netherlands, where all three porefills have been encountered in different wells.

- The method of studying the seismic response at various existing wells covering different reservoir depths was adopted and thorough analysis of the log responses of 13 wells was made.

- A good match between well log data and the post-stack seismic data is established by creating synthetic seismic data. By using fluid substitution and the more recently developed solid substitution theory, subtle changes in seismic response, both pre-stack and post-stack, between the different pore-fills are predicted. Based on these modeled predictions recommendations are made concerning the type of data analysis that should be carried out to discern the different pore-fills on the seismic data.

From the well log analysis:

- No clear relation has been observed between burial depth and petrophysical properties like density and velocity.
- Observed variations in the different wells investigated seem to be related essentially to facies changes and lateral inhomogeneity of the reservoir.
- This spatial variability in properties makes it difficult to create a predictive model with respect to the seismic response to different porefills.

From the seismic modeling study:

- In general the quality of the match between the synthetic and the real seismic data is satisfactory.
- Forward modeling after fluid/solid substitution shows, that especially the AVO response shows clear distinctions between the different pore-fills, mostly expressed by the gradient behavior.
- However, due to the varying input parameters, this response requires calibration to individual wells each time, making it less suitable as a predictive tool for reservoir quality.
- Unfortunately the results of this analysis do not lead to clear recommendations to distinguish between different porefills based on seismic data alone. In order to make this possible, the reservoir properties such as porosity need to be known upfront. A way forward could be to try and make predictions based on the best porosity estimate in the reservoir. The latter could be estimated from seismic data and from geological background knowledge.

6.2.0 Recommendations

Despite the fact that analysis of the results based on seismic alone do not lead to clear recommendations for distinguishing between different porefills based on seismic data alone, the following are recommended;

- Resistivity log types such as Micro-spherically Focused Logs (MSFL), Laterolog Shallow (LLS) and Laterolog deep (LLD) are needed and should be made available for the Buntsandstein in order to reliably analyze the fluid contents of the lithologic intervals. Plus, the SP-Log as permeability indicator
- Siliciclastic petrographic analysis of the Formation should carried out. This will better the understanding of the mineralogic contents of the sand reservoir with respect to the -Uranium distribution radioactivity; Grain-size-distribution, presence of glauconitic illite and K-feldspar content, etc.
- Reservoir heterogeneity and its controls such as permeability, facies shaliness, grain matrix texture, should be integrated into the rock physic model .This is to account for the variability in the geological processes such as diagenetic, etc., in time and space. Reservoir model has to take into account the non-uniformity and anisotropy of the subsurface, since a profound analysis of the geological nature of these heterogeneities is required to UNDERSTAND and therefore PREDICT them.

ACKNOWLEDGEMENT

- First and foremost, I'm grateful to God Almighty for making this master's education as part of His master plan for my life and for the Grace for completion.
- I will like to express my gratitude to Shell International exploration and production for offering to sponsor the studies in general and to the noble professors such as Prof. Alan Green, Prof. C.P.A Wapenaar, etc., who might have initiated the fund.
- Next, I'll like to appreciate the effort of the IDEA League partner universities and their respective personnel who worked tirelessly to ensure quality teaching and coordination while we rotated.
- I'm equally grateful to Wintershall for offering to sponsor the IDEA League programme for quality geophysical skill acquisition for the scholars, and for accepting me in particular for this project. Particularly, I thank the company and all the personnel involved in making my software training in London possible. In particular, thank you Patricia Verburg and Suzy Joosen for all your efforts.
- A big thank you to Andries Wever of Wintershall for all your effort and smart ideas contributed and to make this thesis workable.
- My noble Prof. Rob Arts; is highly appreciated for close supervision, real-time ideas and the general knowledge imparted into me.
- Finally, I'm grateful to my better half; my wife, Victoria for emotional support and for bearing with me while on this course.

REFERENCES

Castagna J. P. Herbert W. Swanz, and Douglas J. Foster, 1998; Framework for AVO gradient and intercept interpretation. GEOPHYSICS, VOL. 63, NO.3 (MAY-JUNE 1998); P. 948–956.

De-hua Han and Michael L. Batzle*, 2004.*Gassmann's equation and fluid-saturation effects on seismic velocities; geophysics, vol. 69, no. 2 (March- April 2004); p. 398–405,8 figs., 2 tables. 10.1190/1.1707059.

Hampson-Russell Software Services Ltd. AVO Theory 1: http://www.ipt.ntnu.no/pyrex/stash/avo_theory.pdf

H.E. Rondeel, D.A.J. Batjes. Geology of Gas and Oil under the Netherlands. Springer,1996.

Isabella Pacek, 2009.Extended Gassmann approach to pore-fill substitution for salt and Fluids, calibrated on Triassic Sandstone Reservoirs in the Southern North Sea. Master thesis Copyright ©2009 Section for Applied Geophysics of TU Delft / ETH Zurich / RWTH Aachen and WINTERSHALL

Jan de Jager Theo E. Wong, Dick A.J. Batjes. Geology of the Netherlands. Royal Netherlands Academy of Arts and Sciences, 2007.

Karen Brawley-Hogg, 1999. Use of AVO and Residual Mapping to Delineate Gething Reservoir Sands in N.E. B.C.: An Integrated and Practical Approach.

L. B Magoon and W. G. Dow, eds., 1994. The Petroleum System –from source to trap: AAPG Memoir 60.

M.C Geluk, 2007. Triassic; in the Geology of the Netherlands. Edited by T.E. Wong, D.A.J. Batjes & J. de Jager. Royal Netherlands Academy of Arts and Sciences, 2007: 85–106.

M. Peeters, 2001: Physical reservoir models: from pictures to properties; Petroleum Geosciences, Vol. 7, 2001 pp. 57-62.1354-0793/01/$15.00 (C) 2001 EAGE/Geological Society of London

Paul M. Krail, 2004; Rock properties and amplitude versus angle. The Leading Edge; October 2004; v. 23; no. 10; p. 986-988; DOI: 10.1190/1.1813360.© 2004 Society of Exploration Geophysicists.

Radim Ciz and Serge A. Shapiro. Generalization of Gassmann equations for porous media saturated with a solid material; Geophysics, Vol. 72, No. 6 November-December 2007; P. A75–A79, 3 Figs.10.1190/1.2772400.

R. Ciz, K. Stürmer, C.H. Arns, M.A. Knackstedt and S.A. Shapiro. Generalization of Gassmann Equations for Porous Rocks Saturated with a Solid Material Theory and Applications; 70th EAGE Conference & Exhibition; Rome, Italy, 9 - 12 June 2008.

R. J. S. Brown and J. Korringa. On the dependence of the elastic properties of a porous rock on the compressibility of the pore fluid. Geophysics, 40:p. 608 (616, 1975.)

Schlumberger. Webpage. http://www.glossary.oilfield.slb.com.
Tapan Mukerji, Gary Mavko and Jack Dvorkin 2998. The Rock Physics Handbook. Cambridge University Press, 1998.

Thomas Funck and Holger Lykke-Andersen, 1998. Comparison of Seismic Reflection Data to A Synthetic Seismogram in a Volcanic Apron at Site 9531.Weaver, P.P.E., Schmincke, H.-U., Firth, J.V., and Duffield, W. (Eds.),1998. Proceedings of the Ocean Drilling Program, Scientific Results, Vol. 157.

Van Adrichem Boogaert & Kouwe, 1994 in 'Geology of the Netherlands):

Vladimir Grechka, 2008; Fluid-Solid substitution in rocks with disconnected porosity: Shell Exploration and Production,200 North Dairy Ashford, Houston, TX, 77079, USA. SEG Las Vegas annual meeting, 2008 (www.segdl.org)

White, R. and Simm, R., 2003. Tutorial: Good practice in well ties, First Break 21(10), 75 - 83.)

Wyllie, M., Gardner, G., and Gregory, A., 1963, Studies of elastic wave attenuation in porous media: Geophysics, **27**, 569-589.

APPENIX A:

Location well in field of study-3D view

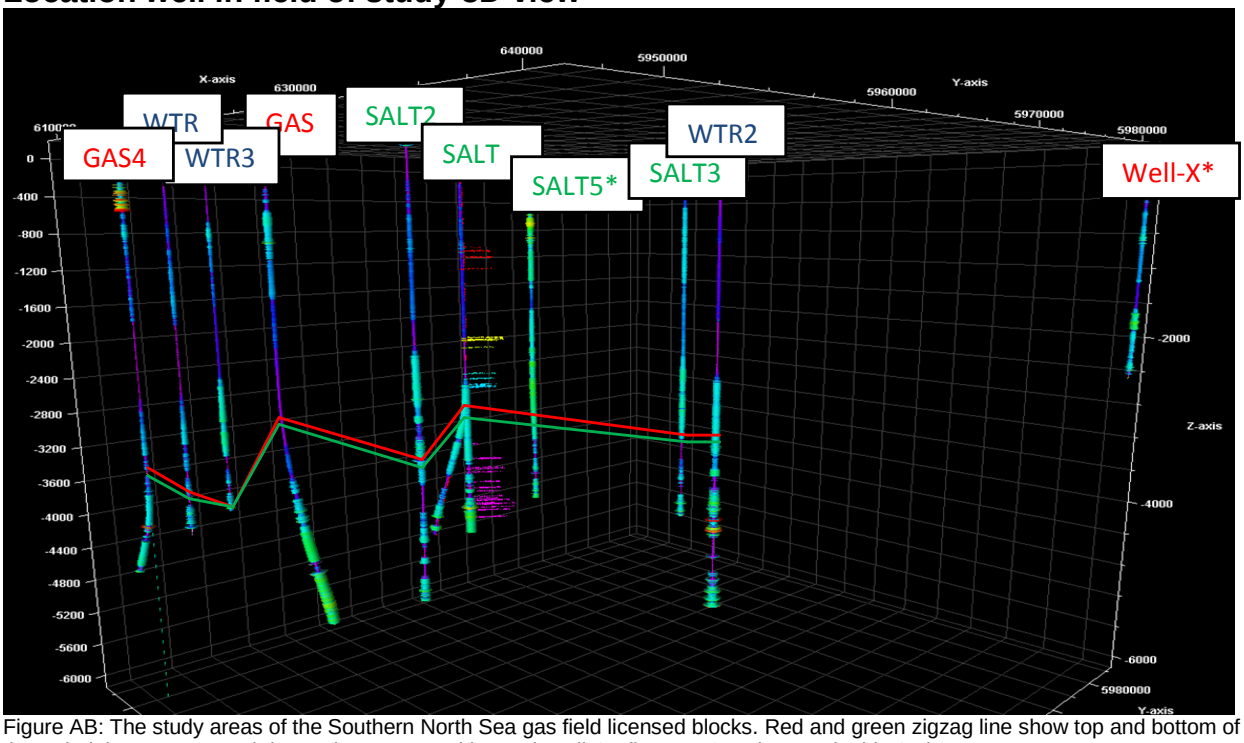


Figure AB: The study areas of the Southern North Sea gas field licensed blocks. Red and green zigzag line show top and bottom of the Volpriehausen reservoir interval encountered by each well.CF figures 16 and AA and table 2 above

APPENDIX C Parameter estimation method by the Ikon Science

The frequency bandwidth 'B' of the seismic data determines the optimum wavelet length 'L' required for a synthetic to match, which in turn limits the range of time windows 'T' that can be used as input to wavelet estimation. This seismic bandwidth can be determined using a statistical wavelet estimation or by any standard spectral analysis software and checked against any filtering applied by the seismic processing sequence.

The graph shows frequency bandwidth v optimum wavelet length (red X , Y axes and red diamond points) and frequency bandwidth v time window min and max (blue X,Y axes and blue dashed lines).

The more bandwidth the seismic data has, the shorter the wavelet should be and therefore the shorter the input seismic data time windows recommended for best results. In the diagram the wavelet length axis numbers are $1/5^{th}$ of the time window axis numbers eg: L = 100 msec is also T = 500 msec. The range of recommended input time windows, for a wavelet of length L, is given by the two dashed lines, 3L & 7L. which together outline a kind of "fairway" within which good wavelet estimations should be possible.

Given a seismic data frequency bandwidth B of 75 hz (axis (1)) , (eg: bandpass filtered to be 5 - 80 hz, 10 - 85 hz , 20 - 95 hz etc), we can see from the graph that the recommended optimum wavelet length L would be 50 msec (axis (2)) and that this length corresponds to a time window T range of 150 – 350 msec (axis (3)).

Reducing wavelet length, given a fixed seismic data frequency bandwidth, will create smoother wavelets from this wavelet estimation process and the more seismic frequencies that can be included in the input seismic trace, the better the phase estimation, as more points are available to define the wavelet's phase line. (see the cartoons beside the B,L,T plot)

Historically most seismic data contained frequencies between 10 and 60 Hz near the surface reducing to 10 – 35 Hz or so in the deeper section. In other words between seismic frequency bandwidths of 50 and 25 Hz. These bandwidths correspond to wavelet lengths around 100 msec and seismic input time windows around 500 msec which is why they are often set as defaults in Roy White wavelet estimation. (see orange annotation and rectangle in diagram). We use 124 msec for "max correlation lag/wavelet length" and 500 msec for "cross correlation range" defaults in WellTie.

The green A indicates an area on the graph where distortion of the estimated wavelet is likely because the wavelet is too short for the seismic data's restricted frequency bandwidth and B an area where longer wavelets than necessary allow noise to be matched to the synthetic as well as signal.

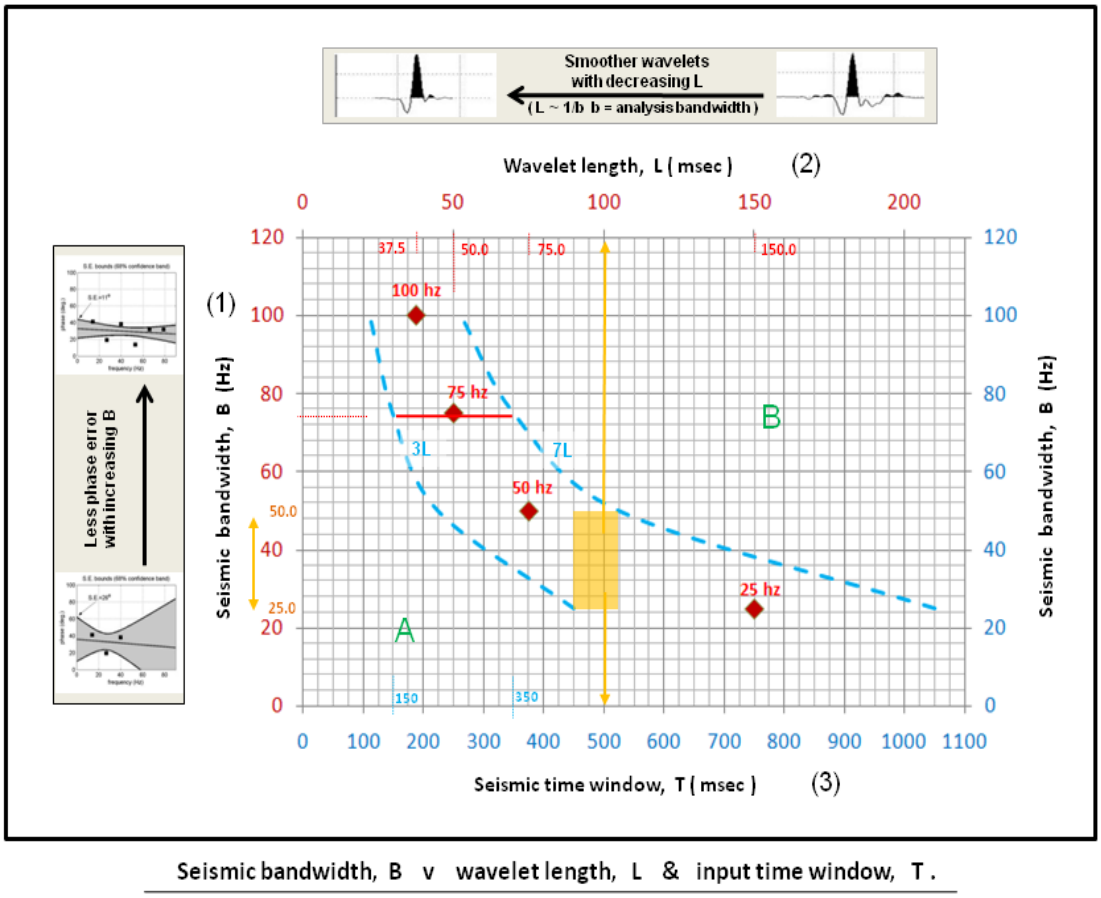


Figure C: Wavelet estimation parameters in display. After Ikon Science RokDoc programme training 2010

Examples of workflows risking distortion (A) might be :

1) Estimating a low frequency bandwidth far offset wavelet, reusing inappropriate near offset (higher frequency bandwidth based) L and T parameters.
2) When forced to use too short an input seismic data time window T because the well's sonic logs were recorded over a restricted time range, around the reservoir interval .

Examples of workflows risking matching noise (B) might be :

1) using input seismic data time windows T that are long enough to allow matching of surface multiples as well as primary signal.
2) It is better to make wavelets too long than too short in most cases.

APPENDIX D: Castagna et al AVO Interpretation guide

Table D1. Top gas sand reflection coefficient versus offset behavior for the three Rutherford and Williams (1989) classes' I–III assuming a typical "background" trend with negative slope. Class IV sands, though not explicitly discussed by Rutherford and Williams, may be considered to be a subdivision of their class III sands.

Class	Relative impedance	Quadrant	I	G	Remarks
I	Higher than overlying unit	IV	+	-	Reflection coefficient (and magnitude) decrease with increasing offset
II	About the same as the overlying unit	II, III or IV	+-	-	Reflection magnitude may increase or decrease with offset, and may reverse polarity
III	Lower than overlying unit	III	-	-	Reflection magnitude creases with offset
IV	Lower than overlying unit	II	-	+	Reflection magnitude de creases with offset